MOLECULAR MECHANISMS OF IMMUNOSUPPRESSIVE EFFECTS OF DIETARY n-3 PUFA, CURCUMIN AND LIMONIN ON MURINE $CD4^+$ T CELLS

A Dissertation

by

WOOKI KIM

Submitted to the Office of Graduate Studies of
Texas A&M University
in partial fulfillment of the requirements for the degree of

DOCTOR OF PHILOSOPHY

December 2008

Major Subject: Nutrition

MOLECULAR MECHANISMS OF IMMUNOSUPPRESSIVE EFFECTS OF DIETARY n-3 PUFA, CURCUMIN AND LIMONIN ON MURINE $CD4^+$ T CELLS

A Dissertation

by

WOOKI KIM

Submitted to the Office of Graduate Studies of
Texas A&M University
in partial fulfillment of the requirements for the degree of

DOCTOR OF PHILOSOPHY

Approved by:

Co-Chairs of Committee,	Robert S. Chapkin
	David N. McMurray
Committee Members,	Roger Smith
	Luc R. Berghman
Chair of Nutrition Faculty,	Stephen B. Smith

December 2008

Major Subject: Nutrition

ABSTRACT

Molecular Mechanisms of Immunosuppressive Effects of Dietary n-3 PUFA, Curcumin and Limonin on Murine $CD4^+$ T Cells. (December 2008)

Wooki Kim, B.S., Yonsei University, Seoul, Korea

Co-Chairs of Advisory Committee: Dr. Robert S. Chapkin
Dr. David N. McMurray

The molecular mechanisms of putative anti-inflammatory nutrients, i.e., fish oil, curcumin and limonin, were investgated with respect to $CD4^+$ T cell function. Initially, using a DO11.10 mouse model which exhibits a transgenic T cell receptor specific to OVA 323-339 peptide, we demonstrated that dietary fish oil suppresses antigen-specific Th1 clonal expansion *in vivo*. Following immunization, the accumulation of adoptively transferred transgenic cells in wild type recipient mouse lymph nodes was suppressed. In addition, cell division analysis by carboxyfluorescein succinimidyl ester (CFSE) revealed that both total cell number in lymph nodes as well as cell division were decreased by fish oil.

Since n-3 polyunsaturated fatty acids (PUFA), active long chain fatty acids in fish oil, elicit favorable effects on a variety of cell types, e.g., anti-tumor effect on colonocytes, amelioration of coronary heart disease and anti-inflammatory effects involving T cells, B cells, dendritic cells and macrophages, we postulated that a fundamental mechanism of action may explain the multiple effects observed. In a series of experiments described herein, we demonstrated that n-3 PUFA alters the

formation/location of membrane subdomains, referenced to as lipid rafts. Specifically, lipid raft formation at the immunological synapse (IS) in $CD4^+$ T cells was suppressed following membrane enrichment with n-3 PUFA. The alteration of lipid rafts down-regulated the localization of select signaling proteins, including F-actin, PKCθ and PLCγ-1, and phosphorylation of PLCγ-1 at the IS. Consequently, $CD4^+$ T cell proliferation was suppressed as assessed by CFSE analysis and radioactive thymidine incorporation.

Phytochemicals have been used for chemopreventive and chemotherapeutic purposes. We examined the putative anti-inflammatory effects of curcumin (1%) and limonin (0.02%) with respect to $CD4^+$ T cell function. Dietary curcumin and limonin suppressed NF-κB activation in $CD4^+$ T cells. In addition, $CD4^+$ T cell proliferation was modulated by 2% curcumin. We further investigated the combined therapeutic potential of phytochemicals and fish oil, containing n-3 PUFA. Interestingly, fish oil and limonin together significantly ($P<0.05$) suppressed T cell proliferation, whereas feeding either fish oil or limonin alone showed little effect.

In summary, our data indicated that dietary fish oil alters proximal signaling of T cells by perturbing lipid raft formation. Curcumin and limoin are capable of suppressing NF-κB in T cells, thereby exhibiting a synergistic effect when combined with fish oil. Further studies are required to elucidate the relationship of dietary dose of active compoments with respect to mechanism of actions.

ACKNOWLEDGEMENTS

I would like to acknowledge many people for helping me during my doctoral work. I would especially like to thank my co-advisors, Dr. Robert S. Chapkin and Dr. David N. McMurray, for their generous time and commitment. Throughout my doctoral work they encouraged me to develop independent thinking and research skills, continually stimulated my analytical thinking and greatly assisted me with scientific writing to lead me from a student to a scientist.

I am also very grateful for having an exceptional doctoral committee and wish to thank Dr. Luc Berghman and Dr. Roger Smith for their continual support and encouragement. In addition, I thank Dr. Smith for his expert operation and analysis of flow cytometry related experiments.

I wish to thank Dr. Rola Barhoumi for providing me with excellent advice and data from microscope-related analyses. I am also very grateful to Dr. Robert Rose and Andrea Taylor for teaching me adoptive transfer techniques. I thank Dr. Michael Walker and Vickie Weir for helping me with cell irradiation.

I am extremely grateful for the assistance, generosity, and advice I received from Chapkin Lab Family; Dr. Laurie Davidson was a mother-in-lab to care for all my laboratory work as well as birthday parties. Dr. Yang-Yi Fan instructed and counseled me regarding invaluable techniques. My work could not have been done without Evelyn Callaway's help with vivarium management. I also thank Dr. Satya Kolar, Qian Jia (JQ) and Rajeshwari Yog for their willingness to help me. Their assistance made it possible

for me to go forward smoothly. I extend my thanks to Dr. Lan Ly for her assistance with the measurement of cell proliferation using radioactive isotopes.

I would like to thank my parents, Mr. Chunwook Kim and Mrs. Shinja Lee, and parents-in-law, Mr. Kibong Song and Mrs. Gyesuk Yang for their support and for praying for me. I owe a special note of gratitude to my lovely wife, Eunsun Song for her being there. Her happy smile and warm hug allowed me to endure the unendurable. My cute daughter Lydia (Sunwoo), as well as the baby-to-be-born (Eunwoo), always kept my heart warm.

Finally, I'd like to thank God, my heavenly Father. Exploring a piece of secret He veiled in nature always keeps me excited. The moment of finding a clue how He created me to respond to a nutrient is when I kneel down and worship Him.

Gratefully, my research was supported in part by The American Society for Nutrition (McNeil Nutritionals Predoctoral Fellowship).

NOMENCLATURE

Ab, antibody

Ag, antigen

AICD, activation-induced cell death

ALA, α-linoleic acid

ANOVA, analysis of variance

AP, activated protein

APC, antigen presenting cell

AA, arachidonic acid

BSA, bovine serum albumin

CARD, caspase recruitment domain-containing protein

CC, corn oil+curcumin

CD, cluster of differentiation

CDAI, Crohn's disease activity index

CFA, complete Freuds' Adjuvant

CFSE, carboxyfluorescein succinimidyl ester

CL, corn oil+limonin

CMTMR, 5-(and-6)-(((4-chloromethyl)benzoyl)amino)tetramethylrhodamine

CO, corn oil

ConA, Concanavalin A

COX, cyclooxygenase

CTx, cholera toxin

Cur, curcumin

DHA, docosahexaenoic acid

DNA, deoxyribonucleic acid

DNP, dinitrophenol

DPA, docosapentaenoic acid

DPM, disintegrations per minute

DRM, detergent-resistant membrane fractions

EGF, epidermal growth factor

ELISA, enzyme linked immunosorbent assay

eNOS, endothelial nitric oxide synthase

EPA, eicosapentaenoic acid

FBS, fetal bovine serum

FC, fish oil+curcumin

FL, fish oil+limonin

FO, fish oil

FRET, fluorescence resonance energy transfer

GM1, monosialotetrahexosylganglioside

GM-CSF, granulocyte macrophage colony stimulating factor

GP, generalized polarization

HMS, homologous mouse serum

HRP, horseradish peroxidase

IBD, inflammatory bowel disease

IFN, interferon

Ig, immunoglobulin

IkB, inhibitor of NF-kB

IKK, IkB kinase

IL, interleukin

iNOS, inducible nitric oxide synthase

IS, immune synapse

LA, linoleic acid

LAT, linker for activation of T cells

LDL, low density lipoprotein

LFA, lymphocyte function-associated antigen

Lim, limonin

LOX, lipoxygenase

LSD, least significant difference

LTE, leukotriene

mAb, monoclonal antibody

ME, mercaptoethanol

MFI, mean fluorescence intensity

MHC, major histocompatibility complex

mRNA, messenger ribonucleic acid

MS, multiple sclerosis

MβCD, methyl-β-cyclodextrin

NF, nuclear factor

NFAT, nuclear factor of activated T cells

PAMP, pathogen-associated molecular patterns

PBMC, peripheral blood mononuclear cells

PBS, phosphate buffered saline

PE-Cy5, phycoerythrin-cyanine 5

PGE, prostaglandin E

PKC, protein kinase C

PLC, phospholipase C

PPAR, peroxisome proliferator-activated receptor

PUFA, polyunsaturated fatty acids

REML, restricted maximum likelihood

ROI, region of interest

RRI, relative relocation index

RvE, resolvin E

SEM, standard error of mean

SFK, Src family kinases

TCR, T cell receptor

Th cell, helper T cell

TLR, Toll-like receptor

TNF, tumor necrosis factor

WT, wild type

ZAP, zeta-chain-associated protein kinase

TABLE OF CONTENTS

CHAPTER Page

LIST OF FIGURES

Page

Page

LIST OF TABLES

Page

CHAPTER I

INTRODUCTION AND LITERATURE REVIEW

Function of $CD4^+$ T cells in immune diseases

$CD4^+$ helper T (Th) cells are essential regulators of the immune response. Upon activation, naïve Th cells differentiate into effector cells (**Fig. 1**). For example, classical Th1 and Th2 lineages are characterized by their cytokine secretion and immune regulation function (1, 2). IL-2 and IFN-γ are signature cytokines produced by Th1 cells which regulate cell-mediated immune response, whereas Th2 cells regulate humoral immune response in part by secreting IL-4, IL-5, IL-10 and IL-13 (3).

Most autoimmune diseases and/or chronic inflammation involve an overactive, self-destructive immune response toward a particular tissue, for example, the pancreas in type 1 diabetes, the central nervous system in multiple sclerosis (MS), various joints in rheumatoid arthritis and the small and large intestine in inflammatory bowel disease (IBD; Crohn's disease and ulcerative colitis). The pathogenesis of immune diseases is made up of a complex network involving a variety of cell types. For example, IBD involves intestinal epithelial cells, lymphocytes, dendritic cells and macrophages (4, 5).

Th1 cells are of pivotal importance for the pathogenesis of IBD (6). A growing body of evidence indicates that IL-23 and TNF-α, as well as Th1-inducing cytokines, drive Th1-induced IBD. Furthermore, an IL-17 producing Th cell lineage activated by IL-23 was recently identified. These cells are classified as distinct pro-inflammatory

---

This dissertation follows the style of *The Journal of Immunology*.

Th17 (Thi) cells (7-9). Hence, autoreactive Th1 cells, as well as Th17 cells, are major players in chronic inflammatory diseases (10-13), and inhibition of the expansion of Th1 cells can be one of the mechanisms by which anti-inflammatory agents exert their effect.

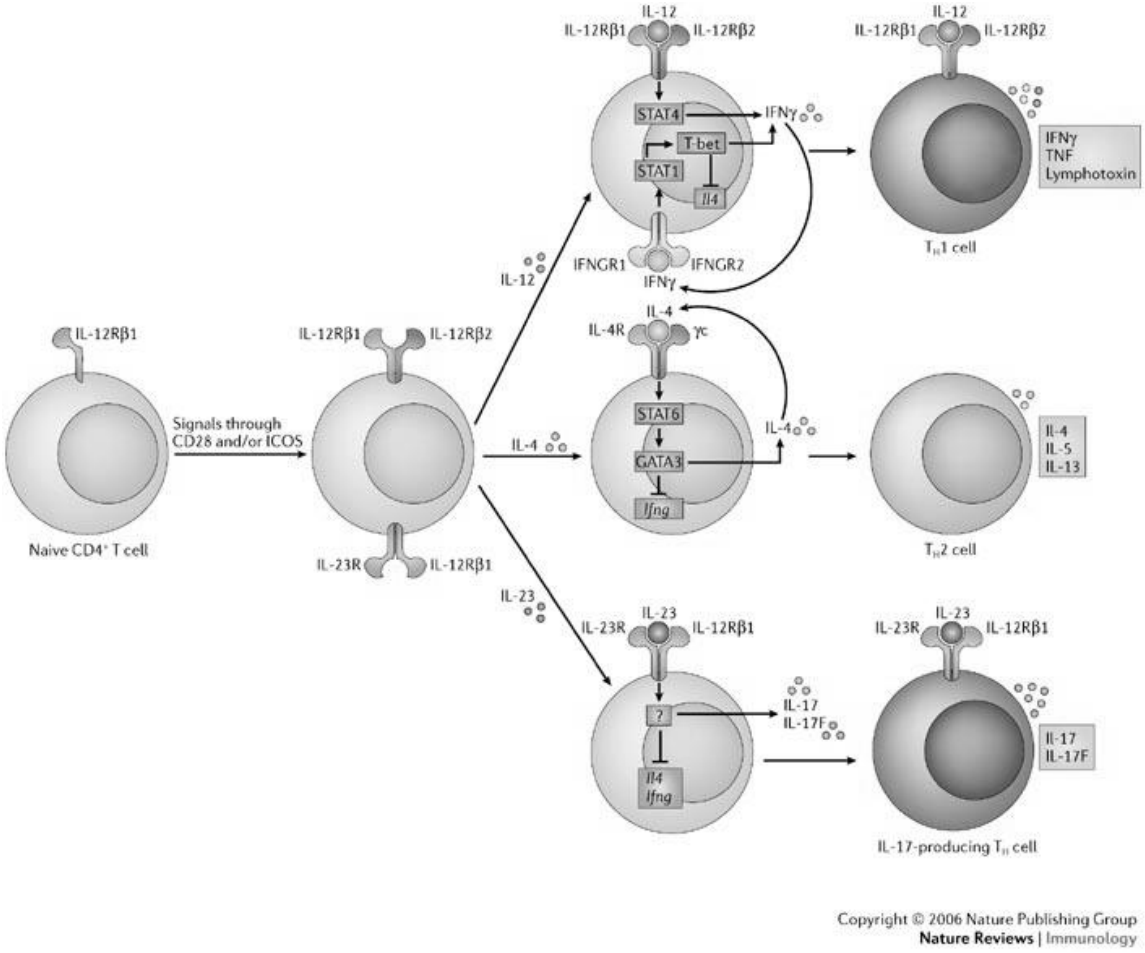

Figure 1. Subpopulations of Th cells. Following stimulation, naïve $CD4^+$ T cells differentiate into either Th1, Th2 or Th17 cells, determined in part by antigen, APC and cytokine interaction. Th1 and Th17 lineages are reported to be pro-inflammatory T cells. Image was reprinted with permission from "Diversification of T-helper-cell lineages: finding the family root of IL-17-producing cells" by Dong, C., 2006, *Nat. Rev. Immunol.* (9). Copyright 2006 by Nature Publishing Group.

T cell activation and lipid rafts

For T cell activation to occur, only cognate peptide-major histocompatibility complexes (MHC), among a total pool of peptide presenting MHC molecules expressed on antigen presenting cells (APC), are recognized by receptors on the T cell to generate an immune response (14). At the contact zone between the T cell and APC (e.g., B cells, macrophages and dendritic cells), the immunological synapse (IS) is formed to facilitate T cell receptor (TCR) binding to antigen (Ag) peptide. Interestingly, during the formation of the IS, T cells polarize their cytoskeleton, including actin and microtubule networks. Furthermore, Thauland *et al*. (15) reported that polarized Th1 and Th2 cells form morphologically distinct IS. Specifically, IS formation of Th1 cells is unique in that a compact central cluster of MHC/TCR surrounded by adhesion molecules is formed. In contrast, Th2 polarized cells exhibit a multifocal IS by forming multiple MHC/TCR accumulations at high Ag concentrations.

The plasma membrane is involved in almost all aspects of cell biology, including morphogenesis, proliferation, migration, invasion, transformation, differentiation, secretion and apoptosis. The classical concept of the cell membrane, i.e., Singer-Nicholson fluid mosaic model of the lipid bilayers, had little influence on membrane protein function (16). However, in the past two decades, a growing body of data indicate that lipids exist in gel, liquid-ordered or liquid-disordered states, depending on the complex environment of the cell. Subsequently, a lipid raft theory has evolved in which liquid-ordered microdomains, i.e. lipid rafts, are floating over the “sea” of bulk membrane, which is in a liquid-disordered state (17). It is postulated that the

preponderance of saturated hydrocarbon chains in sphingolipids allows for cholesterol to be tightly interacted, forming the "packed" liquid-ordered phase. Hence, historically, lipid rafts have been characterized by two operational definitions; the insolubility in cold nonionic detergents, for which lipid rafts are also called detergent-resistant membrane fractions (DRM), and a loss of function associated with cholesterol depletion (18).

Among a variety of functions, lipid rafts are now believed to modulate intracellular signaling cascades, endocytosis, protein trafficking and cell-cell communication in part by altering the lipid-protein composition of the bulk membrane via specialized lipid microdomains (17, 19-21). In terms of immune cell related signaling, lipid rafts are known to be involved in the signal transduction-related processes involving FcεRI receptor (22), T cell receptor (TCR) (23), B cell receptor (BCR) (24), epidermal growth factor (EGF) receptor (25, 26), insulin receptor (27), integrins (28) and endothelial nitric oxide synthase (eNOS) (29). These data indicate that the composition and formation/dissociation status of lipid rafts is likely critical for T cell activation.

Effect of n-3 PUFA on the immune response

With respect to the dietary manipulation of immune function, long chain n-3 polyunsaturated fatty acids (n-3 PUFA), which are enriched in dietary fish oil, have been studied in relation to their anti-inflammatory properties (30-34). With respect to molecular structure, n-3 PUFA have their first double bond at the third carbon from the methyl end. α-linolenic acid (ALA; 18:3n-3), eicosapentaenoic acid (EPA; 20:5n-3) and

docosahexaenoic acid (DHA; 22:6n-3) are examples of n-3 PUFA. Interestingly, DHA is unique in that it is the longest and most unsaturated fatty acid commonly found in membranes (35). In contrast, n-6 PUFA (i.e, linoleic acid (LA; 18:2n-6) and arachidonic acid (AA; 20:4n-6)), which have the first double bond at the sixth carbon from the methyl end, generally exhibit pro-inflammatory properties. Due to the degree of unsaturation and the low activation energy for rotation about the single C-C bonds that separate the unsaturated carbon atoms in the recurring $=CH-CH_2-CH=$ pattern, DHA is thought to form a liquid-disordered structure in biological membrane (36-38). Our proposed anti-inflammatory actions of n-3 PUFA are summarized in **Fig. 2**. The summary of beneficial clinical effects of n-3 PUFA on the immune system has been well documented by other investigators in humans and animal models (39-43).

Alteration of cytokine production

A growing body of data indicate that n-3 PUFA alter cytokine production, which in turn influences the function of a variety of cell types mediating both the induction and resolution of inflammation. Zhao *et al*. reported that ALA inhibits pro-inflammatory cytokine production, such as IL-2, IL-1β, and TNF-α, in peripheral blood mononuclear cells from hypercholesterolemic subjects (44). A reduction in IFN-γ production by FO feeding in multiple sclerosis (MS) patients and a rat model has also been reported by several investigators (45-47). Petursdottir *et al*. demonstrated that dietary FO (18% FO+2% corn oil (CO, contains n-6 PUFA)) decreased the production of both pro-inflammatory TNF-α and anti-inflammatory IL-10 in Concanavalin A (ConA) stimulated

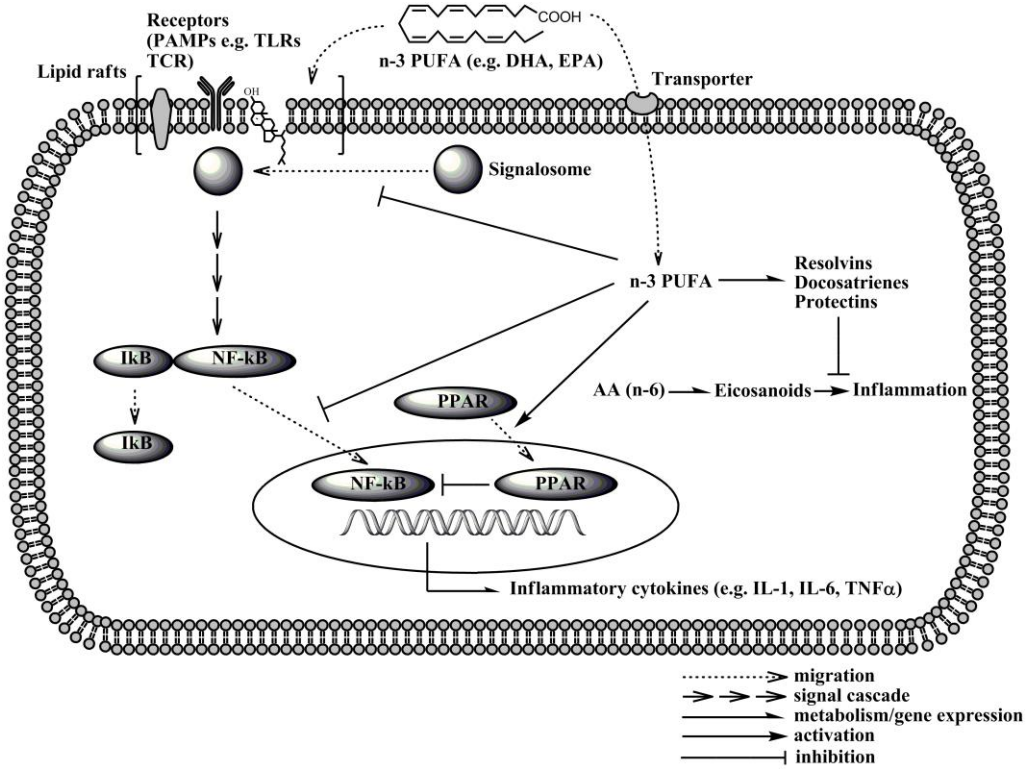

Figure 2. Proposed molecular model by which EPA and DHA modulate immune cell function and inflammation. n-3 PUFA suppress nuclear receptor activation, e.g., NF-kB, arachidonic acid-cyclooxygenase derived eicosanoids, and alter plasma membrane micro-organization (lipid rafts). We propose that lipid rafts may be targets for the development of n-3 PUFA-containing dietary bioactive agents to down-modulate chronic inflammatory responses. AA, arachidonic acid ($20:4^{\Delta 5,8,11,14}$, an n-6 PUFA); DHA, docosahexaenoic acid ($22:6^{\Delta 4,7,10,13,16,19}$); (EPA, eicosapentaenoic acid ($20:5^{\Delta 5,8,11,14,17}$); NF-kB, nuclear factor kB; IkB, inhibitor of NF-kB; IL, interleukin; PPAR, peroxisome proliferator-activated receptor; PUFA, polyunsaturated fatty acids; TLR, Toll-like receptors are a member of the pattern recognition receptor family. These receptors recognize highly conserved pathogen-associated molecular patterns (PAMPs) to generate an immune response; TNF, tumor necrosis factor-alpha.

mouse splenocytes (48), emphasizing the complexity of cytokine biology in inflammation. In addition, Kim *et al*. delineated the effect of n-3 PUFA in inflammation by demonstrating that dietary FO elicited anti-inflammatory effects via increases in lipid peroxidation and superoxide generation in the murine kidney (49).

Effect on CD4$^+$ T cell function

In terms of n-3 PUFA effects on CD4$^+$ T cells, Arrington *et al*. from our laboratory reported that IL-2 secretion by mitogenic anti-CD3/anti-CD28 stimulation of murine splenic T cells was suppressed by dietary DHA (34). In a parallel experiment, they further demonstrated that IL-2 production by Jurkat T cells was suppressed by 50 μM AA or DHA, compared to LA. Interestingly, DHA treatment suppressed IL-2 secretion compared to AA treatment only when CD28 was engaged in T cell activation, indicating that n-3 PUFA also affect the function of co-stimulatory CD28 signaling (33).

Since IL-2 production is critical for T cell proliferation, Switzer *et al*. from our laboratory examined the effect of n-3 PUFA on activation-induced cell death (AICD) of mouse splenic CD4$^+$ T cells. They showed that dietary FO enhanced Th1 polarization and AICD *ex vivo*. They also reported that the n-3 PUFA enriched FA composition of T cell membranes was maintained in long-term culture in the presence of homologous mouse serum (HMS). In contrast, cell culture with FBS displaced n-3 PUFA derived from FO feeding, resulting in the loss of dietary effect (50). Other investigators have demonstrated that apoptosis is enhanced by DHA in murine CD4$^+$ T cells as well as T cell lines (51). The induction of apoptosis by n-3 PUFA might explain why fewer cells entered the cell cycle after long-term culture (52).

Zhang *et al*. from our laboratory also investigated the effect of n-3 PUFA on antigen-induced CD4$^+$ T cell proliferation. They confirmed that n-3 PUFA are capable of suppressing proliferation of mouse antigen-specific (DO11.10) CD4$^+$ T cells in the presence of HMS (52). The effects of serum on antigen-specific T cell activation was in

accordance with previous observations indicating that HMS is required in long-term culture to preserve n-3 PUFA-induced changes in plasma membrane microdomain fatty acyl composition and cell functionality (50). They further reported that dietary FO modulates the Th1/Th2 balance toward the Th2 pole in the presence of HMS. In subsequent experiments, it was demonstrated that Th2 proliferation was not affected by FO, indicating that FO selectively suppressed Th1 development (30).

Overall, these findings suggest that n-3 PUFA suppress $CD4^+$ T cell proliferation and function. $CD4^+$ T cells are one of the major immunoregulators and therefore a target cell type for immunosuppressive dietary agents including n-3 PUFA.

Eicosanoids, protectins and resolvins

It was shown that dietary intake of AA is correlated with plasma levels of AA-derived pro-inflammatory eicosanoids, prostaglandin (PGE_2) and leukotriene (LTE_4) (53). This is noteworthy because dietary EPA competes for the key enzymes, i.e. cyclooxygenase (COX)-2 and 5-lipoxygenase (LOX) to be converted to PGE_3 and LTE_5, respectively (54). Furthermore, FO also suppressed the expression of iNOS and COX-2, thereby ameliorating inflammatory markers, for example, PGE_2 and LTB_4 (49, 55, 56).

Of interest, resolvins (RvE1 and RvE2), docosatrienes and neutroprotectins derived from DHA and EPA were recently classified as anti-inflammatory mediators (57). For example, it was reported that RvE1 displayed potent ability to regulate leukocyte/dendritic cell trafficking, block IL-12 production, counter-regulate TNF-α induced NF-κB signaling, and protect against murine colitis (58). Others have further

demonstrated that these n-3 PUFA derived metabolites can counter-regulate and terminate inflammation (59, 60), which may explain why the biosynthesis of these metabolites seem to be defective in patients with chronic inflammation (59, 61).

It is noteworthy that the AA pool size is large and conversion of metabolic precursors to AA is relatively slow, whereas the DHA pool is relatively small and therefore susceptible to dietary alteration (62).

PPAR agonist

Hontecillas *et al*. reported that the loss of peroxisome proliferator-activated receptor (PPAR)-γ enhanced Ag-specific proliferation and overproduction of pro-inflammatory IFN-γ in response to IL-12 using effector $CD4^+$ T cells from PPAR-γ knockout mice (63), indicating the anti-inflammatory role of PPAR-γ. Furthermore, PPAR-γ knockout resulted in the loss of anti-inflammatory regulatory T cells (Treg) required to prevent effector T cell-induced colitis (63). This is noteworthy, because micromolar levels of n-3 PUFA can activate PPAR-γ (64, 65), which in turn is capable of antagonizing a "life signaling" transcription factor, i.e. nuclear factor NF-κB (66).

Protein lipidation and intracellular targeting

For TCR initiated T cell activation, it is critical that co-receptors and signaling proteins are palmitoylated. Palmitate, a 16-carbon saturated fatty acid (16:0), is known to be essential for the targeting of many proteins into lipid rafts. For example, localization of CD4 into lipid rafts requires palmitoylation of CD4 molecules (67). Src family

kinases (SFK), Lck and Fyn, are dual-acylated by myristate (14:0) and palmitate in order to localize into lipid rafts. Interestingly, Webb *et al*. showed that inhibition of palmitoylation resulted not only in dislocation of SFK from rafts but also the failure of TCR signaling and T cell activation (68, 69).

Zeyda *et al*. reported that EPA treated Jurkat T cells exhibited a displaced linker for activation of T cell (LAT) from lipid rafts compared to the saturated stearic acid (18:0) treated control group, as assessed by biochemical separation of DRM and Western blot of LAT using specific antibodies (70). In the same experiment, they showed that not only the location of LAT but also the phosphorylation status of LAT and phospholipase C (PLC)-γ1 was suppressed, indicating suppressed activation of signaling proteins by n-3 PUFA (70). This observation is relevant because LAT is palmitoylated at two cysteine residues, which might drive the migration of LAT into lipid rafts. However, the biological impact of LAT localization into rafts has been recently challenged. Zhu *et al*. demonstrated that mutated LAT, which locates out of lipid rafts, functioned comparably to the wild-type LAT, suggesting that LAT palmitoylation and/or raft targeting is not necessary for LAT function (71). Therefore, further studies are required to determine the effect of n-3 PUFA on LAT localization in T cell activation.

Dietary alteration of lipid rafts

Since lipid rafts are thought to regulate many cell functions, a number of studies have examined the effects of fatty acid manipulation on T cell lipid rafts. Stulnig *et al*. reported the enrichment of n-3 PUFA in plasma membranes of Jurkat T cells by addition

of fatty acids into the culture media (70, 72-76). These manipulations were associated with a marked displacement of Src family kinases, e.g., Lck and Fyn, from DRM indicating that the alteration of lipid rafts affects the intracellular localization of signaling proteins. Interestingly, the displacement of Lck correlated with diminished calcium signaling indicating the functional role of lipid rafts in T cell activation (72). Our laboratory also previously showed that highly purified dietary DHA ethyl ester and FO, in which n-3 PUFA are highly enriched, were incorporated into murine splenic T cell lipid rafts and soluble membrane phospholipids, resulting in a 30% reduction in raft sphingomyelin content (32, 77).

Recently, using immunogold electron microscopy of plasma membrane sheets coupled with spatial point analysis which enabled visualization of morphologically featureless microdomains, our laboratory has shown that DHA altered the size and distribution of lipid rafts in HeLa cells. Specifically, DHA treatment significantly reduced the interparticle distance of lipid raft marker proteins. In contrast, distance of marker proteins of bulk membrane was not affected by DHA treatment indicating that n-3 PUFA can selectively increase clustering of proteins in cholesterol-dependent microdomains, i.e. lipid rafts (78, 79). These observations can be explained in part by the fact that n-3 PUFA, specifically DHA, has a low affinity for cholesterol, providing a lipid-driven mechanism for lateral phase separation of cholesterol/sphingolipid-rich lipid microdomains from the surrounding liquid-disordered (l_d) phase (80-84). Similarly, Patra *et al*. has demonstrated that enrichment of ceramide, derived from the hydrolysis of sphingomyelin in the outer leaflet of the plasma membrane, resulted in coalescence of

lipid raft sub-domains into large-membrane macrodomains, in part by excluding cholesterol from bulk membrane. In addition, the displacement of cholesterol from lipid rafts suppressed the association of the raft-binding and cholesterol binding proteins (85).

Anti-inflammatory phytogenic polyphenols

Curcumin

Curcumin [(E,E)-1,7-bis-(4-hydroxy-3-methoxyphenyl)-1,6-heptadiene-3,5-dion or diferuloymethane, **Fig. 3A**] is a food-derived yellow pigment extracted from *Curcuma longa* (Linn). Curcumin has been shown to have chemopreventive and chemotherapeutic properties in animal models (86) and humans (87, 88). In addition, numerous studies indicate that curcumin has anti-inflammatory properties (89) by inhibiting the activation of nuclear transcription factors including NF-κB (90, 91) and activated protein 1 (AP-1) (92, 93). Milacic *et al*. (94) recently reported that curcumin directly binds to and inhibits proteasomes, by which NF-κB activity was suppressed in a human colon cancer cell line. Fujiyama *et al*. have shown that 3.5% dietary curcumin feeding to mice prevented the development of dextran sulphate sodium (DSS)-induced colitis in part by blocking NF-κB activity (86, 95). In addition, clinical data from ulcerative colitis patients treated with curcumin indicated the suppressive effect on relapse (95). Another recent clinical pilot study also supports the contention that dietary curcumin intake reduces the Crohn's Disease Activity Index (CDAI) (96). Sharma *et al*. also reported that curcumin suppressed NF-κB and COX-2 expression in human oral premalignant and cancer cells (97).

A. Curcumin

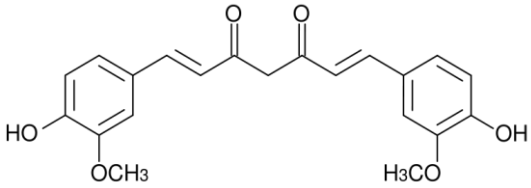

M.W. 368.38 g/mol

B. Limonin

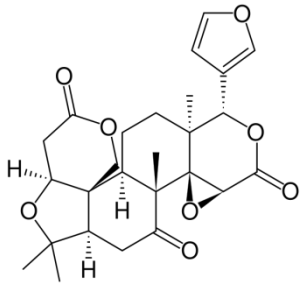

M.W. 470.52 g/mol

Figure 3. Chemical structures of curcumin and limonin.

Curcumin has been shown to down-regulate a variety of cell growth related genes. For example, Gertsch *et al*. reported that mRNA levels of granulocyte macrophage colony stimulating factor (GM-CSF), cyclin D1 and IFN-γ were down-regulated in Jurkat T cells and human peripheral blood mononuclear cells (PBMC) following addition of curcumin into the culture media. Furthermore, IL-2 and IL-6 mRNAs levels were suppressed in Jurkat T cells (89).

Zhang *et al*. studied the effect of curcumin on Th1/Th2 balance in a chronic colitis mouse model. Interestingly, intraperitoneal injection of curcumin decreased the expression of IL-12, IFN-γ, TNF-α and IL-2 (Th1 cytokines) and increased the expression of IL-4 and IL-10 (Th2 cytokines) in colon mucosa. In addition, the IFN-γ/IL-4 ratio in splenocytes and blood circulation was suppressed by curcumin, indicating that curcumin shifts the Th1/Th2 balance to the Th2 pole (98). In accordance, Kang *et*

al. reported that curcumin suppressed IL-2 production in macrophages, which in turn inhibited the Th1 cytokine profile in murine $CD4^+$ T cells (99).

Limonin

Limonin (7,16-dioxo-7,16-dideoxylimondiol, **Fig. 3B**) is derived from citrus fruit. It has been demonstrated that dietary limonin reduced colon cancer development in part by suppressing COX-2 and iNOS expression in rats (100, 101). It is noteworthy that both COX-2 and iNOS are in part regulated by NF-κB, which is generally a pro-inflammatory signal (102, 103). Hence, the putative anti-inflammatory properties of limonin merit study. Yu *et al*. reported that limonin suppressed production of superoxide radical formation and offered protection against LDL oxidation. These data suggest that limonin exhibits antioxidant-like properties (104). Furthermore, limonin improved vascular permeability, the decrease of paw edema and AA-induced ear swelling, suggesting that limonin is a bioactive molecule exhibiting anti-inflammatory properties.

Advances in methodologies and mouse models

Use of Laurdan to visualize lipid rafts in living cells

There have been several methodologies developed to identify and visualize the lipid rafts. For instance, flotation of DRM fractions and immunofluorescence microscopy by antibody patching have been used to identify putative raft association and raft proteins (105, 106). In addition, immunoelectron microscopy and single fluorophore tracking microscopy were utilized to track the location of raft components (107).

Fluorescence resonance energy transfer (FRET) was also applied to determine whether two raft components are spatially impacted (108). However, due to their nano scale sizes (<50 nm in diameter) and highly dynamic formation and dissociation (up to 10^{-8} $cm^{-2}sec^{-1}$) of larger domains (17, 109), microdomain morphology has been hard to visualize.

Recently, it was demonstrated that the fluorescent probe Laurdan can align itself parallel with the hydrophobic tails of phospholipids in membranes (110-112). Owing to its ability to emit two different wavelengths according to the fluidity of the microenvironment, Laurdan can be used to measure membrane fluidity and visualize lipid rafts in living cells by two-photon microscopy (111). Since lipid raft formation was expected to be induced by the formation of the IS (110), non IS forming APC and /or non IS regions of plasma membrane in the $CD4^+$ T cells can be used as negative controls.

Fat-1 (n-3 desaturase) mouse

Since mammals cannot produce n-3 PUFA from the major n-6 PUFA found in the diet due to the lack of Δ15-desaturase activity, it is necessary to enrich the diet with eicosapentaenoic acid (EPA, 20:5n-3) and/or DHA in order to assess their biological properties *in vivo*. Recently, the *fat-1* gene encoding an n-3 fatty acid desaturase was cloned from *Caenorhabditis elegans* and expressed in mammalian cells (113). This enzyme can catalyze the conversion of n-6 PUFA to n-3 PUFA by introducing a double bond into fatty acyl chains. Hence, transgenic mice expressing *fat-1* allow us to investigate the biological properties of n-3 PUFA without having to incorporate these fatty acids into the diet.

Jia *et al*. from our laboratory previously reported that *fat*-1 transgenic mice exhibit a reduction in colitis-induced colon cancer (114). In a parallel experiment, they also demonstrated that transgenic mice recovered better from chronic vs acute dextran sodium sulphate (DSS) exposure, indicating that n-3 PUFA differently modulate the acute vs chronic phases of inflammation.

DO11.10 TCR transgenic mouse

The DO11.10 Rag $2^{-/-}$ transgenic mouse model has been used to study antigen-specific T cell activation and differentiation. The DO11.10 mouse expresses a transgenic T cell receptor (TCR), which recognizes only an ovalbumin (OVA) 323-339 peptide, (115). The transgenic TCR also can be identified using the clonotypic monoclonal antibody (mAb) KJ1–26 (116). The deletion of *rag2* gene enabled virtually all peripheral $CD4^+$ T cells from these mice to be TCR transgenic, compared to ~25% TCR positive $CD4^+$ T cells in the periphery of the conventional DO11.10 mouse (117). This mouse model is advantageous in that one can induce an antigen-specific T cell response excluding the effect of non-specifically responding lymphocytes. Pompos *et al*. have shown that dietary n-3 PUFA suppressed OVA peptide stimulated proliferation of splenocytes and IL-2 secretion in DO11.10 TCR transgenic mice (117). To extend this observation, our laboratory previously revealed that purified $CD4^+$ T cells from the DO11.10 $Rag2^{-/-}$ mice fed FO had significantly decreased proliferation in response to OVA peptide, when cultured in the presence of HMS (52). These data conclusively

demonstrate that dietary n-3 PUFA suppress antigen-specific $CD4^+$ T cell functions *ex vivo*.

The genetic background determines the default Th1/Th2 development of naïve Th cells under neutral conditions and the DO11.10 mouse is on a Th1-prone B10.D2 background (118, 119). In fact, more than 90% of the $CD4^+$ cells were shown to be Th1 cells after Th1 polarization in culture (52). Zhang *et al*. from our laboratory revealed that FO feeding did not alter the percentage of Th1 cells generated under stringent Th1 polarizing conditions, suggesting that dietary FO does not affect the Th1 differentiation process in mice. In contrast, FO feeding suppressed Th1 clonal expansion driven by IL-2 (52).

Summary

Data indicate that dietary n-3 PUFA have anti-inflammatory properties in both animal models and humans. However, the molecular/cellular mechanisms of action are not fully elucidated to date. Therefore, herein, we further studied the effect of n-3 PUFA on lipid raft formation in naïve $CD4^+$ T cells and Ag-specific *in vivo* proliferation of Th1 cells. With respect to phytochemicals, curcumin and limonin exert anti-inflammatory effects in part by affecting $CD4^+$ T cell function. To date, no study has investigated the effect of dietary curcumin and limonin on $CD4^+$ T cells. Therefore, we determined how dietary curcumin and limonin with or without n-3 PUFA supplementation alter murine $CD4^+$ T cell function.

Hypotheses and specific aims

Hypothesis 1. Dietary n-3 PUFA inhibit antigen-stimulated Th1 development in vivo

Aim 1. Determine the effect of n-3 PUFA on recipient mouse lymph nodes.

Aim 2. Determine the effect of n-3 PUFA on the proliferation of donor cells in recipient mouse organs.

Hypothesis 2. n-3 PUFA promote lipid raft formation at the immune synapse, thereby altering signaling molecule recruitment and activation in $CD4^+$ T cells

Aim 1. Visualize and measure lipid rafts at the IS.

Aim 2. Determine the localization of select signaling proteins at the IS.

Aim 3. Determine the activation status of key signaling proteins at the IS.

Aim 4. Measure the proliferation of $CD4^+$ T cells in response to various stimuli.

Hypothesis 3. Dietary curcumin and/or limonin suppress antigenic $CD4^+$ T cell proliferation via down-regulation of NF-kB activation

Aim 1. Quantify NF-kB activation.

Aim 2. Measure IL-2 production.

Aim 3. Measure $CD4^+$ T cell proliferation.

Aim 4. Determine if FO supplementation with or without curcumin/limonin elicit maximal anti-inflammatory properties by “combination chemotherapy”.

CHAPTER II

DIETARY n-3 PUFA SUPPRESS Th1 CLONAL EXPANSION OF $CD4^+$ T CELLS *IN VIVO**

Introduction

Our laboratory previously demonstrated that n-3 PUFA inhibit expansion of antigen-specific Th1 cells, *ex vivo* (52). In that study, DO11.10 $Rag2^{-/-}$ TCR transgenic mice were fed either CO control diet or FO for 2 wk, followed by $CD4^+$ T cell purification, Th1 polarization and long-term stimulation by antigenic or mitogenic stimuli in culture. In addition, 2.5% homologous mouse serum (HMS) was utilized to prevent culture-induced alteration of plasma membrane fatty acids. It is important to note that the use of HMS, along with an *ex vivo* culture system, complicates the physiological relevance of the study.

DO11.10 TCR transgenic mice cannot be directly immunized with cognate OVA323-339 peptide in order to investigate *in vivo* immune response, due to the abnormal immune response to direct *in vivo* antigen challenge at the artificially high frequency of OVA peptide-specific T cells (120). Therefore, Kearney *et al*. (120) developed an adoptive transfer model in which TCR transgenic T cells were injected into a non-transgenic recipient, and transgenic T cells could be reliably detected using KJ1-26 mAb, which is specific to transgenic TCR.

---

* Reprinted with permission from "Dietary fish oil inhibits antigen-specific murine Th1 cell development by suppression of clonal expansion" by Zhang, P. *et al*., 2006. *J Nutr.* 136, 2391-2398. Copyright 2006 by American Society of Nutritional Sciences.

Complete Freuds' adjuvant (CFA) is known to induce Th1 differentiation (121). The resultant immune response following subcutaneous injection induces the accumulation of antigen-specific transgenic T cells only in the draining lymph nodes, allowing one to harvest and investigate Th1 polarized cells *in vivo*. Interestingly, rounds of T cell division can be assessed by CFSE profile analysis as previously reported (122). Taking advantage of the adoptive transfer system, Th1 polarized immunization and CFSE profile analysis, here we show that antigen-driven Th1 clonal expansion was suppressed by n-3 PUFA *in vivo*, in accordance with previous *ex vivo* observations.

Materials and Methods

Animals and diets

All experimental procedures using laboratory animals were approved by the Texas A&M University Laboratory Animal Care Committee. Pathogen-free B10.D2 and syngeneic TCR transgenic DO11.10 $Rag2^{-/-}$ mice were purchased from Taconic Farms, bred, and maintained at Texas A&M University. Representative results of DO11.10 genotyping is avalible in Appendix A-1. At the onset of the study, B10.D2 and DO11.10 $Rag2^{-/-}$ mice (8–10 wk of age) were fed a control semi-purified diet containing 5% CO by weight during the 7 d acclimation period, followed by a 2 wk feeding period with the same control diet or a FO diet (1% CO + 4% FO). B10.D2 mice were maintained on the same diets following adoptive transfer and immunization. All diets met the NRC nutrition requirements and varied only in lipid content (32). The basic diet composition, expressed as g/100 g was as follows: casein, 20; sucrose, 42; cornstarch, 22; cellulose, 6;

AIN-76 mineral mix, 3.5; AIN-76 vitamin mix, 1; DL-methionine, 0.3; choline chloride, 0.2; Tenox 20A, 0.1; and oil, 5 (32).

$CD4^+$ T cell purification

After feeding, mice were killed by CO_2 asphyxiation. Spleens and lymph nodes (brachial and mesenteric) were removed from DO11.10 $Rag2^{-/-}$ mice and placed in RPMI complete medium (RPMI 1640 medium with 25 mmol/L HEPES (Irvine Scientific), supplemented with 5% fetal bovine serum (FBS) or homologous mouse serum (HMS 2.5% + 2.5% FBS), 10^5 U/L penicillin and 100 mg/L streptomycin (Irvine Scientific), 2 mmol/L L-glutamine, and 10 µmol/L 2-mercaptoethanol). T cells were purified by a negative selection column method as previously described (34). The detailed protocol is included in Appendix B-2. HMS was collected according to the method of Pompos *et al*. (117). In general, spleens from DO11.10 $Rag2^{-/-}$ mice were smaller than from conventional mice in accordance with a previous report (123), and the number of lymphocytes obtained was much lower compared to conventional C57BL/6 mice (1.7×10^6 vs. 20×10^6, n=5-6, $P<0.05$).

Adoptive transfer and immunization

$CD4^+$ T cells were purified from spleens and lymph nodes (brachial, axillary and mesenteric) of DO11.10 donor mice as described above and labeled using CFSE. Briefly, purified $CD4^+$ T cells were mixed with 10 µM CFSE in PBS containing 0.1% bovine serum albumin and incubated at 37°C. After 10 min, 10% FBS RPMI was added and the

cells were placed on ice for 5 min to quench excessive CFSE in media. Following 3 successive washes with PBS, cells were adjusted to $3x10^7$cells/ml, loaded into 30-guage insulin syringes, and injected (100 µl) via tail vein into B10.D2 recipient mice maintained on the same diet as donor mice. One day after adoptive transfer, recipient mice were immunized with OVA peptide (300 µg/mouse) and CFA via subcutaneous injection at two dorsal sites on the back according to the protocol of Lee *et al* (124). Full details can be found in Appendix B-2.

Immune cell collection and flow cytometry

Three days after immunization, mice were sacrificed by CO_2 asphyxiation. Draining (axillary, brachial, and inguinal) lymph nodes were collected from individual recipient mice. Viable lymphocytes were counted by trypan blue exclusion. Approximately $2x10^6$ cells were collected and labeled using KJ1-26 monoclonal antibody specific for detection of DO11.10 transgenic TCR as described in Appendix B-2. Briefly, cells were incubated with Fc block (5 µg/ml) at 4°C for 15 min, washed with buffer (PBS with 1% heat-inactivated FBS and 0.09% sodium azide, pH 7.4), stained using 2 µg/ml KJ-126 mAb at 4°C for 30 min, and analyzed using flow cytometry. Green fluorescence from CFSE was collected through a 530/30-nm bandpass filter and red fluorescence from phycoerythrin-cyanine 5 (PE-Cy5) through a 670-nm longpass filter. List mode data were acquired on at least 20,000 KJ1-26-positive events or until the sample was consumed. Data analysis was performed using ModFitLT (Verity Software House, Topsham, ME). A lymphocyte region was established using forward

and side light scattering properties, and a region for KJ1-26-positive events within the lymphocyte region was defined. Using the Proliferation Wizard, KJ1-26-positive lymphocytes from unimmunized mice were used to establish the position of non-dividing cells, and the data for cells from immunized mice were modeled using that point for the parent generation. Parent generations were established independently for each set of CFSE-stained, adoptively transferred lymphocytes (52). Donor $CD4^+$ T cells and recipient cells from lymph nodes served as KJ1-26 staining controls (Appendix A-2).

Statistics

To elucidate the effects of diet, average proliferation percentages of antigen-specific T cells were determined as described elsewhere (125). Each sub-dataset of every four consecutive generations was analyzed using a quadratic random effect model that incorporated the correlation structure and random effects of individual samples (126). It was determined that the quadratic model performed well for data from four consecutive generations. Individual samples were preserved as the experimental units through the correlation structure of the data. The model was fit using REML (restricted maximum likelihood) (127). Wald tests were performed for any main effects or interactions. Analyses on the sub-datasets were performed using R (version 1.9.1, R Foundation for Statistical Computing).

Results

Dietary fish oil suppressed Ag-specific Th1 proliferation of CD4$^+$ T cells

DO11.10 Rag2$^{-/-}$ donor mice and B10.D2 recipient mice were fed either a control diet (CO) or a FO diet for 2 wks. CD4$^+$ T cells from lymph nodes of donors were labeled with CFSE to follow cell division. Cells were adoptively transferred into recipient mice fed the same diet as the donor. B10.D2 mice were immunized 1 d after adoptive transfer, and 3 d after immunization, lymph nodes were harvested. The absolute number of viable lymphocytes recovered from lymph nodes of FO-fed recipient mice was significantly reduced (p=0.014) ($2.4\pm0.6x10^6$) compared to CO-fed recipients ($1.0\pm0.2x10^7$, n=3) (**Fig. 4**). In addition, KJ-126 stained cells were analyzed by flow cytometry indicating that the percentage of transgenic donor cells among the total lymphocytes in recipient lymph nodes was suppressed in FO fed group. (**Fig. 5**)

To determine the ability of n-3 PUFA to modulate antigen-induced T cell activation *in vivo*, flow cytometric gating was used to detect cellular division (**Fig. 6**). Consistent with previous studies using peptide-stimulated DO11.10 T cells, flow cytometric analysis showed that the transferred cells of both groups underwent 9 cell divisions *in vivo* following immunization (125, 128). Interestingly, FO-fed mice exhibited a reduction (p=0.078) in the percentage of transgenic CD4$^+$ T cells in lymph nodes (FO 1.35±0.34 vs CO 2.12±0.37, n=6). Determination of the average number of cell divisions (expressed as average generation number) of antigen-specific T cells revealed that FO fed animals exhibited a higher percentage of early generation cells (**Fig. 7**). Specifically, percentages of cells in generations 3 (p=0.047) and 6 (p=0.006)

were elevated in cells following FO treatment. In contrast, percentages of cells in generations 8 ($p<0.001$) and 9 ($p<0.001$) were reduced in the FO vs CO fed animals. We conclude that antigen-specific $CD4^+$ daughter cells were arrested in their progression through the proliferation cycle in FO-fed mice.

Discussion

In order to extend our *ex vivo* observations on clonal expansion to antigen-stimulated T cells in a whole animal, we utilized the vital dye CFSE within the context of an adoptive transfer model to examine antigen-specific T cell activation and Th1 proliferation *in vivo*. In agreement with our *in vitro* findings (52), we observed fewer antigen-specific $CD4^+$ T cells in FO-fed recipient mice following immunization with OVA peptide mixed with a Th1 polarizing adjuvant. This, combined with a reduction in daughter cell accumulation (**Fig. 6**), conclusively demonstrates that dietary FO suppresses Th1 development *in vivo*. The lower number of transgenic T cells in the lymph nodes of FO-fed recipient mice may also be explained by an effect of (n-3) PUFA on T cell trafficking into and out of the nodes and/or on the extent of local lymphoproliferation or AICD. We hypothesize that the suppressive effects (described above) are due to modifications in lipid raft composition, which may subsequently alter IL-2 receptor downstream signaling. The exact mechanisms of involvement of lipid rafts in inducing these changes will be the subject of further investigation and will provide insight into how dietary (n-3) PUFA can favorably modulate Th1-mediated autoimmune diseases.

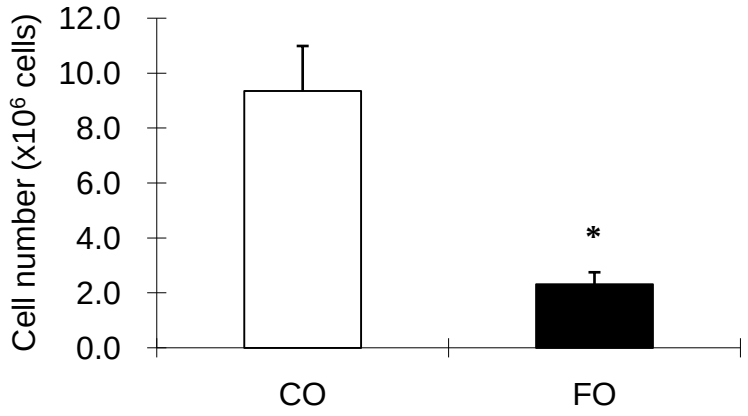

Figure 4. FO decreased (P<0.05) recipient lymph node viable cell number. Three days after immunization, recipient mice were sacrificed and total viable cells in draining lymph nodes were counted. Data represent mean ± SEM from 4 mice per group.

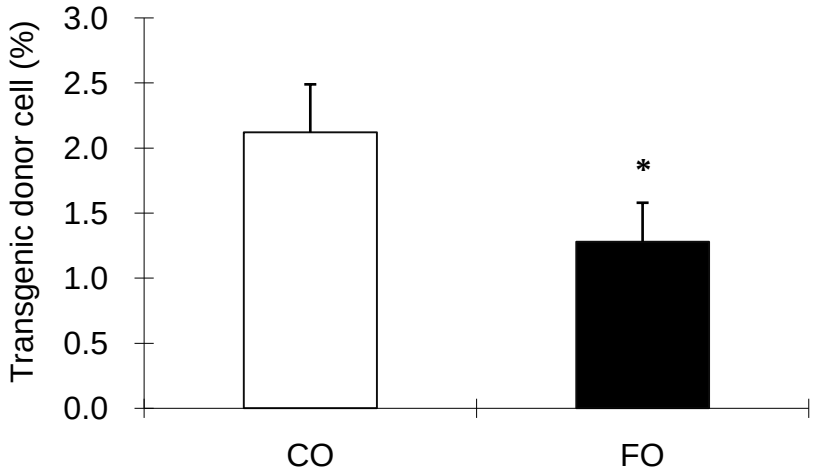

Figure 5. FO decreased (P<0.05) the percentage of transgenic $CD4^+$ donor cells. The number of KJ1-26^+ cells were divided by the total lymph node cell number. Data represent mean ± SEM from 7 mice per group.

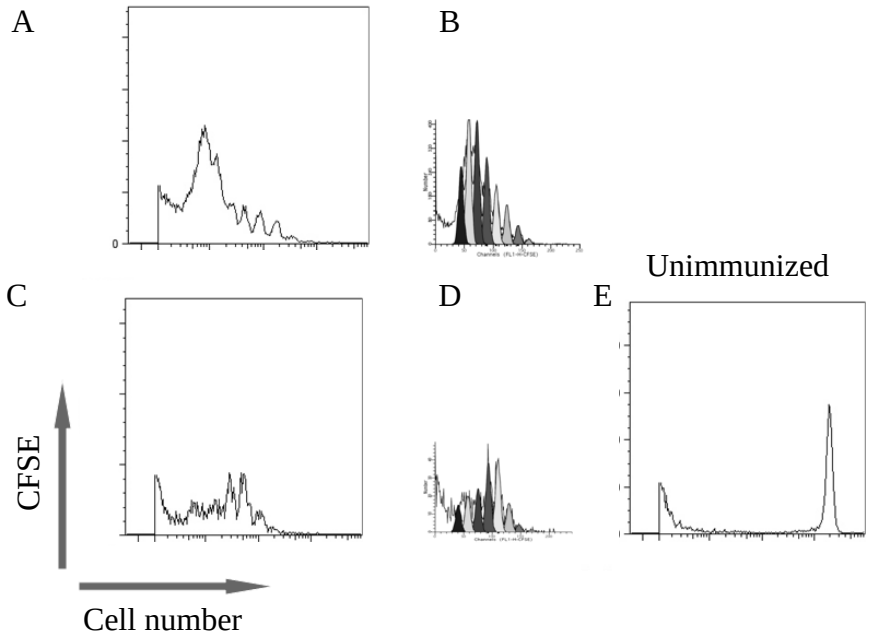

Figure 6. Determination of cell division number and daughter cell profiles. (A) and (C) are representative analyses from CO and FO fed mice, respectively. Computer modeling was performed (B and D) to identify each generation and cell division number using MOdFitLT^{TM}. (E) Unimmunized control.

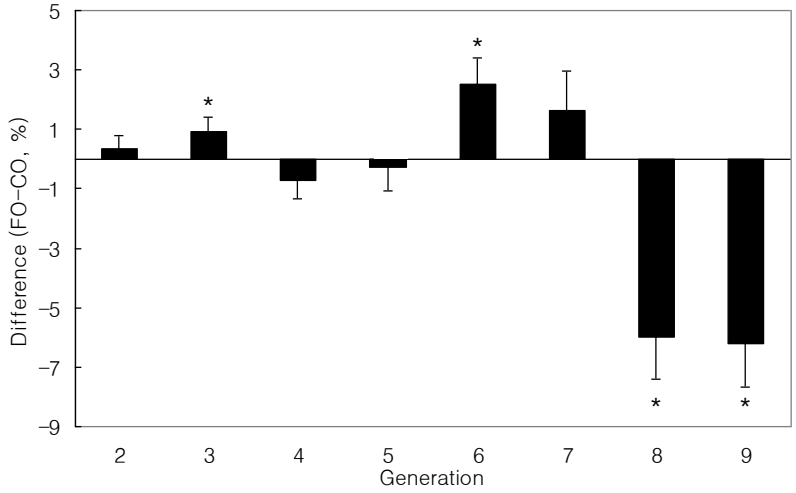

Figure 7. Dietary n-3 PUFA modulate T cell clonal expansion *in vivo*. Values represent data sets derived from consecutive generations and were plotted by expressing the generation number against the difference of the averages between the estimated FO% and CO% at the generation. The data shown were compiled from a total of 6 mice for each diet group from 3 separate experiments. Values greater than 0 indicated that in the FO group, the % of cells in a specific generation exceeds the CO group. The P-value was calculated using the Wald test (*P<0.05).

CHAPTER III

n-3 POLYUNSATURATED FATTY ACIDS SUPPRESS THE LOCALIZATION AND ACTIVATION OF SIGNALING PROTEINS AT THE IMMUNOLOGICAL SYNAPSE IN $CD4^+$ T CELLS BY AFFECTING LIPID RAFT FORMATION*

Introduction

The Singer and Nicholson lipid bilayer model of the plasma membrane (16) has evolved significantly to include specialized microdomains, i.e., lipid rafts. Lipid rafts can be classified as morphologically featureless, detergent-resistant membranes (DRM)[3] due to their insolubility in cold nonionic detergents (129). Their highly enriched cholesterol and sphingolipid content suggests that they are in a liquid ordered (l_o) state, whereas the bulk membrane is in a liquid disordered (l_d) state (17). The biochemical characterization of lipid rafts has provided new insight into the regulation and function of plasma membrane proteins. For example, it is now known that T cell intracellular signaling cascades, endocytosis, protein trafficking and cell-cell communication are modulated in part by altering the lipid-protein composition of the bulk membrane and specialized lipid microdomains (17, 19-21).

Dietary fish oil, rich in n-3 polyunsaturated fatty acids (PUFA), can alter immune cell function and aid in the resolution of chronic inflammation, e.g., arthritis,

---

* Reprinted with permission from "n-3 polyunsaturated fatty acids suppress the localization and activation of signaling proteins at the immunological synapse in $CD4^+$ T cells by affecting lipid raft formation" by Kim, W. *et al*., 2008, *J Immunol*, 181, 6236-6243. Copyright 2008 by The American Association of Immunologists.

Crohn's disease, dermatitis, psoriasis and ulcerative colitis (35, 130-132). To further investigate the anti-inflammatory properties of fish oil, we have demonstrated that n-3 PUFA modulate $CD4^+$ T cell immune responses in part via reduction in Th1 clonal expansion (52), IL-2 secretion and IL-2 receptor α-chain mRNA transcription (77). However, the molecular mechanisms by which n-3 PUFA suppress $CD4^+$ T cell function are not fully understood.

It has been reported that the fatty acid composition of lipid rafts and the bulk membrane in Jurkat T cells was altered by addition of n-3 PUFA to the culture media (133). Our laboratory also demonstrated the modulation of T cell lipid rafts by dietary n-3 PUFA in a mouse model (32). In the latter study, it was demonstrated that dietary fish oil as well as purified docosahexaenoic acid (DHA, 22:6n-3), a major bioactive n-3 PUFA, altered $CD4^+$ T cell plasma membrane fatty acid composition, specifically in phosphatidylserine and phosphatidylethanolamine, which are abundant in the cytofacial leaflet of the cell membrane (134). In contrast, fatty acid profiles in sphingomyelin, phosphatidylinositol, and phosphatidylcholine, which are major lipids in the exofacial leaflet (134) in which TCR is linked, were not altered. These observations may partially explain why n-3 PUFA alter signaling pathways without affecting expression and/or affinity of the TCR/CD3 complex (135, 136). Furthermore, in complementary studies, changes in lipid raft fatty acid composition were associated with a decrease in the translocation of protein kinase C (PKC)θ, a key molecule regulating $CD4^+$ T cell activation, into lipid rafts in mitogen stimulated T cells (77). In contrast, n-3 PUFA incubation displaced F-actin, talin, LFA-1α, but not PKCθ from the IS, where T cells

and APC form a conjunction (74). In terms of cell signaling triggered by TCR, it was reported that a scaffold protein, caspase recruitment domain-containing protein 11 (CARD11, CARMA1) is recruited into the IS and plays an essential role in linking Ag recognition, PKCθ activation via translocation into lipid rafts and NF-kB nuclear translocation (137). From these studies, it is apparent that n-3 PUFA may modulate T cell function via alteration of lipid raft structure and the translocation of signaling molecules.

We have recently reported that long chain PUFA alter the size and distribution of lipid rafts in HeLa cells, as determined by immuno-gold electron microscopy (78). These data suggest that plasma membrane organization of inner leaflets is fundamentally altered by n-3 PUFA enrichment. However, to date, the direct visualization of T cell lipid rafts at the IS following n-3 PUFA membrane enrichment has not been reported. Recently, it was demonstrated that the fluorescent probe Laurdan can align itself parallel with the hydrophobic tails of phospholipids in membranes (110-112). Owing to its ability to emit two different wavelengths according to the fluidity of the microenvironment, Laurdan can be used to measure membrane fluidity and visualize lipid rafts in living cells by two-photon microscopy (111).

Since mammals cannot produce n-3 PUFA from the major n-6 PUFA found in the diet due to the lack of Δ15-desaturase activity, it is necessary to enrich the diet with eicosapentaenoic acid (EPA, 20:5n-3) and/or DHA in order to assess their biological properties *in vivo*. Recently, the *fat-1* gene encoding an n-3 fatty acid desaturase was cloned from *Caenorhabditis elegans* and expressed in mammalian cells (113). This

enzyme can catalyze the conversion of n-6 PUFA to n-3 PUFA by introducing a double bond into fatty acyl chains. Hence, transgenic mice expressing *fat-1* allow us to investigate the biological properties of n-3 PUFA without having to incorporate these fatty acids in the diet. Using the *fat-1* mouse model, we report for the first time the effect of n-3 PUFA on (a) the formation of lipid rafts in living $CD4^+$ T cells at the immunological synapse, (b) membrane translocation of signaling molecules, (c) phosphorylation (activation status) of key signaling proteins and (d) the proliferation of $CD4^+$ T cells.

Materials and Methods

Animals, diets, and $CD4^+$ T cell purification

Fat-1 transgenic mice were generated and backcrossed onto a C57BL/6 background by breeding heterozygous mice (113, 114). Littermates were used in all experiments as previously described (114). All procedures followed guidelines approved by Public Health Service and the Institutional Animal Care and Use Committee at Texas A&M University. Mice were genotyped using tail DNA. To confirm the phenotype, total lipids were isolated from splenic $CD4^+$ T cells and the fatty acid profile was characterized by gas chromatography as previously described (32). The detailed protocols for *fat-1* phenotyping and genotyping are described in Appendix B-3 and 4, respectively. Representative chromatograms and RT-PCR results from fat-1 and WT mice are available in Appendix A-3 and 4, respectively. Animals were fed a 10% safflower oil diet (n-6 PUFA rich, Research Diets) *ad libitum* with a 12 h light/ dark

cycle. The diet contained 40 (g/100 g diet) sucrose, 20 casein, 15 corn starch, 0.3 DL-methionine, 3.5 AIN 76A salt mix, 1.0 AIN 76A mineral mix, 0.2 choline chloride, 5 fiber (cellulose), 10 safflower oil. $CD4^+$ T cells from *fat-1* or WT mice were isolated from spleens by a magnetic microbead positive selection method (Miltenyi Biotec) according to the manufacturer's recommendation.

Laurdan labeling

Purified (91.0 ± 1.0% determined by flow cytometry, n=3) $CD4^+$ T cells were stained with Laurdan (Invitrogen) for lipid raft visualization. The detailed protocol for positive $CD4^+$ T cell purification is available in Appendix B-5. Briefly, 5 μmol/L Laurdan was prepared in serum-free RPMI medium and incubated with $2x10^6$ cells/ml for 30 min at 37℃ (110) (Full details are provided in Appendix B-7). Cells were subsequently washed and resuspended in serum-free Leibovitz's medium. To evaluate the effect of cholesterol depletion on lipid raft formation, cells were pretreated with 10 mmol/L methyl-β-cyclodextrin (MβCD, Sigma) in fatty acid-free RPMI media containing 0.1% BSA for 3 min prior to Laurdan labeling (138) The detailed protocol is provided in Appendix B-7.

$CD4^+$ T cell activation and two-photon microscopy

For mitogenic activation, $CD4^+$ T cells were cocultured with CD3-specific Ab expressing hybridoma cells (clone 145-2C11, ATCC, anti-CD3 hybridoma) in complete medium [RPMI 1640 medium with 25 mmol/L HEPES (Irvine Scientific), supplemented

with 5% heat-inactivated FBS (Invitrogen), 10^5 U/L penicillin and 100 mg/L streptomycin (Gibco), 2 mmol/L L-glutamine (Glutamax®, Gibco), and 10 µmol/L 2-ME (Sigma)]. To validate immune synapse formation, T cells were also incubated with an irrelevant DNP-specific Ab expressing hybridoma cells (clone UC8-1B9, anti-DNP hybridoma) (139). In select experiments, hybridoma cells were prelabeled with Cell Tracker orange-fluorescent tetramethylrhodamine (CMTMR, Invitrogen, full protocol is provided in Appendix B-7). Laurdan labeled $CD4^+$ T cells were coincubated with hybridoma cells at a ratio of 5:1. Cell mixtures were seeded onto poly-L-lysine (Sigma) precoated chambered coverglass slides ($2x10^6$ $CD4^+$ T cells/chamber). After a 30 min incubation period at 37°C, Laurdan was measured by two-photon microscopy (Zeiss LSM 510 META NLO, 40x objective 1.3 NA oil) at 400-460 nm and 470-530 nm (**Fig. A-D**) to calculate generalized polarization (GP)-values, which indicate l_o and l_d states of the membrane, respectively (111). A representative calculation of GP-value is available in Appendix A-5. The Coherent Chameleon femtosecond pulsed Ti:Sapphire laser was set at an excitation of 770 nm.

GP-value calculation

All images were converted to 8-bit/channel TIFF format and were processed using Adobe Photoshop CS3®. The mean intensities of each color channel were measured in either whole cells or contact regions of the synapse by drawing a polygon around each cell boundary (whole cell) (**Fig. 8F**) or by drawing an oval at the T cell membrane proximal to the hybridoma cell (**Fig. 8E**). GP-values were obtained by the

formula, GP=($I_{400-460}$-$I_{470-530}$)÷($I_{400-460}$+$I_{470-530}$), where *I* stands for intensities of each region of interest for the blue and green channels, respectively (110, 111) Full details are described in Appendix B-8. A representative calculation of GP-value is available in Appendix A-5.

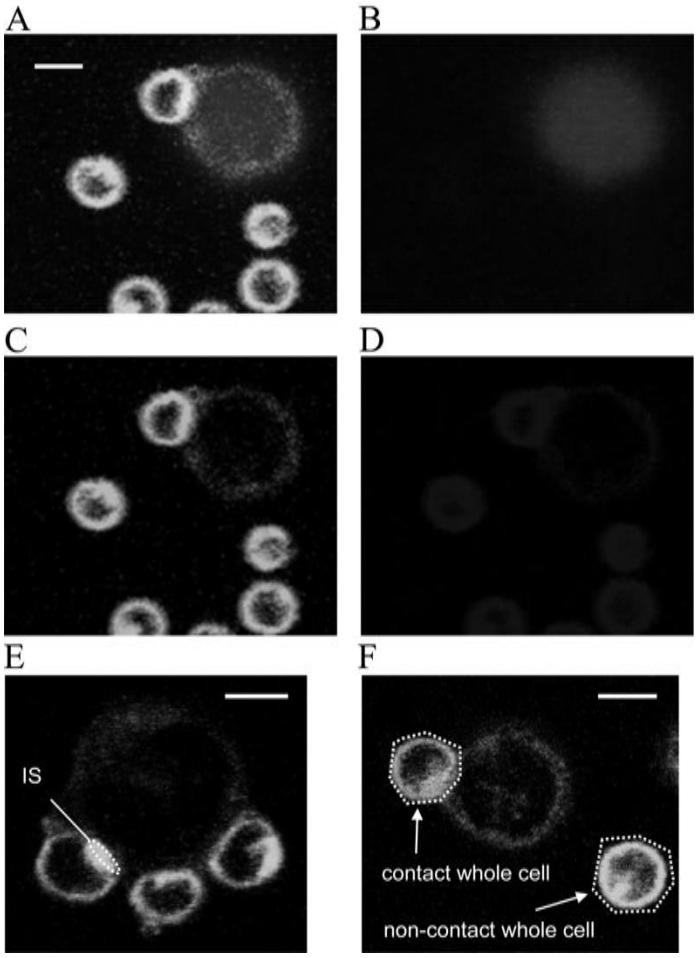

Figure 8. Two-photon microscopy images of Laurdan labeled T cells. 8-bit TIFF format captured images were analyzed in (A) RGB, (B) red (CMTMR), (C) green ($I_{470-530}$) or (D) blue ($I_{400-460}$) channels, respectively. Regions of interest (ROI) at (E) T cell immune synapse, (F) contact whole cell and non-contact whole cell were selected by drawing an oval or polygon as shown in white dotted lines. Mean intensities from blue and green channels were recorded to calculate GP-values as described in the Methods. Scale bar, 5 µm.

Quantification of protein localization, activation and GM1 relocation

To assess the relocalization of signaling proteins or cytoskeletal F-actin, isolated $CD4^+$ T cells were mixed with hybridoma cells (5:1) and seeded onto poly-L-lysine precoated coverglass slides. After a 30 min incubation period, cells were fixed in 4% formaldehyde for 20 min, rinsed with PBS, and incubated with 10 mmol/L glycine in PBS for 10 min at room temperature to quench aldehyde groups. Cell membranes were permeabilized by exposure to 0.2% Triton X-100 in PBS for 5 min at room temperature, followed by PBS washing. Cells were subsequently covered with blocking solution (1% BSA/0.1% NaN_3 in PBS) and incubated at 4°C overnight with primary Abs, rabbit Abs specific to either PKCθ (Santa Cruz Biotechnology), linker for activation of T cells (LAT), phospho-LAT (Upstate Biotechnology), CARMA1, phospholipase C (PLC)γ-1, phospho-PLCγ-1 (Cell Signaling Technology) as previously reported (77) (Detailed protocol is provided in Appendix B-9). After PBS washing, cells were incubated with secondary Alexa Fluor® 568 goat Ab to rabbit IgG (Molecular Probes). In order to visualize F-actin and ganglioside GM1 localization, cells were incubated with F-actin-specific phallotoxin-Alexa Fluor 568® (Molecular Probes) or GM1-specific cholera toxin B subunit-fluorescein isothiocyanate (CTx-FITC, Sigma), respectively. Following serial ethanol dehydration steps, samples were mounted onto glass slides with ProLong Antifade reagent (Molecular Probes) (77). Fluorescence images were acquired by confocal microscopy to determine both the translocation and phosphorylation status (activation) of signaling proteins in $CD4^+$ T cells. Either a BioRad Radiance 2000MP (argon laser excitation at 568 nm and emission at 590 nm, 63x objective 1.4 NA water)

or Zeiss LSM 510 META NLO (argon laser excitation at 543 nm and emission with a LP 560 nm, 63x objective 1.4 NA oil) system was used for image acquisition. Cell images were captured in 8-bit TIFF format and the percentage of cells with protein patching at the IS was counted to assess the relocalization of signaling proteins or F-actin (raw data can be found in Appendix A-6). GM1 recruitment into the IS was quantified by relative relocation index (RRI) (140). Briefly, polygons were drawn to designate the IS, the contact whole cell and background area. RRI was calculated by the formula, RRI=[mean fluorescence intensity (MFI) at the IS-background]÷(MFI at the contact whole cell-background). Raw data are included in Appendix A-7. Quantitative analysis of MFI was performed using Adobe Photoshop® CS3 for Windows.

$CD4^+$ T cell proliferation assay

The effect of n-3 PUFA on T cell proliferation was evaluated by the [^{3}H]-thymidine incorporation and CFSE labeling as previously described (52, 141). Briefly, $2x10^5$ purified $CD4^+$ T cells were stimulated using either control RPMI complete medium, $5x10^5$ anti-CD3 hybridoma cells which were pretreated with 10 µmol/L mitomycin C (Sigma) for 30 min to block cell division, plate bound CD3-specific mAb (1 mg/L) and soluble CD28-specific mAb (10 mg/L, BD Pharmingen) (anti-CD3/28 mAbs) or PMA (1 pg/L) and Ionomycin (500 nmol/L) (PMA/Ionomycin). Cells were cultured for 72 h in round-bottom 96-well multiplates. For CFSE profile analysis, $CD4^+$ T cells were pretreated with 5 µmol/L CFSE in PBS supplemented with 5% FBS for 10 min (141). After 72 h in culture as described above, CFSE was analyzed by flow

cytometry (FACSCalibur, BD) as previously reported (52). Briefly, cells were harvested by centrifugation and resuspended in PBS. To determine viability, propidium iodide (PI, Sigma) was added to each sample prior to analysis. CFSE fluorescence was detected using a 530/30 band pass filter and PI fluorescence through a 650LP filter. CFSE fluorescence was sufficiently intense to be detected through a 650LP filter. Viable cells were determined using a plot of CFSE vs PI fluorescence, based on the fluorescence patterns of a sample with CFSE but no PI. This gate also excluded most of the hybridoma cells because of their higher level of autofluorescence. An additional lymphocyte gate was set based on forward and side light scattering properties. CFSE profiles were analyzed by ModFit LT 3.0 (Verity Software House). Data were expressed as difference of percentage (Δpercentage, *fat-1* - WT) at each daughter cell generation. Raw data and calculation can be found in Appendix A-8. For the [^{3}H]-thymidine incorporation, 4 μCi [^{3}H]-thymidine/well (New England Nuclear) was added to the cultures for the final 6 h. Cells were harvested using a 96-well cell harvester (Packard Instrument) and thymidine uptake was measured using liquid scintillation counting (Beckman Coulter). Results are expressed as proliferation index, which is derived by dividing disintegrations per minute (DPM) of stimulated wells by DPM of basal control. Raw data are included in Appendix A-9.

Statistics

Data were analyzed using Student's t-test to compare *fat-1* and WT cells. The Kolmogorov-Smirnov method was applied to test the normality of the data distribution.

Statistical interaction of the variables (genotype and ROI) was tested by two-way ANOVA. To compare multiple treatment means, one-way ANOVA and LSD multiple post-hoc tests were used (SPSS 15.0 for Windows). Data are expressed as mean ± SEM and differences of $P<0.05$ were considered statistically significant.

Results

n-3 PUFA enhances the formation of lipid rafts at the immune synapse

Both *fat-1* transgenic and wild type (WT) control offspring were fed a 10% safflower oil diet enriched in n-6 PUFA throughout the duration of study as described in Materials and Methods. Splenic $CD4^+$ T cell total lipid fatty acid compositional analyses revealed an increase in n-3 PUFA [EPA (P=0.010), docosapentaenoic acid (DPA 22:5n-3, P=0.007) and DHA (P=0.015)] and a decrease in n-6 PUFA, specifically arachidonic acid (20:4n-6, P=0.053), adrenic acid (22:4n-6, P=0.041) and DPA (22:5n-6, P=0.008) in *fat-1* transgenic mice (**Fig. 9**). In addition, the ratio of n-6 to n-3 PUFA was significantly (P=0.003) suppressed in *fat-1* (5.13 ± 1.18), compared to WT T cells (35.71 ± 6.38). These data indicate that an appropriate activity of n-3 fatty acid desaturase was present and that T cells from *fat-1* mice were enriched in n-3 PUFA.

To investigate the effect of endogenous n-3 PUFA on lipid raft formation at the IS, Laurdan labeled $CD4^+$ T cells were cocultured with anti-CD3 hybridoma cells at 37℃ in 5% CO_2 for 30 min. Images of conjugate $CD4^+$ T cells and hybridomas were captured, while non-contact $CD4^+$ T cells served as a negative control. Two-way ANOVA of generalized polarization (GP)-values revealed that there was no statistical

interaction between genotype and regions of interest (ROI) (P=0.430). GP-values were significantly (P<0.001, LSD post-hoc test) increased at the IS (0.412 ± 0.017 WT vs 0.452 ± 0.014 *fat-1*) compared to non-contact T cells (0.329 ± 0.008 WT vs 0.372 ± 0.008 *fat-1*) or contact whole cells (0.363 ± 0.010 WT vs 0.377 ± 0.008 *fat-1*) (**Fig. 10A**). Overall, raft formation was enhanced in *fat-1* vs WT cells in both resting (P=0.016) and stimulated (P=0.022) $CD4^+$ T cells. The DNP-specific Ab expressing hybridoma was used as a negative control, and failed to exhibit an increase in the GP index at the IS (**Fig. 10B and C**). These data demonstrate that the n-3 PUFA-dependent increase in the GP index is IS dependent.

In independent experiments, $CD4^+$ T cells were pretreated with 10 mmol/L MβCD for 3 min to specifically deplete cholesterol from lipid rafts as described

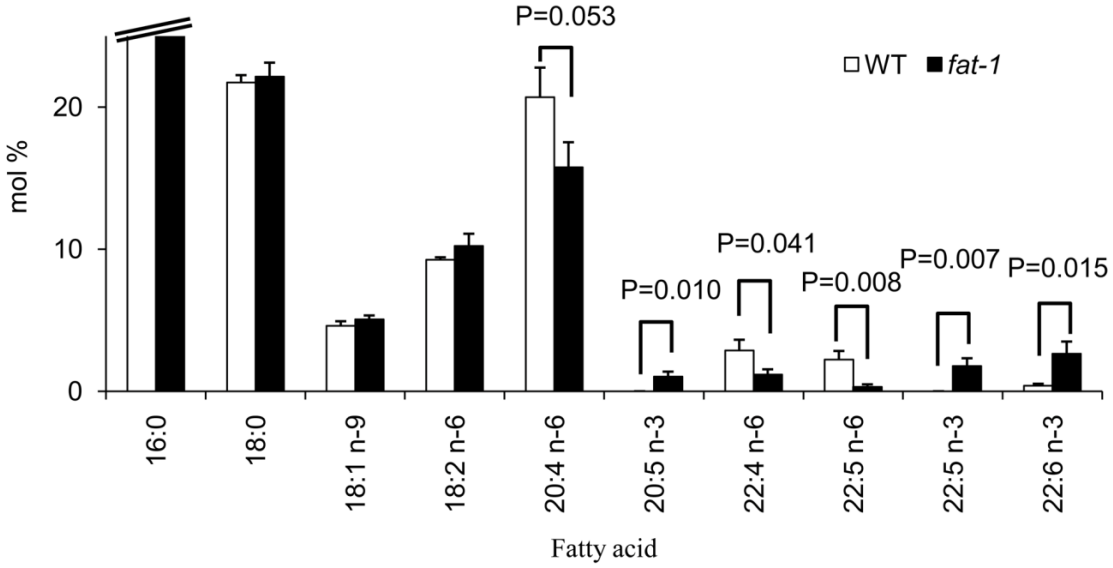

Figure 9. Fatty acid composition of $CD4^+$ T cell total lipids in WT and *fat-1* mice. Splenic $CD4^+$ T cells were isolated from wild type (WT) or *fat-1* transgenic mice. Total phospholipids were isolated and fatty acid composition was analyzed by gas chromatography, n=5.

previously (138). Laurdan analysis revealed that the elevated GP values associated withIS formation (ΔGP=0.195 ± 0.030, *fat-1* and 0.139 ± 0.015, WT, n=6-14 cells per mouse from 1-2 mice per genotype) was diminished following MβCD treatment (ΔGP=0.053 ± 0.022, *fat-1* and ΔGP=0.059 ± 0.033, WT), indicating that changes in the GP index at the IS are cholesterol dependent.

In complementary experiments, GM1-specific microcluster recruitment was assessed using CTx-FITC. CTx has been used to mark membrane microdomains in the exofacial leaflet, although a significant fraction of GM1 is found outside l_o regions (142). Interestingly, in contrast to the enhanced l_o domain formation at the IS (**Fig. 10B**), GM1 recruitment was not altered in *fat-1* $CD4^+$ T cells (**Fig. 10D and E**).

n-3 PUFA suppress the localization of signaling proteins into the IS

Following Ag recognition by the TCR, signaling cascades proximal to the IS are initiated by relocalization of a complex of molecules, i.e., protein kinases (Fyn, Lck, ZAP-70, PLCγ-1), scaffolding proteins (LAT, Grb-2, SLP-76, CARMA1) and cytoskeletal proteins (F-actin) into the IS (20, 137, 143). In this study, the effect of n-3 PUFA on the localization of select signaling molecules in the plasma membrane at the IS was quantified. **Fig. 11A** shows representative cell images obtained following incubation with rabbit mAb specific to mouse LAT and the secondary Alexa Fluor® 568 Ab specific to rabbit IgG. Relocalization of PKCθ, PLCγ-1 and F-actin into the IS, expressed as the percentage conjugate with patching, were suppressed in *fat-1* transgenic cells by 30% (P=0.050), 32% (P=0.081) and 36% (P=0.020), respectively (**Fig. 11B**). In

contrast, the intracellular localization of LAT and CARMA1 at the IS was not altered by n-3 PUFA.

n-3 PUFA down-regulate PLCγ-1 phosphorylation at the IS

Since phosphorylation of LAT and PLCγ-1 occurs at the very early stages of T cell activation, either phospho-LAT or phospho-PLCγ-1 specific Ab was used to visualize the effect of n-3 PUFA on T cell activation. Specifically, the percentage conjugate patching of phospho-Y195 (LAT) (144) and phospho-Y783 (PLCγ-1) (145) was examined and showed that PLCγ-1 phosphorylation was suppressed by 29% (P=0.034) in n-3 PUFA enriched cells at the IS, whereas LAT phosphorylation was not altered (P=0.464) (**Fig. 12A and B**).

n-3 PUFA suppress $CD4^+$ T cell proliferation

$CD4^+$ T cells were labeled with CFSE and cultured for 72 h for the purpose of determining whether the effect of n-3 PUFA on lipid rafts and signaling protein recruitment/activation was associated with an alteration in T cell proliferation. Using flow cytometry analysis, non-viable cells were gated out based on their uptake of PI (**Fig. 13A, D and G**) and lymphocytes were identified by forward and side scatter plot analysis (**Fig. 13B, E and H**). The parental peak was obtained by examining unstimulated control cells, which did not divide (**Fig. 13C**), whereas cell division was visualized by the shift of CFSE peak to the left (52, 141). To identify each daughter generation, computer-aided modeling was performed (**Fig. 13F and I**). Examination of

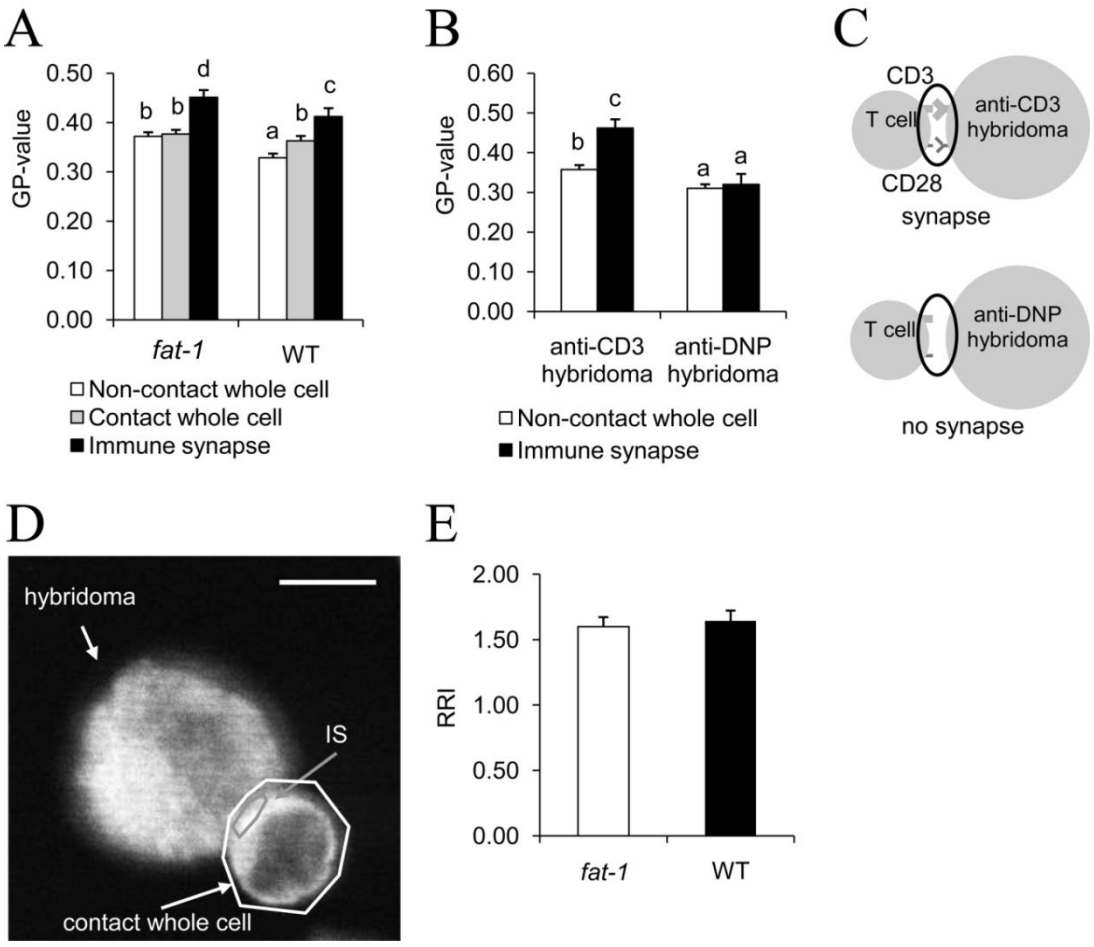

Figure 10. Lipid raft formation and GM1 relocalization at the IS of $CD4^+$ T cells. (A) GP-values, which indicate microenvironment fluidity in the plasma membrane, were quantified in $CD4^+$ T cells obtained from either *fat-1* or WT mice (8-14 cells per mouse from 3-4 mice per genotype were examined to obtain a total of n=27-51 observations). Bars with different letters indicate significant differences at $P<0.05$ across all treatment groups within panel A. (B) IS-dependent increase of GP-values was confirmed by anti-DNP hybridoma cells (negative control, n=6-9 cells from one mouse per genotype). Bars with different letters indicate significant differences at $P<0.05$ across all treatment groups within panel B. (C) Schematic of IS formation (top) and non-IS contact (bottom), respectively. (D and E) Immunofluorescence analysis of GM1 recruitment into the IS. Purified $CD4^+$ T cells and anti-CD3 hybridomas were coincubated, fixed, permeabilized, labeled with CTx-FITC. Confocal microscopic images were captured and MFI was measured at the IS relative to the whole cell to calculate RRI, as described in the Methods. (D) Representative image of GM1 localization. Scale bar, 5 μm. (E) The relocation of GM1 at the IS was assessed by RRI of CTx-FITC (n=31-32 cells from 3 mice per genotype).

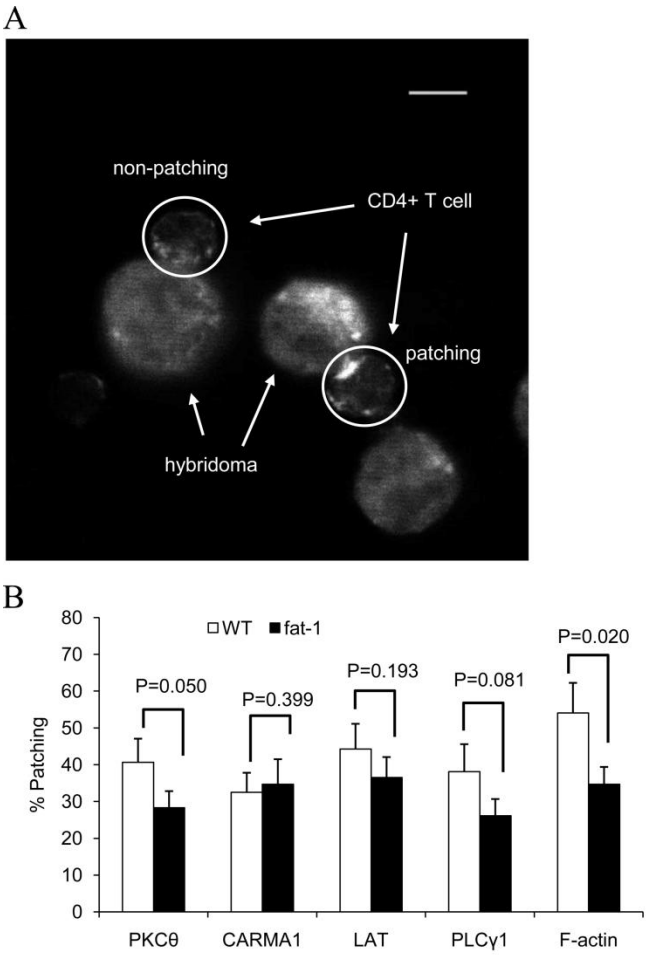

Figure 11. Immunofluorescence analysis and localization of signaling molecules into the IS. Purified $CD4^+$ T cells and anti-CD3 hybridomas were coincubated, fixed, permeablized, and labeled with Abs specific to either PKCθ, CARMA1, LAT, PLCγ-1 or F-actin, as described in the Methods. (A) Representative images of LAT localization to the IS in *fat-1* cells. Image contrast was adjusted. Scale bar, 5 µm. (B) Protein localization was assessed by percent patching (the number of patching cells divided by the number of total cells examined, n=37-101 cells from 2-5 mice per genotype for each protein).

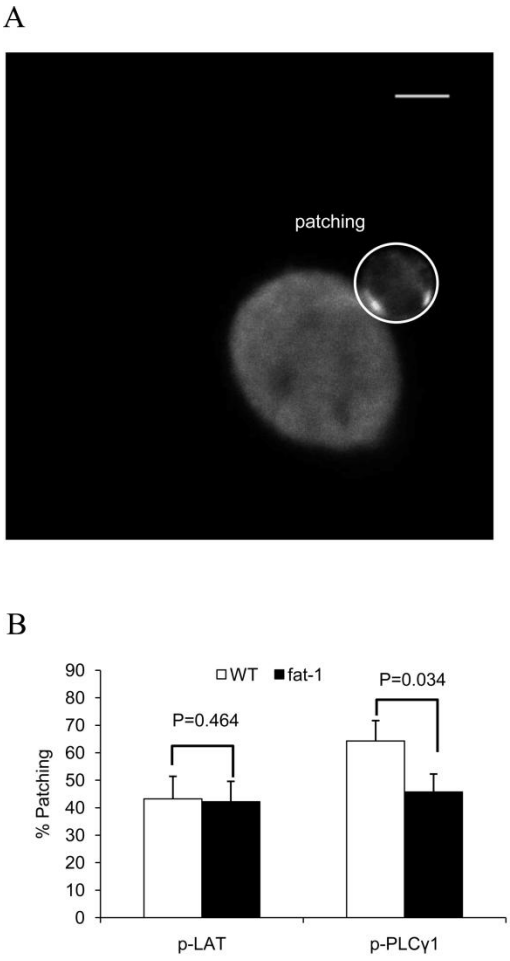

Figure 12. Phosphorylation status of signaling proteins at the IS. Purified $CD4^+$ T cells and anti-CD3 hybridomas were coincubated, fixed, permeablized, and labeled with Abs specific to either phospho-LAT or phospho-PLCγ-1, as described in the Methods. (A) Representative image of LAT phosphorylation at the IS in *fat-1* cells. Image contrast was adjusted. Scale bar, 5 µm. (B) Protein activation was assessed by percent patching (n=37-59 cells from 3-4 mice per genotype for each protein).

the percentage of each daughter cell generation revealed that *fat-1* $CD4^+$ T cell proliferation was suppressed in response to anti-CD3 hybridoma stimulation. Specifically, a higher percentage of non-divided parental cells (Δpercentage=5.87, P=0.028) and lower percentage of daughter cells at generation 4 (Δpercentage=-0.98,

P=0.037), 5 (Δpercentage=-1.73, P=0.042) and 6 (Δpercentage=-1.38, P=0.065) were obtained (**Fig. 14A**). In addition, $CD4^+$ T cells stimulated by either anti-CD3/28 mAbs or PMA/Ionomycin exhibited a similar trend; larger fraction at generation 1 (Δpercentage=4.30, P=0.085 anti-CD3/28 mAbs, Δpercentage=3.58, P=0.001 PMA/Ionomycin) and a reduced number of cells at generation 4 (Δpercentage=-3.34, P=0.081 anti-CD3/28 mAbs), suggesting a suppression of cell division in the *fat-1* group (**Fig. 14B and C**).

In a complementary experiment, $CD4^+$ T cell proliferation was assessed by the incorporation of [^{3}H]-thymidine. In accordance with the CFSE profile data, thymidine uptake expressed as the proliferation index revealed that *fat-1* $CD4^+$ T cell division was significantly suppressed by 52% (P<0.001), 45% (P=0.002) and 56% (P=0.001) in anti-CD3 hybridoma, anti-CD3/28 mAbs and PMA/Ionomycin stimulated cells, respectively (**Fig. 15**).

Discussion

It has been postulated that n-3 PUFA, because of their perceived broad acting effects on mammalian physiology, act at a fundamental level common to all cells, i.e., by altering the physical properties of biological membranes (74, 80-84, 131, 132). More specifically, we hypothesized that the anti-inflammatory effects of n-3 PUFA on $CD4^+$ T cells would be explained, in part, by suppressing/disrupting lipid raft formation at the IS. To elucidate the membrane bioactive properties of n-3 PUFA in T cells, the *fat-1* transgenic mouse model was utilized because it is uniquely capable of converting n-6

PUFA to n-3 PUFA endogenously by introducing a cis double bond into fatty acyl chains (113, 146). Data from initial experiments showed that the *fat-1* gene was functionally expressed in splenic $CD4^+$ T cells and that the plasma membrane was enriched in n-3 PUFA (**Fig. 9**).

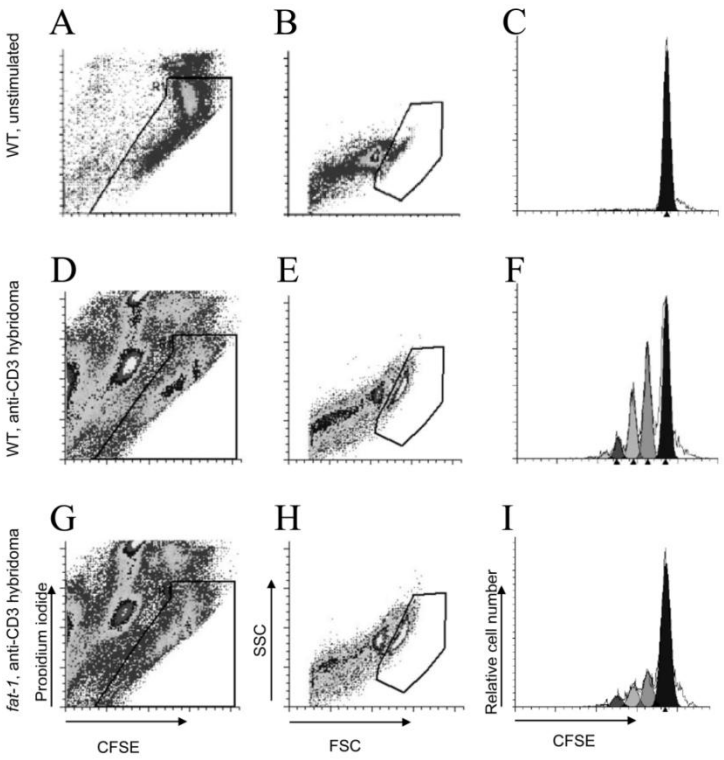

Figure 13. Representative CFSE profiles. Data from either basal WT T cells (A-C), anti-CD3 hybridoma stimulated WT (D-F) or *fat-1* (G-I) $CD4^+$ T cells were shown. Regions for viable cells (A, D and G) and lymphocytes (B, E and H) were set based on propidium iodide incorporation and forward/side scatter plots, respectively. Viable lymphocytes were defined as those events falling within both the viability and lymphocyte regions. Computer-aided modeling of each daughter generation (C, F and I) was performed as described in the Methods. The non-divided parental peak was obtained from the unstimulated control group (C). The left shift of peaks (F and G) indicated successive rounds of cell division.

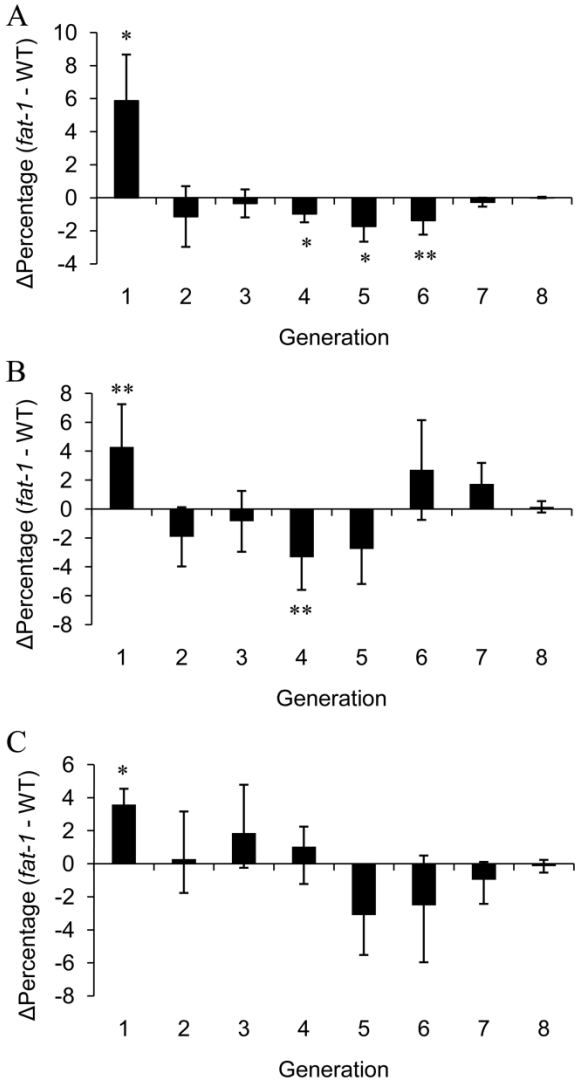

Figure 14. The difference in the percentage of T cells (Δpercentage) at each generation. The difference was obtained by subtracting the percentage of the WT group from the percentage of *fat-1*. Positive bars show that *fat-1* cultures had more cells in those generations, whereas negative bars show fewer *fat-1*cells. (A) anti-CD3 hybridoma, (B) anti-CD3/28 mAbs and (C) PMA/Ionomycin stimulated (n=6-10 cultures from 3-5 mice per genotype for each stimulus) ($^{*}P<0.05$, $^{**}P<0.10$).

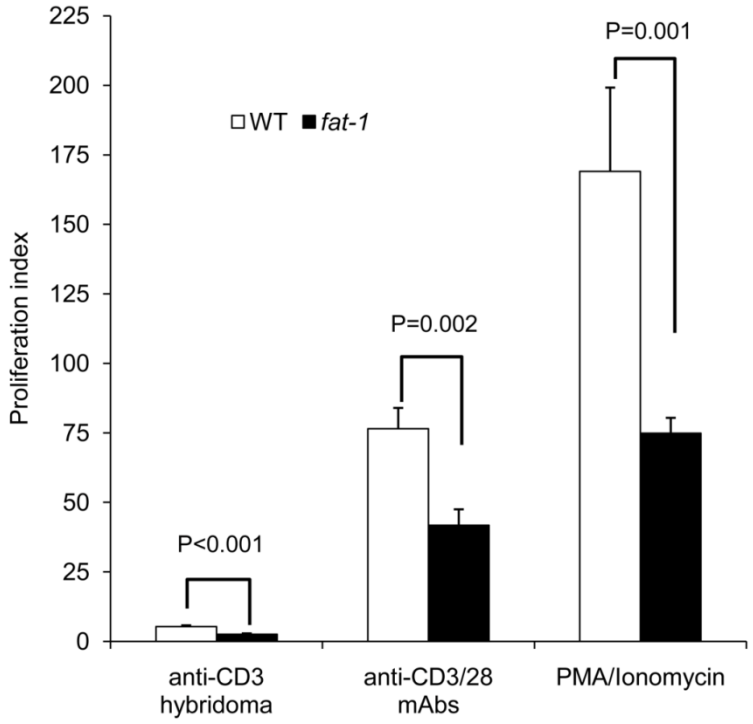

Figure 15. Proliferation of $CD4^+$ T cells expressed as proliferation index. Proliferation index was calculated by DPM stimulated ÷ DPM unstimulated in response to either anti-CD3 hybridoma, anti-CD3/28 mAbs or PMA/Ionomycin (n=6-10 cultures from 3-5 mice per genotype for each stimulus).

We have demonstrated previously that n-3 PUFA suppress murine $CD4^+$ T cell proliferation by remodeling lipid raft fatty acid composition and by altering PKCθ colocalization (77). In that study, $CD4^+$ T cells were stimulated by culture plate-bound mAb to CD3 (anti-CD3 mAb) to induce the colocalization of PKCθ with GM1, a marker of lipid rafts. However, the direct visualization of lipid rafts at the IS is necessary in order to investigate microdomain assembly and localization at the plasma membrane. Hence, in the present study, we incubated $CD4^+$ T cells with Laurdan to directly measure membrane fluidity and visualize lipid rafts by two-photon microscopy. For this purpose,

anti-CD3 hybridoma cells were used as Ag presenting cells to form an IS, since they express cell surface costimulatory B7 and intercellular adhesion molecule (ICAM-1) (139). In a major step toward developing a unifying mechanistic hypothesis addressing how dietary PUFA modulate cell membrane microdomains, we demonstrate for the first time that n-3 PUFA actually promote lipid raft formation at the IS (**Fig. 10A-C**). These results can be explained in part by the fact that n-3 PUFA, specifically DHA, has a low affinity for cholesterol, providing a lipid-driven mechanism for lateral phase separation of cholesterol/sphingolipid-rich lipid microdomains from the surrounding l_d phase (80-84). Hence, the insertion of DHA into the bulk membrane should enhance the coalescence of cholesterol-rich lipid raft-like domains in living cells. These findings are consistent with previous observations using immuno-gold electron microscopy of plasma membrane sheets coupled with spatial point analysis of validated microdomain markers (78). In that study, we demonstrated that DHA increased lipid raft clustering in HeLa cells, indicating that plasma membrane organization of inner leaflets is fundamentally altered by n-3 PUFA-enrichment.

With regard to the role of lipid rafts in T cell activation, T cells from patients suffering from autoimmune disease synthesized more GM1 following TCR activation (20), suggesting that GM1 enriched domains play a critical role in the activation of immune responses. However, cholesterol overloading in healthy T cells reduced the lateral mobility of receptors and signaling molecules providing a link between plasma membrane cholesterol content and immunosenescence (20). These observations are controversial because GM1 and cholesterol, which are both thought to be lipid raft

building blocks (17), play different roles in T cell activation and regulation. Therefore, we measured the recruitment of GM1 into the IS by labeling with CTx-FITC in order to evaluate the effect of n-3 PUFA on GM1-specific lipid rafts. Of interest, GM1 relocation as assessed by RRI was not altered by n-3 PUFA (**Fig. 10E**). This observation is consistent with a previous report, where GM1 localization as assessed by biochemical isolation of DRM was not affected by PUFA treatment (72). Interestingly, the fatty acid composition of phospholipids in the exofacial leaflet of T cells, where GM1 is enriched, was not altered by n-3 PUFA (32). In addition, long chain PUFA are predominantly enriched in phospholipids localized to the cytofacial leaflet (32, 147). Based on these findings, the data suggest that the incorporation of n-3 PUFA into cytofacial leaflet phospholipids alters the lateral composition of lipid rafts in the plasma membrane, thereby altering the IS microenvironment to impact thresholds for the activation TCR mediated cell signaling.

The proximal events of cell signaling following Ag recognition by the TCR are initiated by the localization of signaling molecules into the IS (20). To evaluate the effect of n-3 PUFA on the localization of select signaling proteins, the percentage of cells with multi-protein signaling complexes relocalized to the IS was enumerated by immunofluorescence microscopy. Consistent with a perturbation in lipid raft structure, n-3 PUFA enriched $CD4^+$ T cells exhibited a suppressed localization of PKCθ, PLCγ-1 and F-actin into the IS (**Fig. 11**). We also reported that PKCθ colocalization with GM1 in anti-CD3 mAb stimulated T cells was suppressed by dietary fish oil and purified DHA ethyl ester administration (77). Although a significant fraction of GM1 can be found

outside l_o regions (142, 148), the dislocation of PKCθ from GM1 enriched domains may explain in part why PKCθ accumulation at the IS was suppressed by n-3 PUFA, while lipid raft formation was enhanced. In addition, we also show that the localization of PLCγ-1 and F-actin was selectively suppressed by n-3 PUFA, whereas LAT and CARMA1 localization was not altered. In contrast, in a previous study, F-actin, LAT and PKCθ localization into the IS was not altered by n-3 PUFA (EPA) treatment compared to n-6 PUFA (arachidonic acid) (74). Indeed, both n-3 and n-6 PUFA treatment equally suppressed the localization of F-actin, talin, leukocyte function-associated molecule-1α, LAT and CD3ε into the IS, compared to the saturated stearic acid (18:0) treated control group. The apparent differences between these studies may be attributed to the fact that Jurkat human T cells were directly incubated with 50 μmol/L fatty acid followed by antigenic stimulation (74).

Since not only the spatial migration but also the phosphorylation status of LAT and PLCγ-1 is critical for T cell activation (144, 145) and dietary FO has been shown to modulate PLCγ-1 phosphorylation in rat lymphocytes (149), we counted cells with phospho-specific immunofluorescent patching in order to assess the activation status of those proteins. In accordance with the localization results, LAT phosphorylation was not affected by n-3 PUFA, however PLCγ-1 phosphorylation was suppressed in *fat-1* transgenic T cells (**Fig. 12**). These data indicate that n-3 PUFA selectively modulate the localization and/or activation status of signaling proteins in TCR-mediated T cell activation.

The understanding of the function of the IS is still evolving. For example, membrane condensation and signaling protein translocation to the IS has been shown to be critical for TCR triggered T cell activation (110). In contrast, compelling data suggest central supramolecular activation cluster (cSMAC) of mature IS may promote TCR/CD3 internalization and recycling (124). In addition, TCR microclusters initiate T cell signaling in seconds (150) following binding to peptide-MHC complex but the signal becomes weaker when cSMAC is formed in minutes (151, 152). These observations suggest that the dynamic nature of the IS and perhaps rapid formation/dissolution of rafts promote TCR signaling. It is possible, therefore, that n-3 PUFA by stabilizing lipid rafts at the IS disrupt lipid-protein interactions and perturb membrane structure/function.

Alteration of $CD4^+$ T cell lipid raft microdomains and proximal T cell signaling by n-3 PUFA in *fat-1* cells resulted in the suppression of proliferation (**Fig. 14A and 15**), indicating the critical importance of lipid raft localization of proteins such as PKCθ, PLCγ-1 and F-actin to TCR signaling. To test if the mechanism of suppression by n-3 PUFA was limited to the IS or proximal signaling cascades, T cells were stimulated with either anti-CD3/28 mAbs or PMA/Ionomycin to bypass IS formation and TCR mediated signaling, respectively. T cell proliferation by anti-CD3/28 mAbs and PMA/Ionomycin was suppressed as assessed by CFSE profiles and thymidine uptake, indicating that the down-regulation of T cell proliferation by n-3 PUFA is not limited to TCR-mediated activation. Indeed, CFSE profile analysis revealed that the largest Δpercentage was associated with the non-dividing parental generation when T cells were stimulated with the IS forming anti-CD3 hybridoma cell model (**Fig. 14**), consistent with a very strong

suppression of T cell proliferation. These data are consistent with previous reports that n-3 PUFA are anti-inflammatory and immunomodulatory *in vivo* (77, 153).

In general, hyperactivation of $CD4^+$ T cells is associated with enhanced susceptibility to autoimmune disorders and chronic inflammatory diseases (131, 132). Recently, our laboratory reported that *fat-1* mice exhibited an enhanced ability to resolve dextran sodium sulphate-induced intestinal inflammation and injury (114). Since subsets of $CD4^+$ T cells are known to be critical mediators of chronic inflammation, results from our study may partially explain why n-3 PUFA favorably modulate the inflammation-dysplasia-carcinoma axis.

In conclusion, we have shown that n-3 PUFA promote the formation of lipid rafts and perturb the reorganization of signaling machinery which is critical to T cell activation. These results provide a critical new paradigm in understanding the molecular mechanisms through which dietary n-3 PUFA modulate T cell activation. Additional studies are needed to further elucidate the effect of dietary n-3 PUFA on T cell signaling networks.

CHAPTER IV

DIETARY CURCUMIN AND LIMONIN SUPPRESS MURINE $CD4^+$ T CELL PROLIFERATION AND INTERLEUKIN-2 PRODUCTION IN PART BY SUPPRESSING NF-κB ACTIVATION

Introduction

Inflammation is an imperative host defense response comprising both innate and adaptive immune systems. Interestingly, chronic inflammation is a disease state which is associated with a higher risk of cancer development (131, 154-156). With respect to the adaptive immune response, $CD4^+$ T cells regulate inflammatory responses, in part, by clonal expansion into effector T helper cell subsets and cytokine production. The function of $CD4^+$ T cells is affected by a variety of factors such as genetic background, antigen peptide, adjuvant, antigen presenting cell subset, as well as nutrients.

Dietary fat, a major energy source, can modify membrane structure thereby playing an important role in cell signaling in a variety of cell types. The anti-inflammatory properties of diets rich in n-3 PUFA, e.g., eicosapentaenoic acid (EPA, $20{:}5^{\Delta5,8,11,14,17}$) and docosahexaenoic acid (DHA, $22{:}6^{\Delta4,7,10,13,16,19}$) which are highly enriched in cold water fish, on T cell function have been established in both humans and experimental animals (41, 42, 157-161). In contrast, dietary lipids rich in n-6 PUFA, found in vegetable oils and animal fats, e.g., linoleic acid ($18{:}2^{\Delta9,12}$) and arachidonic acid ($20{:}4^{\Delta5,8,11,14}$), can be deleterious with respect to some inflammatory diseases (reviewed in (41)). This is significant because the typical Western diet contains 10 to 20 times

more n-6 than n-3 PUFA (162). Though the molecular mechanisms of anti-inflammatory n-3 PUFA are not fully elucidated to date, a growing body of data indicate that n-3 PUFA modulate $CD4^+$ T cell function, in part, by altering plasma membrane microenvironment , thereby modulating intracellular localization of signaling molecules (32, 77). This may aid in the resolution of a series of chronic inflammatory diseases, such as arthritis, Crohn's disease, dermatitis, psoriasis and ulcerative colitis (35, 130-132).

The molecular mechanisms of T cell activation have been well documented. Antigenic T cell activation through the T cell receptor (TCR)/CD3 complex requires antigen peptide (Ag) in the context of major histocompatibility complex class II of antigen presenting cells (APC), directing the subsets of adaptive immune responses, i.e. cell-mediated or humoral immunity. With respect to the heterogeneous plasma membrane phospholipid bilayer, cholesterol/sphingomyelin rich microdomains, i.e., lipid rafts (17, 129, 163) are thought to be platforms for receptor residence and signaling molecule migration (20). In addition, signaling molecules are recruited to the immunological synapse where T cells and APCs make physical contact after TCR/CD3 ligation to Ag. Following the induction of signal cascades proximal to TCR initiated signaling, nuclear factors (NF) translocate from cytosol into the nucleus to elicit the expression of an array of cytokines. It is now appreciated that NF-kB delivers a "life signal" by stimulating pro-inflammatory cytokines such as interleukin (IL)-2 and interferon (INF)-γ in T cells (164, 165). IL-2 gene transcription is a hallmark feature of T cell activation, which is also regulated by AP-1 and NFAT nuclear factors (**Fig. 16**).

Interestingly, Fan *et al*. from our laboratory reported that dietary fish oil (FO), as well as purified DHA, suppressed the recruitment of signaling molecules into lipid rafts, NF-kB/AP-1 activation and IL-2 production, linking alteration in lipid raft composition to reduced IL-2 production (77). In that study, $CD4^+$ T cells were stimulated using mitogenic monoclonal antibodies to CD3 and CD28 (anti-CD3/28 mAbs), which avoided the engagement of an immunological synapse.

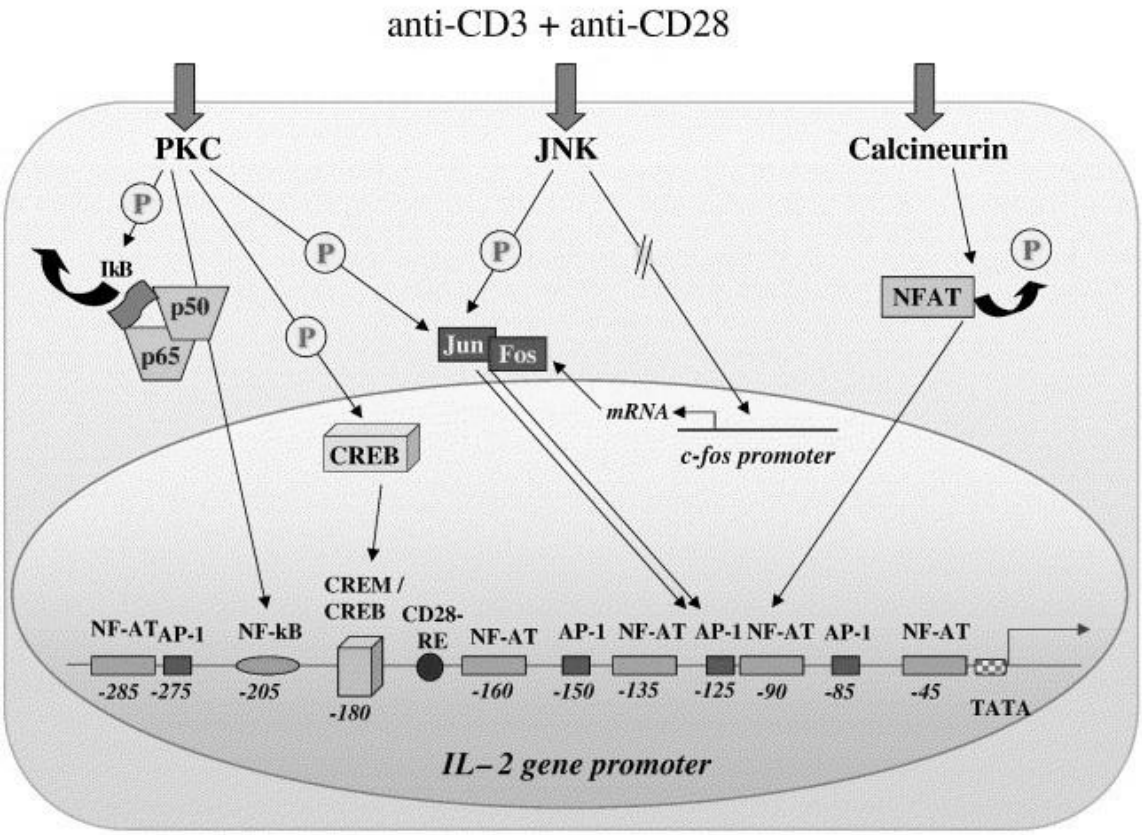

Figure 16. Transcriptional regulation of IL-2 in T cells. Image was reprinted with permission from "Transcriptional repression of interleukin-2 in human systemic lupus erythematosus" by Katsiari, C.G. 2006, *et al*, *Autoimmun. Rev.* (166). Copyright 2005 by Elsevier B.V.

The experimental model system of T cell activation has evolved significantly to include DO11.10 $Rag2^{-/-}$ TCR transgenic mouse models. T cells from these transgenic mice respond specifically to a peptide of ovalbumin (OVA323-339) to mimic physiological Ag selection by Ag-specific T cells (115). In addition, OVA peptide antigen presentation by APC forms an immunological synapse with T cells, following which T cells redistribute signaling molecules and organelles such as mitochondria (167).

Phytochemicals have been investigated for decades as chemotherapeutic agents for cancer and chronic inflammatory diseases. Of interest, it has been reported that curcumin (diferuloylmethane, Cur), a major active component of turmeric (*Curcuma longa Linn*), exhibited anti-inflammatory effects by suppression of the NF-κB signaling pathway in ovarian and pancreatic cancer cell-line models (168-170). In addition, Vanamala *et al*. from our laboratory has shown that limonin (7,16-Dioxo-7,16-dideoxylimondiol, Lim), a citrus fruit extract compound, down-regulates iNOS and COX-2, which are regulated in part by NF-kB, in a rat mucosal cancer model (100). These data suggest that limonin may also be a putative NF-kB inhibitor and therefore capable of modulating $CD4^+$ T cell function. However, the function of curcumin and limonin with regard to $CD4^+$ T cell activation has not been elucidated to date.

Hence, in this study, using antigen-specific or mitogenic stimulation, we hypothesized that (a) dietary curcumin and limonin suppress $CD4^+$ T cell function by modulating NF-kB activity and (b) dietary "combination chemotherapy", using n-3 PUFA plus either curcumin or limonin, will maximally suppress IL-2 secretion and cell proliferation.

Materials and Methods

Animals, diets, and cell purification

All procedures followed guidelines approved by Public Health Service and the Institutional Animal Care and Use Committee at Texas A&M University. TCR transgenic DO11.10 $Rag2^{-/-}$ mice were purchased from Taconic Farms, Inc. (Germantown, NY), bred and maintained at Texas A&M University. The composition of experimental diets is shown in **Table 1** and met the NRC nutrition requirements. Briefly, diets differed with respect to fat source and the addition of Cur or Lim. The FO diet contained 4% FO+1% corn oil (CO) to meet essential fatty acids requirement, while the 5% CO diet served as a control. 1% Cur or 0.02% Lim was added to both CO and FO diets at the expense of cellulose. Mice were fed (1 wk) a wash-out CO diet followed by (2 wk) experimental diet feeding. $CD4^+$ T cells from mice were isolated from spleens by a magnetic microbead positive selection method (Miltenyi Biotec) according to the manufacturer's recommendation (Working protocol can be found in Appendix B-5). For antigenic stimulation, splenic lymphocytes from chow-fed BALB/c mice were used as APCs. Briefly, lymphocytes were isolated by density gradient centrifugation using Lympholyte-M® (Cedarlane Labs) and incubated in 25 µg/ml Mitomicin C (Sigma) for 30 min, followed by a washing step to remove excessive Mitomicin C (refer to Appendix B-10 for details).

Table 1. Experimental diet composition of curcumin and limonin supplement.

	Composition (g/100g)					
Ingredients	CO*	CC	CL	FO	FC	FL
Casein (Bio-serv)	20.0	20.0	20.0	20.0	20.0	20.0
Sucrose (Bio-serv)	42.0	42.0	42.0	42.0	42.0	42.0
Corn starch (Bio-serv)	22.0	22.0	22.0	22.0	22.0	22.0
Cellulose (Bio-serv)	6.0	5.0	5.98	6.0	5.0	5.98
AIN-76 mineral mix (Bio-serv)	3.5	3.5	3.5	3.5	3.5	3.5
AIN-76 vitamin mix (Bio-serv)	1.0	1.0	1.0	1.0	1.0	1.0
DL-Methionine (Bio-serv)	0.3	0.3	0.3	0.3	0.3	0.3
Choline chloride (Bio-serv)	0.2	0.2	0.2	0.2	0.2	0.2
CO (Dyets, Inc.)	5.0	5.0	5.0	1.0	1.0	1.0
FO (Omega protein)	-	-	-	4.0	4.0	4.0
Curcumin (Sabinsa Co.)	-	1.0	-	-	1.0	-
Limonin**	-	-	0.02	-	-	0.02
Total	100.0	100.0	100.0	100.0	100.0	100.0

*CO, corn oil; CC, corn oil+curcumin; CL, curcumin+limonin; FO, fish oil; FC, fish oil+curcumin; FL, fish oil+limonin

**Limonin was purified and provided by Dr. Patil, Vegetable and Fruit Improvement Center, Texas A&M University

T cell activation using antigen or mitogen

In order to test either cell proliferation or IL-2 production/nuclear factor activation, $2x10^5$ DO11.10 $CD4^+$ T cells/ml were cultured in 200 µl medium in an U-bottomed 96-well culture plate or in 2 ml medium in a flat bottom 24-well culture plate, respectively, in a 5% CO_2 incubator at 37 ^oC for 72 hr in the presence of the following stimuli. For antigen-specific stimulation, $CD4^+$ T cells were co-cultured with $5x10^5$ APC/ml in the presence of 0.1 µmol/L OVA323-339 peptide (Biosource) in complete medium [RPMI 1640 medium with 25 mmol/L HEPES (Irvine Scientific), supplemented with 5% heat-inactivated FBS (Invitrogen), 10^5 U/L penicillin and 100 mg/L streptomycin (Gibco), 2 mmol/L L-glutamine (Glutamax® , Gibco), and 10 µmol/L 2-ME (Sigma)]. Plate bound CD3-specific mAb (1 ng/L) and soluble CD28-specific mAb (5 ng/L, BD Pharmingen) (anti-CD3/28 mAbs) were used for mitogenic stimulation.

Nuclear extraction and quantification of NF-κB, NFAT and AP-1 activation

Following a 72 hr incubation of $CD4^+$ T cells as described above, nuclei were pelleted and extracted using a Nuclear Extraction kit (Active Motif). The levels of activated NF-κB, NFAT and AP-1 were measured using an ELISA-based Trans AM NF-κB p65, NFATc1 and AP-1 c-Jun Transcription Factor Assay kits (Active Motif), respectively, as previously described (77). Briefly, induction of NF-κB, NFAT or AP-1 in the nuclear extracts was quantified by nucleotide (5'-GGGACTTTCC-3' for NF-κB, 5'-T/AGGAAA-3' for NFAT or 5'-TGA(C/G)TCA-3' for AP-1) binding using specific Abs to NF-κBp65, NFATc1 or c-Jun followed by secondary HRP conjugated Abs and

chromogenic substrate. A sensitive colorimetric readout was quantified by either chemiluminescence (NF-κB) or spectrophotometry at 450 nm with a reference wavelength of 655 nm (NFAT and AP-1). Competition experiments were performed by incubating the extracts with the labeled probe in the presence of excess (20 pmol/L) of unlabeled wild-type NF-κB, NFAT or AP-1 oligonucleotide. TPA and calcium ionophore-stimulated Jurkat T cell extracts were used as a positive control, resulting in a 18-fold activation of NF-κB in comparison to the negative control (Jurkat T cell extract plus NF-κB wildtype oligonucleotide competitor). Similarly, a 4-fold (NFAT) and a 9-fold (AP-1) level of activation were observed in the positive controls (PHA-stimulated Jurkat T cell nuclear extract and TPA-stimulated K-562 nuclear extract, respectively) relative to the negative controls (Jurkat nuclear extract plus NFAT wild-type oligonucleotide competitor and K-562 nuclear extract plus AP-1 wild-type oligonucleotide competitor). Serial dilution of control nuclear extract revealed a dose dependent sensitivity of the kits (Appendix A-19). The induction of nuclear factors was expressed as fold increase, which was derived by (colorimetric readout of stimulated cells) ÷ (colorimetric readout of unstimulated cells).

IL-2 quantification

IL-2 secretion was measured in cell culture supernatants. Following a 72 hr cell stimulation period, culture media was harvested and stored at -80℃ until analysis by Quantikine mouse IL-2 ELISA kit (R&D Systems) as previously described (77). The

amount of IL-2 in the media was calibrated by linear regression of serially diluted standards provided in the kit (Appendix A-20).

Cell proliferation assay

For CFSE profile analysis, $CD4^+$ T cells were pretreated with 5 µmol/L CFSE (Molecular Probes) in PBS supplemented with 5% FBS for 10 min (141). After 72 h in culture as described above, CFSE was analyzed by flow cytometry (FACSCalibur, BD) as previously reported (52). Briefly, cells were harvested by centrifugation (200x g for 10 min at RT) and resuspended in PBS. To determine viability, propidium iodide (1 µg/ml) (PI, Sigma) was added to each sample prior to analysis. CFSE fluorescence was detected using a 530/30 band pass filter and PI fluorescence through a 650LP filter. CFSE fluorescence was sufficiently intense to be detected through a 650LP filter. Viable cells were determined using a plot of CFSE vs PI fluorescence, based on the fluorescence patterns of a sample with CFSE but no PI. This gate also excluded most of the APC because of their higher level of autofluorescence (Appendix A-21). An additional lymphocyte gate was set based on forward and side light scattering properties (Appendix A-22). CFSE profiles were analyzed by FlowJo (Tree Star). Data were expressed as difference of percentage compared to CO control (Δpercentage) at each daughter cell generation. For the [^{3}H]-thymidine incorporation, 4 µCi [^{3}H]-thymidine/well (New England Nuclear) was added to the cultures for the final 6 h. Cells were harvested using a 96-well cell harvester (Packard Instrument) and thymidine uptake was measured using liquid scintillation counting (Beckman Coulter).

Statistics

To compare multiple treatment means, one-way ANOVA and Duncan's multiple comparison or Least Significant Difference (LSD) were used (SPSS 15.0 for Windows). Kolmogorov-Smirnov method was applied to test the normality of the data distribution. Statistical interaction of the two dietary variables (fat source and phytochemicals) was tested by two-way ANOVA. Data are expressed as mean ± SEM and differences of $P<0.05$ were considered statistically significant.

Results

Dietary curcumin and limonin suppress NF-κB activation

With respect to the physiological relevance of the diets used in this study, fish oil (4%), limonin (0.02%), and curcumin (1.0%) diets are within the estimated range consumed by humans (52, 88, 171, 172). Body weight gains of mice were not affected by the experimental diets following a 2 wk feeding period (data in Appendix A-10).

In order to investigate the effect of Cur and Lim on nuclear transcription factor activation, nuclei were extracted from $CD4^+$ T cells following a 72 h stimulation period with OVA peptide or mAbs. NF-kB translocation analysis revealed that both Cur and Lim suppressed NF-kB activation in both antigen- and mitogen-stimulated cells ($P<0.001$, one-way ANOVA) (**Fig. 17**). Two-way ANOVA analysis was performed to determine whether the Cur and Lim effect differed depending on the fat source. The statistical outcome indicated that there was no interaction of the two variables, fat source and phytochemical ($P=0.610$, anti-CD3/28 mAbs; $P=0.712$, OVA/APC). These data

indicate that FO did not influence NF-κB activation, as opposed to Cur and Lim which suppressed activation (**Fig. 17**). Since the promoter region of a key T cell growth promoting cytokine, *IL-2*, also contains NFAT and AP-1 response elements (**Fig. 16**), we measured the effect of Cur and Lim on NFAT and AP-1 activation. The results demonstrate that NFAT activation was not affected by the experimental diets compared to CO control diet as shown in **Fig. 18**. Of interest, FO diet promoted ($P<0.05$) AP-1 activation by 1.38 fold and 3.46 fold in the response to either anti-CD3/28 or APC+OVA peptide, respectively (**Fig. 19**).

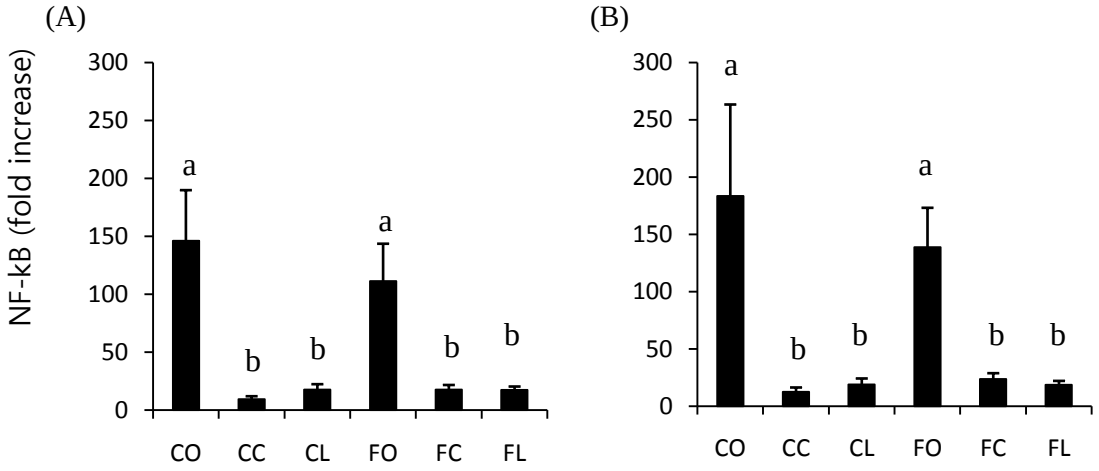

Figure 17. Activation of NF-κB in $CD4^+$ T cells. Cells were stimulated by either (A) anti-CD3/28 mAbs or (B) APC+OVA peptide as described in the Methods. Fold increase of chemiluminescence was expressed relative to unstimulated controls. Bars with different letters indicate significant differences ($P<0.05$) within the panel (CO, corn oil control; CC, CO+1% curcumin; CL, CO+0.02% limonin; FO, 4% fish oil+1% CO; FC, FO+1% curcumin; FL, FO+0.02% limonin, n=6-7 mice per diet).

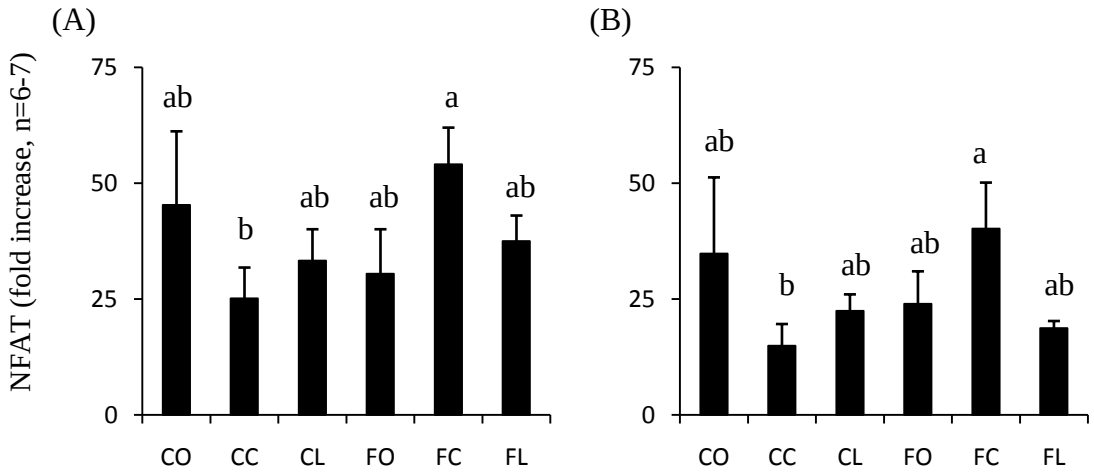

Figure 18. Activation of NFAT in $CD4^+$ T cells. Purified $CD4^+$ T cells were stimulated by either (A) anti-CD3/28 mAbs or (B) APC+OVA peptide as described in the Methods. Fold increase of fluorescence absorbance at 450 nm was expressed relative to unstimulated controls. Bars with different letters indicate significant difference ($P<0.05$) within the panel. (CO, corn oil control; CC, CO+1% curcumin; CL, CO+0.02% limonin; FO, 4% fish oil+1% CO; FC, FO+1% curcumin; FL, FO+0.02% limonin, n=6-7 mice per diet).

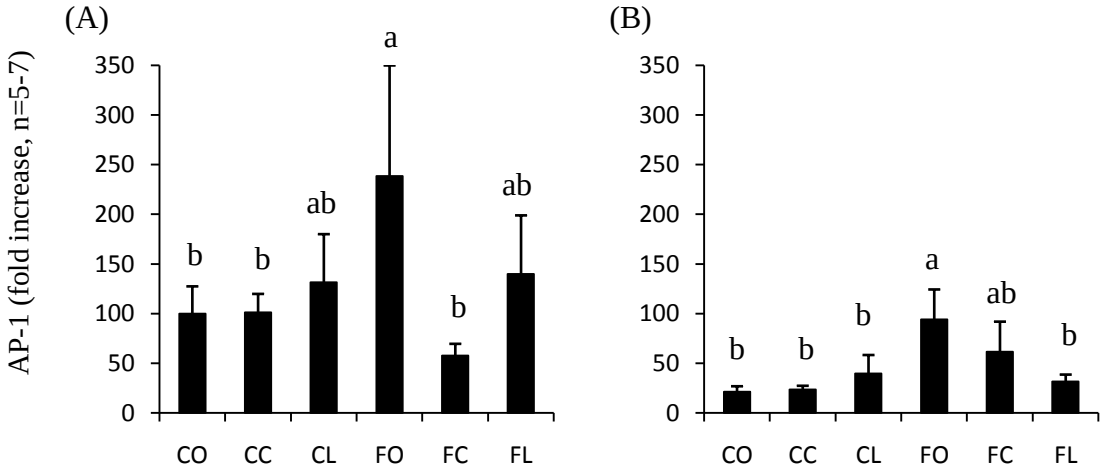

Figure 19. Activation of AP-1 in $CD4^+$ T cells. Purified $CD4^+$ T cells were stimulated by either (A) anti-CD3/28 mAbs or (B) APC+OVA peptide as described in the Methods. Fold increase of fluorescence absorbance at 450 nm was expressed relative to unstimulated controls. Bars with different letters indicate significant difference ($P<0.05$) within the panel. (CO, corn oil control; CC, CO+1% curcumin; CL, CO+0.02% limonin; FO, 4% fish oil+1% CO; FC, FO+1% curcumin; FL, FO+0.02% limonin, n=5-7 mice per diet).

Dietary curcumin and limonin reduce IL-2 production

In order to link suppression of NF-kB to T cell function, IL-2 secretion into the culture medium was measured. Interestingly, IL-2 production was not altered by the experimental diets in mitogen-stimulated cultures (**Fig. 20A**). In contrast, IL-2 production was suppressed ($P<0.05$) by Cur and Lim supplementation, as well as FO, compared to CO control by 56-71% when $CD4^+$ T cells were stimulated by OVA323-339 peptide. However, Cur and Lim supplementation with FO did not further suppress IL-2 secretion (**Fig. 20B**).

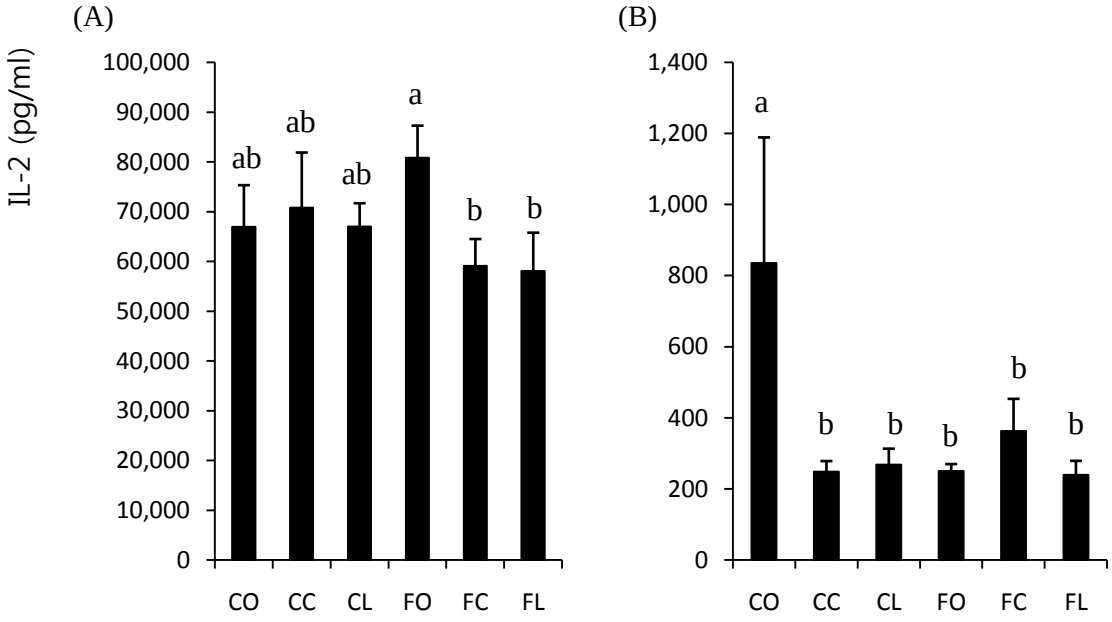

Figure 20. IL-2 production by $CD4^+$ T cells. Cells were stimulated by either (A) anti-CD3/28 mAbs or (B) APC+OVA peptide as described in the Methods. Bars with different letters indicate significant differences ($P<0.05$) within the panel (CO, corn oil control; CC, CO+1% curcumin; CL, CO+0.02% limonin; FO, 4% fish oil+1% CO; FC, FO+1% curcumin; FL, FO+0.02% limonin, n=6-7 mice per diet).

Dietary curcumin and limonin suppress CD4$^+$ cell proliferation

In order to investigate the effect of suppressed NF-κB activation and IL-2 on CD4$^+$ T cell function, cell proliferation was measured using two independent methods. Analysis of CFSE profiles (**Fig. 21**) indicated that CD4$^+$ T cell division was suppressed by dietary Cur and Lim added to CO. Specifically, compared to CO control diet group, Cur fed animals had significantly ($P<0.05$) more cells following anti-CD3/28 stimulation at generations 1, 2 and 3 (Δ percentage= 2.83, 2.89, 6.45, respectively) and fewer cells at generation 5 (Δ percentage=-7.69, **Fig. 22A**). Similarly, Cur supplementation in combination with FO (**Fig. 22D**) reduced the percentage of cells at generations 4 and 5 (Δ percentage=-9.58 and -4.02, respectively). In contrast, Lim supplement did not alter the proliferation of CD4$^+$ T cells (**Fig. 22B**) and the FO diet had little effect, except in generation 1 (Δ percentage=2.65, **Fig. 22C**). Of interest, the Lim and FO combination (**Fig. 22E**) exhibited a synergistic suppressive effect on CD4$^+$ T cell proliferation with significantly more cells in generations 1 and 2 (Δ percentage=2.88 and 2.61, rescpectively) and fewer cells in generation 5 (Δ percentage=-4.70, P=0.066). Similarly, with an Ag-specific stimulation by OVA peptide+APC, Cur supplementation to the CO diet (**Fig. 23A**) resulted in more cells at generations 3 and 4 (Δ percentage= 5.46 and 5.40, respectively) whereas fewer cells were observed at generations 5 and 6 (Δ percentage=-5.71 and -4.94, respectively). Cur+FO treatment resulted in more cells at generations 1 (Δ percentage=3.79, P=0.059) and 2 (Δ percentage=1.73, P=0.072) and fewer cells at generations 4 and 5 (Δ percentage=-7.67 and -8.31, respectively, **Fig. 23D**).

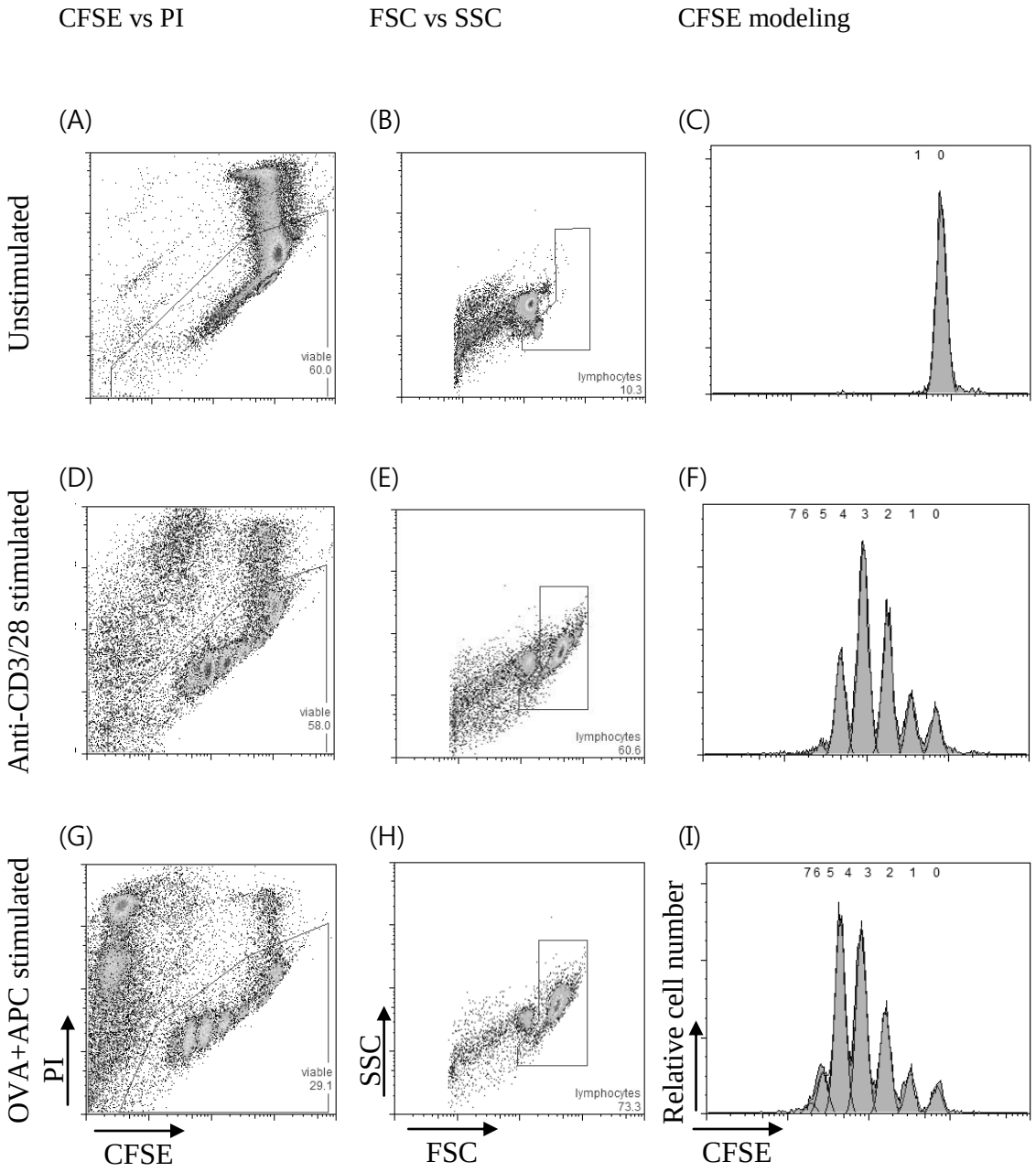

Figure 21. Representative flow cytometry plots and CFSE modeling. Data from a CO-fed control mouse were shown. Unstimulated (A-C), anti-CD3/28 stimulated (D-F) or OVA+APC stimulated (G-I) $CD4^+$ T cell cultures were analyzed by flow cytometry. Propidium iodide negative cells were gated (A, D, G) which excluded non-viable parental $CD4^+$ T cells (A) and auto-fluorescent APC (G), followed by lymphocyte gating by FSC vs SSC plot (B, E, H). Computer-aided modeling of CFSE plot indicated that the peak of unstimulated cells (C) shifts to left (F and I) as cells divide.

(A) CC-CO (B) CL-CO

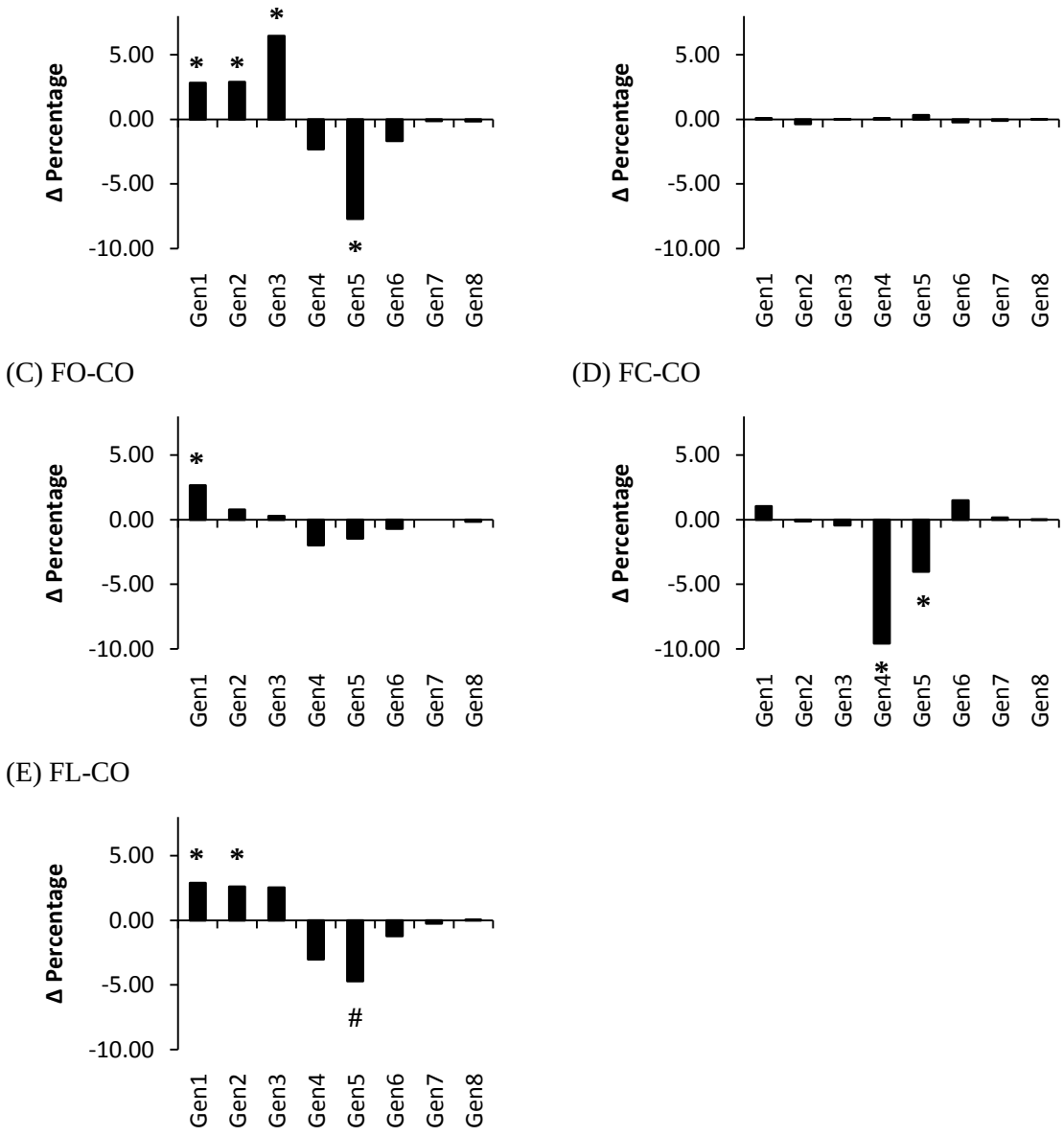

Figure 22. Suppression of $CD4^+$ T cell division in mitogen-stimulated cultures as assessed by CFSE anlalysis. Δ Percentages of each generation in anti-CD3/28 stimulated $CD4^+$ T cells. Purified $CD4^+$ T cells were labled by CFSE. Following a 72 hr stimulation period *ex vivo*, CFSE profile was analyzed by flow cytometry as described in the Methods. Data are presented as the difference of percentage of cells in each daughter generation compared to the corn oil control diet group (CO, corn oil control; CC, CO+1% curcumin; CL, CO+0.02% limonin; FO, 4% fish oil+1% CO; FC, FO+1% curcumin; FL, FO+0.02% limonin, n=10-12 cultures from 5-6 mice, *$P<0.05$, $^{\#}P<0.1$)

However, Lim and/or FO supplement did not alter Ag-specific $CD4^+$ T cell proliferation (Fig. 23B,C,E).

In parallel experiments, cell proliferation was quantified by uptake of radioactive [^{3}H] thymidine (**Fig. 24**). In contrast to the CFSE analysis, thymidine uptake was not significantly altered in the response to mitogenic anti-CD3/28 mAbs. Ag-specific OVA peptide+APC-induced [^{3}H] thymidine uptake was suppressed ($P<0.05$) by Cur supplementation to both CO and FO based diets by 30.82% and 43.40%, respectively.

Discussion

In order to investigate the anti-inflammatory properties of dietary curcumin and limonin, we assessed NF-κB activity in mitogenic anti-CD3/28 mAbs or antigenic OVA peptide+APC stimulated murine $CD4^+$ T cells. NF-κB p65 nuclear translocation was suppressed by both 1% curcumin and 0.02% limonin. Since NFAT and AP-1 nuclear factors are reported to regulate not only IL-2 gene expression but also T cell proliferation/function (166, 173-175), NFATc1 and AP-1 c-Jun nuclear translocation were measured. Of interest, dietary curcumin and limonin did not suppress NFATc1 and c-Jun activation in response to either mitogen or antigen. The selective suppression of NF-κB by dietary curcumin and limonin can be explained in part by the mechanism of protein activation. In a resting state, NF-κB family proteins, i.e., c-Rel, p50 (NF-κB1), p52 (NF-κB2), p65 (RelA) and RelB, form homo- or heterodimers which are bound to the inhibitor of NF-κB (IκB). Once T cells are activated, IκB is phosphorylated by IκB

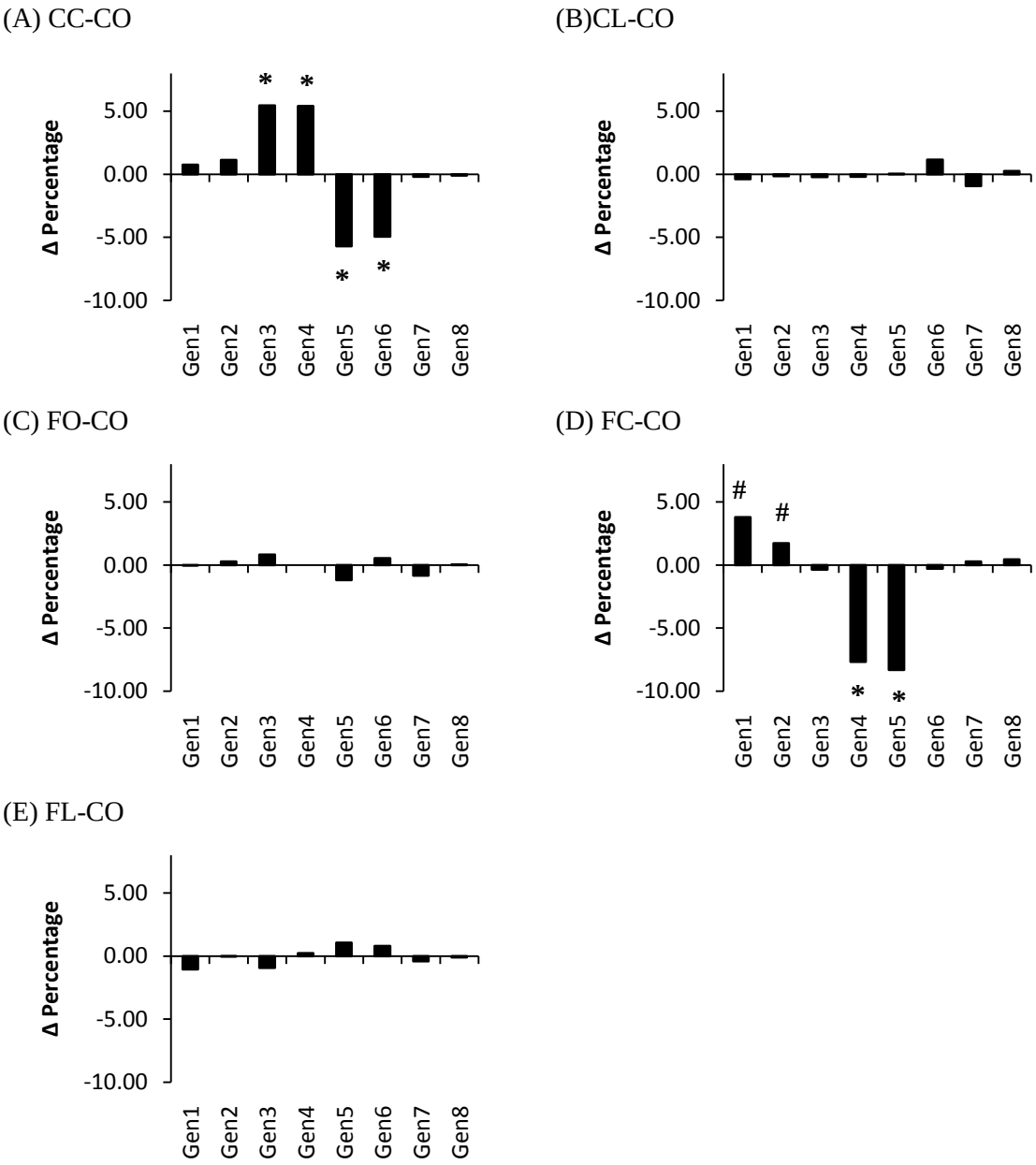

Figure 23. Suppression of $CD4^+$ T cell division in antigen-stimulated cultures as assessed by CFSE anlalysis. Δ Percentages of each generation in OVA peptide+APC stimulated $CD4^+$ T cells. Purified $CD4^+$ T cells were labled by CFSE. Following a 72 hr stimulation period *ex vivo*, CFSE profile was analyzed by flow cytometry as described in the Methods. Data are presented as the difference of percentage of cells in each daughter generation compared to the CO control diet group (CO, corn oil control; CC, CO+1% curcumin; CL, CO+0.02% limonin; FO, 4% fish oil+1% CO; FC, FO+1% curcumin; FL, FO+0.02% limonin, n=10-12 cultures from 5-6 mice, *$P<0.05$, $^{\#}P<0.1$)

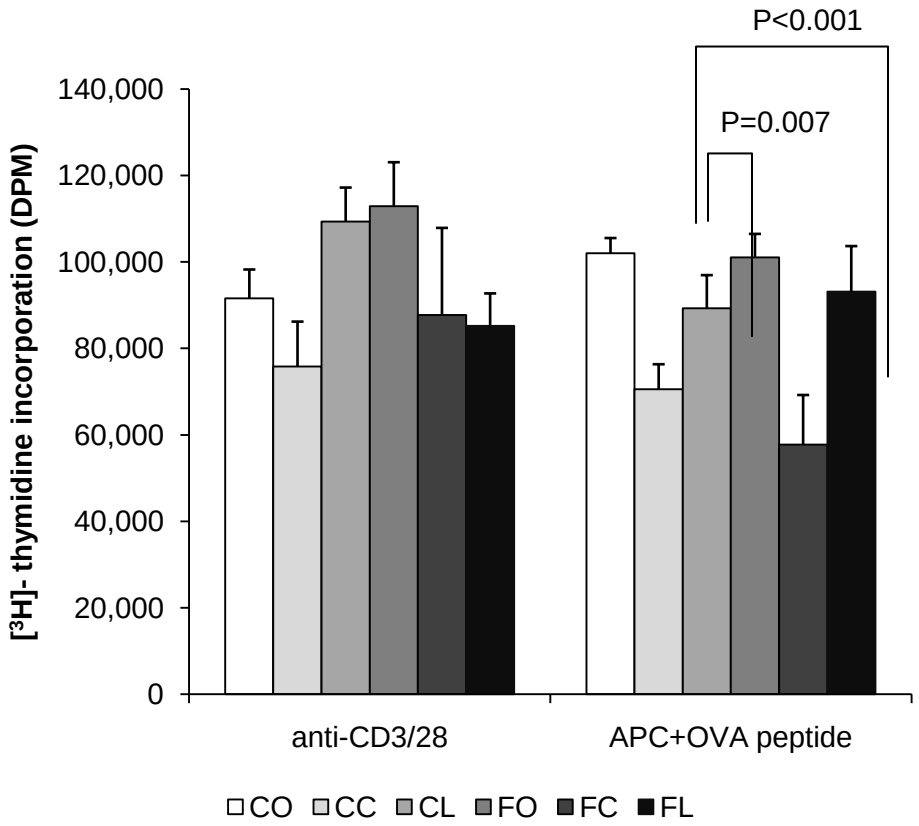

Figure 24. T cell proliferation assessed by thymidine incorporation. Purified $CD4^+$ T cells from each diet group were labeled with CFSE and cultured for 72 hr with either mitogenic or antigenic stimuli. Radioactive [^{3}H]-thymidine uptake was counted using a liquid scintillation counter..DPM, disintegrations per minute; CO, corn oil control; CC, CO+1% curcumin; CL, CO+0.02% limonin; FO, 4% fish oil+1% CO; FC, FO+1% curcumin; FL, FO+0.02% limonin, n=10-12 cultures from 5-6 mice.

kinases (IKK) and detaches from the NF-κB dimer. Phospho-IκB is further degraded by the proteasomal pathway in an ubiquitin-dependent manner (176).

NF-κB dimer migrates into the nucleus to bind to the response element of target genes including IL-2. In contrast, NFAT activation requires direct dephosphorylation of the nuclear factor by calcineurin (166), and AP-1 c-Jun is up-regulated by phosphorylation and formation of a heterodimer with newly synthesized c-Fos. This is noteworthy, because Milacic *et al*. (94) recently reported that curcumin directly binds to

and inhibits proteasomes, resulting in suppressed dissociation of IκB from NF-κB and therefore NF-κB suppression in a human colon cancer cell line. In addition, Aggarwal *et al*. (88) demonstrated that curcumin also inhibits IKK activity. With respect to dietary FO, our laboratory has previously reported that DHA, a major active fatty acid in FO, suppresses PKCθ, which also has IKK activity. Hence, we hypothesized that FO, curcumin and limonin affect different molecular targets; FO alters proximal signaling whereas the phytochemicals antagonize NF-κB. In order to test this hypothesis, FO was combined with either curcumin or limonin.

We further examined the consequence of the suppression of NF-κB p65 by curcumin and limonin with respect to T cell function. IL-2 production was suppressed in antigen stimulated cultures, whereas mitogen stimulated cells produced the same amounts of IL-2 across the dietary treatments. The function of NF-κB subunits in regard to T cell activation has been well studied (173). Liou et al. reported that c-Rel is required for lymphocyte proliferation (177). Rao et al. observed that IL-2 gene transcription in $CD4^+$ T cells is dependent on c-Rel, but not p65 (178). In contrast, Lederer et al. reported that the p65-p50 heterodimer accounts for the NF-κB-mediated IL-2 upregulation (179). IL-2 secretion data from this study suggest that NF-κB p65 does not directly regulate IL-2 production in $CD4^+$ T cells. In addition to transcriptional regulation of IL-2, mRNA degradation in activated T cells was also reported (180). These previous findings suggest further studies are required to elucidate the mechanism by which diet influences IL-2 production and NF-κB inhibition.

The functional result of dietary modulation was assessed by examining $CD4^+$ T cell proliferation using two different methods. Purified $CD4^+$ T cells were labeled by CFSE and stimulated for 72 hr. Cells were either analyzed by flow cytometry or radioactive [^{3}H]-thymidine incorporation. The advantage of CFSE analysis compared to the traditional thymidine incorporation assay was reported by others. Specifically, CFSE analysis has been shown to be more sensitive than the [^{3}H]-thymidine assay to quantify cell division (181-183). The thymidine incorporation analysis demonstrated that cell proliferation was significantly suppressed by curcumin supplementation to either corn oil or fish oil based diets when T cells were stimulated by antigen peptide. Interestingly, T cell proliferation by mitogenic stimulation was not affected by dietary intervention. In contrast, CFSE data revealed that dietary curcumin supplementation to corn oil and fish oil diets suppressed T cell proliferation following both mitogenic- and antigenic stimulation compared to the CO control diet. To our knowledge, this is the first study to investigate the anti-inflammatory effects of FO with either curcumin or limonin on $CD4^+$ T cells.

We next tested the hypothesis that dietary "combination therapy" by curcumin and limonin supplementation to fish oil maximally suppresses $CD4^+$ T cell function. Interestingly, fish oil control diet (4% FO+1% CO) did not suppress NF-κB activation. In contrast, our laboratory has previously demonstrated that dietary FO, as well as purified DHA, suppressed NF-κB nuclear translocation in part by affecting fatty acid composition of plasma membrane including lipid rafts (77). These apparent disparate outcomes may be explained by the different mouse strain and stimuli used. In addition,

the use of homologous mouse serum during the long-term 72 h culture in the previous study may have augmented the lipid effect by maintaining an n-3 PUFA enriched membrane microenvironment (77).

Fish oil diet suppressed IL-2 secretion, which was not further suppressed by curcumin or limonin supplementation. We further investigated the combination effect on T cell proliferation. In accordance with the NF-κB data, $CD4^+$ T cell proliferation was modestly affected in the FO control diet. This is likely explained in part by the loss of n-3 PUFA from the plasma membrane in a long-term culture (30, 50). Limonin supplementation to the CO control diet did not suppress T cell proliferation either. Of interest, FO+Lim supplementation significantly suppressed T cell proliferation in anti-CD3/28 stimulated cultures. Taken together, these data suggest that n-3 PUFA indirectly affect NF-κB activation by altering membrane composition, but curcumin and limonin directly suppress NF-κB translocation. The combination treatments were shown to augment the anti-inflammatory effects.

In summary, the anti-inflammatory effects of dietary curcumin and limonin on $CD4^+$ T cell proliferation are attributed in part to the suppression of NF-κB. Interestingly, there was no obvious association between NF-κB status and IL-2 secretion. We further show that the combination of fish oil and curcumin or limonin elicits a maximal suppressive effect with respect to $CD4^+$ T cell activation.

CHAPTER V

SUMMARY AND CONCLUSIONS

Humans have an adaptive immune system consisting of cell-mediated and humoral immune responses. It is well known that $CD4^+$ T cells control the balance between these two immune responses. Upon infection, the immune system differentiates into one of those two immune responses, or both, depending on the type of pathogen and the individual's age, genetic background and environment such as diet. Interestingly, it has been reported that prolonged activation of $CD4^+$ T cell-mediated immune responses contributes to many chronic inflammatory and autoimmune diseases .

A growing body of epidemiological and clinical studies show that dietary fish oil, which is enriched in n-3 PUFA, attenuates immune-mediated inflammatory diseases (39-43). The major bioactive constituents of fish oil are eicosapentaenoic acid (EPA) and docosahexaenoic acid (DHA). Inuit in Greenland, whose diets are rich in EPA and DHA from fish, exhibit a very low incidence of certain chronic inflammatory diseases (43, 184). Subsequently, many clinical trials also demonstrated that FO supplementation results in clinical improvement in patients with rheumatoid arthritis (40, 41), inflammatory bowel diseases (42, 43, 185), psoriasis (186-188), lupus (189), and multiple sclerosis (190-193). However, to date, detailed molecular mechanisms related to this beneficial effect have not been elucidated.

$CD4^+$ T cells can be further categorized into at least 4 subpopulations, Th1, Th2, Th17 and Treg cells, determined by cytokine secretion and transcriptional factor

activation (1-3, 7-9). Interestingly, Th1 and Th17 subsets have been thought to be responsible for chronic inflammation and autoimmune diseases (10-13). Our lab as well as others previously demonstrated that n-3 PUFA suppress Th1 clonal expansion *ex vivo* (30, 52), which may explain in part the beneficial effect of dietary fish oil. To extend these observations, we used an *in vivo* model by adoptively transferring OVA323-339 peptide-specific DO11.10 $CD4^+$ T cells into WT recipient mice. Following immunization by OVA peptide with complete Freunds' Adjuvant, the accumulation of donor cells in recipient mouse draining lymph nodes were suppressed in fish oil fed animals (**Fig.4 and 5**). In addition, this lower number of cells can be explained by suppressed cell proliferation, determined by CFSE profile analysis (**Fig. 6 and 7**).

To identify a unifying mechanism of pleiotropic n-3 PUFA on a variety of cell types, we examined the alteration of plasma membrane composition/function and consequent cell signaling by n-3 PUFA in $CD4^+$ T cells. Using an endogenously n-3 PUFA producing transgenic mouse model, i.e., the *fat-1* mouse, we show that the accumulation of cholesterol/sphingolipid-enriched microsubdomain of plasma membrane, i.e., lipid rafts, at the immunological synapse was enhanced by n-3 PUFA as assessed by labeling with the fluorescent dye Laurdan which reflects the fluidity of the T cell membrane microenvironment (**Fig. 10**). Interestingly, the suppression of intracellular localization of signaling proteins (F-actin, PKCθ and PLCγ-1) into the IS was associated with enhanced lipid raft formation (**Fig. 11**). In addition, the phosphorylation status of PLCγ-1 at the IS was also down-regulated (**Fig. 12**). As a consequence, $CD4^+$ T cells derived from *fat-1* transgenic mice exhibited a suppressed

ability to proliferate as assessed by two independent methods, CFSE labeling (**Fig. 14**) and radioactive thymidine incorporation (**Fig. 15**). These findings are novel because lipid rafts are generally considered as platforms for T cell signaling and disruption of these subdomains has been postulated to be associated with suppressed T cell function. However, our data emphasize that not only the quantity of lipid rafts but also the quality/diversity of lipid rafts should be addressed in further studies.

Phytochemicals are also proposed to prevent or treat chronic inflammation and cancers. Among several bioactive phytochemicals, curcumin and limonin have been suggested to suppress cellular "life signals" in part by suppressing the NF-κB pathway in various cell types (100, 168-170). Curcumin is a yellow pigment found in curry and limonin is a byproduct of citrus fruit juice production. By feeding DO11.10 mice with 1% curcumin or 0.02% limonin diets, which were previously reported to represent physiologically relevant doses in humans (52, 88, 171, 172), we show that both curcumin and limonin suppress NF-κB p65 nuclear translocation in $CD4^+$ T cells (**Fig. 17**). Further analysis of AP-1 c-Jun and NFATc1 revealed that these agents selectively suppressed NF-κB (**Fig. 18 and 19**). $CD4^+$ T cell proliferation was also suppressed by curcumin in response to either mitogenic or antigenic stimulation, as assessed by CFSE analysis (**Fig. 22 and 23**). In contrast, IL-2 production was not directly associated with the NF-κB pathway (**Fig. 21**). Collectively, these data demonstrate that n-3 PUFA modulate proximal T cell signaling by enhancing lipid raft formation at the IS. In contrast, curcumin and limonin suppress NF-κB activation. Interestingly, dietary

combination of fish oil with limonin further suppressed $CD4^+$ T cell proliferation in response to anti-CD3/28 stimulation (**Fig. 22**).

In summary, dietary n-3 PUFA, curcumin and limonin attenuate $CD4^+$ T cell-mediated immune responses in well-established mouse models. We propose that n-3 PUFA modulate different molecular targets relative to curcumin and/or limonin. Hence, the combination of n-3 PUFA and curcumin or limonin may be capable of synergizing to suppress chronic inflammatory diseases.

REFERENCES

1. Mosmann, T. R., and R. L. Coffman. 1989. TH1 and TH2 cells: different patterns of lymphokine secretion lead to different functional properties. *Annu Rev Immunol* 7:145-173.
2. Dong, C., and R. A. Flavell. 2000. Cell fate decision: T-helper 1 and 2 subsets in immune responses. *Arthritis Res* 2:179-188.
3. Mosmann, T. R., and S. Sad. 1996. The expanding universe of T-cell subsets: Th1, Th2 and more. *Immunol Today* 17:138-146.
4. Young, Y., and M. T. Abreu. 2006. Advances in the pathogenesis of inflammatory bowel disease. *Curr Gastroenterol Rep* 8:470-477.
5. Leon, F., L. E. Smythies, P. D. Smith, and B. L. Kelsall. 2006. Involvement of dendritic cells in the pathogenesis of inflammatory bowel disease. *Adv Exp Med Biol* 579:117-132.
6. Pallone, F., and G. Monteleone. 2001. Mechanisms of tissue damage in inflammatory bowel disease. *Curr Opin Gastroenterol* 17:307-312.
7. Neurath, M. F. 2007. IL-23: a master regulator in Crohn disease. *Nat Med* 13:26-28.
8. Harrington, L. E., R. D. Hatton, P. R. Mangan, H. Turner, T. L. Murphy, K. M. Murphy, and C. T. Weaver. 2005. Interleukin 17-producing $CD4^+$ effector T cells develop via a lineage distinct from the T helper type 1 and 2 lineages. *Nat Immunol* 6:1123-1132.

9. Dong, C. 2006. Diversification of T-helper-cell lineages: finding the family root of IL-17-producing cells. *Nat Rev Immunol* 6:329-333.

10. Bradley, L. M., V. C. Asensio, L. K. Schioetz, J. Harbertson, T. Krahl, G. Patstone, N. Woolf, I. L. Campbell, and N. Sarvetnick. 1999. Islet-specific Th1, but not Th2, cells secrete multiple chemokines and promote rapid induction of autoimmune diabetes. *J Immunol* 162:2511-2520.

11. Ando, D. G., J. Clayton, D. Kono, J. L. Urban, and E. E. Sercarz. 1989. Encephalitogenic T cells in the B10.PL model of experimental allergic encephalomyelitis (EAE) are of the Th-1 lymphokine subtype. *Cell Immunol* 124:132-143.

12. Singh, V. K., S. Mehrotra, and S. S. Agarwal. 1999. The paradigm of Th1 and Th2 cytokines: its relevance to autoimmunity and allergy. *Immunol Res* 20:147-161.

13. Sanchez-Munoz, F., A. Dominguez-Lopez, and J. K. Yamamoto-Furusho. 2008. Role of cytokines in inflammatory bowel disease. *World J Gastroenterol* 14:4280-4288.

14. Acuto, O., S. Mise-Omata, G. Mangino, and F. Michel. 2003. Molecular modifiers of T cell antigen receptor triggering threshold: the mechanism of CD28 costimulatory receptor. *Immunol Rev* 192:21-31.

15. Thauland, T. J., Y. Koguchi, S. A. Wetzel, M. L. Dustin, and D. C. Parker. 2008. Th1 and Th2 cells form morphologically distinct immunological synapses. *J Immunol* 181:393-399.

16. Singer, S. J., and G. L. Nicolson. 1972. The fluid mosaic model of the structure of cell membranes. *Science* 175:720-731.

17. Pike, L. J. 2004. Lipid rafts: heterogeneity on the high seas. *Biochem J* 378:281-292.

18. Edidin, M. 2003. The state of lipid rafts: from model membranes to cells. *Annu Rev Biophys Biomol Struct* 32:257-283.

19. Hanzal-Bayer, M. F., and J. F. Hancock. 2007. Lipid rafts and membrane traffic. *FEBS Lett* 581:2098-2104.

20. Jury, E. C., F. Flores-Borja, and P. S. Kabouridis. 2007. Lipid rafts in T cell signalling and disease. *Semin Cell Dev Biol* 18:608-615.

21. Brassard, P., A. Larbi, A. Grenier, F. Frisch, C. Fortin, A. C. Carpentier, and T. Fulop. 2007. Modulation of T-cell signalling by non-esterified fatty acids. *Prostaglandins Leukot Essent Fatty Acids* 77:337-343.

22. Sheets, E. D., D. Holowka, and B. Baird. 1999. Membrane organization in immunoglobulin E receptor signaling. *Curr Opin Chem Biol* 3:95-99.

23. Janes, P. W., S. C. Ley, A. I. Magee, and P. S. Kabouridis. 2000. The role of lipid rafts in T cell antigen receptor (TCR) signalling. *Semin Immunol* 12:23-34.

24. Cheng, P. C., M. L. Dykstra, R. N. Mitchell, and S. K. Pierce. 1999. A role for lipid rafts in B cell antigen receptor signaling and antigen targeting. *J Exp Med* 190:1549-1560.

25. Waugh, M. G., D. Lawson, and J. J. Hsuan. 1999. Epidermal growth factor receptor activation is localized within low-buoyant density, non-caveolar membrane domains. *Biochem J* 337 (Pt 3):591-597.

26. Le Roy, C., and J. L. Wrana. 2005. Clathrin- and non-clathrin-mediated endocytic regulation of cell signalling. *Nat Rev Mol Cell Biol* 6:112-126.

27. Mastick, C. C., M. J. Brady, and A. R. Saltiel. 1995. Insulin stimulates the tyrosine phosphorylation of caveolin. *J Cell Biol* 129:1523-1531.

28. Wary, K. K., A. Mariotti, C. Zurzolo, and F. G. Giancotti. 1998. A requirement for caveolin-1 and associated kinase Fyn in integrin signaling and anchorage-dependent cell growth. *Cell* 94:625-634.

29. Shaul, P. W., E. J. Smart, L. J. Robinson, Z. German, I. S. Yuhanna, Y. Ying, R. G. Anderson, and T. Michel. 1996. Acylation targets emdothelial nitric-oxide synthase to plasmalemmal caveolae. *J Biol Chem* 271:6518-6522.

30. Zhang, P., R. Smith, R. S. Chapkin, and D. N. McMurray. 2005. Dietary (n-3) polyunsaturated fatty acids modulate murine Th1/Th2 balance toward the Th2 pole by suppression of Th1 development. *J Nutr* 135:1745-1751.

31. Switzer, K. C., D. N. McMurray, J. S. Morris, and R. S. Chapkin. 2003. (n-3) Polyunsaturated fatty acids promote activation-induced cell death in murine T lymphocytes. *J Nutr* 133:496-503.

32. Fan, Y. Y., D. N. McMurray, L. H. Ly, and R. S. Chapkin. 2003. Dietary (n-3) polyunsaturated fatty acids remodel mouse T-cell lipid rafts. *J Nutr* 133:1913-1920.

33. Arrington, J. L., D. N. McMurray, K. C. Switzer, Y. Y. Fan, and R. S. Chapkin. 2001. Docosahexaenoic acid suppresses function of the CD28 costimulatory membrane receptor in primary murine and Jurkat T cells. *J Nutr* 131:1147-1153.

34. Arrington, J. L., R. S. Chapkin, K. C. Switzer, J. S. Morris, and D. N. McMurray. 2001. Dietary n-3 polyunsaturated fatty acids modulate purified murine T-cell subset activation. *Clin Exp Immunol* 125:499-507.

35. Siddiqui, R. A., K. A. Harvey, G. P. Zaloga, and W. Stillwell. 2007. Modulation of lipid rafts by Omega-3 fatty acids in inflammation and cancer: implications for use of lipids during nutrition support. *Nutr Clin Pract* 22:74-88.

36. Seo, J., R. Barhoumi, A. E. Johnson, J. R. Lupton, and R. S. Chapkin. 2006. Docosahexaenoic acid selectively inhibits plasma membrane targeting of lipidated proteins. *FASEB J* 20:770-772.

37. Feller, S. E., K. Gawrisch, and A. D. MacKerell, Jr. 2002. Polyunsaturated fatty acids in lipid bilayers: intrinsic and environmental contributions to their unique physical properties. *J Am Chem Soc* 124:318-326.

38. Huber, T., K. Rajamoorthi, V. F. Kurze, K. Beyer, and M. F. Brown. 2002. Structure of docosahexaenoic acid-containing phospholipid bilayers as studied by (2)H NMR and molecular dynamics simulations. *J Am Chem Soc* 124:298-309.

39. Calder, P. C. 2006. n-3 polyunsaturated fatty acids, inflammation, and inflammatory diseases. *Am J Clin Nutr* 83:1505S-1519S.

40. Kremer, J. M., W. Jubiz, A. Michalek, R. I. Rynes, L. E. Bartholomew, J. Bigaouette, M. Timchalk, D. Beeler, and L. Lininger. 1987. Fish-oil fatty acid

supplementation in active rheumatoid arthritis. A double-blinded, controlled, crossover study. *Ann Intern Med* 106:497-503.

41. Kremer, J. M. 2000. n-3 fatty acid supplements in rheumatoid arthritis. *Am J Clin Nutr* 71:349S-351S.

42. Belluzzi, A., C. Brignola, M. Campieri, A. Pera, S. Boschi, and M. Miglioli. 1996. Effect of an enteric-coated fish-oil preparation on relapses in Crohn's disease. *The New England journal of medicine* 334:1557-1560.

43. Belluzzi, A., S. Boschi, C. Brignola, A. Munarini, G. Cariani, and F. Miglio. 2000. Polyunsaturated fatty acids and inflammatory bowel disease. *Am J Clin Nutr* 71:339S-342S.

44. Zhao, G., T. D. Etherton, K. R. Martin, P. J. Gillies, S. G. West, and P. M. Kris-Etherton. 2007. Dietary alpha-linolenic acid inhibits proinflammatory cytokine production by peripheral blood mononuclear cells in hypercholesterolemic subjects. *Am J Clin Nutr* 85:385-391.

45. Wallace, F. A., E. A. Miles, C. Evans, T. E. Stock, P. Yaqoob, and P. C. Calder. 2001. Dietary fatty acids influence the production of Th1- but not Th2-type cytokines. *J Leukoc Biol* 69:449-457.

46. Kleemann, R., F. W. Scott, U. Worz-Pagenstert, W. M. Nimal Ratnayake, and H. Kolb. 1998. Impact of dietary fat on Th1/Th2 cytokine gene expression in the pancreas and gut of diabetes-prone BB rats. *J Autoimmun* 11:97-103.

47. Gallai, V., P. Sarchielli, A. Trequattrini, M. Franceschini, A. Floridi, C. Firenze, A. Alberti, D. Di Benedetto, and E. Stragliotto. 1995. Cytokine secretion and

eicosanoid production in the peripheral blood mononuclear cells of MS patients undergoing dietary supplementation with n-3 polyunsaturated fatty acids. *J Neuroimmunol* 56:143-153.

48. Petursdottir, D. H., and I. Hardardottir. 2007. Dietary fish oil increases the number of splenic macrophages secreting TNF-alpha and IL-10 but decreases the secretion of these cytokines by splenic T cells from mice. *J Nutr* 137:665-670.

49. Kim, Y. J., H. J. Kim, J. K. No, H. Y. Chung, and G. Fernandes. 2006. Anti-inflammatory action of dietary fish oil and calorie restriction. *Life Sci* 78:2523-2532.

50. Switzer, K. C., Y. Y. Fan, N. Wang, D. N. McMurray, and R. S. Chapkin. 2004. Dietary n-3 polyunsaturated fatty acids promote activation-induced cell death in Th1-polarized murine CD4+ T-cells. *J Lipid Res* 45:1482-1492.

51. Siddiqui, R. A., L. J. Jenski, K. Neff, K. Harvey, R. J. Kovacs, and W. Stillwell. 2001. Docosahexaenoic acid induces apoptosis in Jurkat cells by a protein phosphatase-mediated process. *Biochim Biophys Acta* 1499:265-275.

52. Zhang, P., W. Kim, L. Zhou, N. Wang, L. H. Ly, D. N. McMurray, and R. S. Chapkin. 2006. Dietary fish oil inhibits antigen-specific murine Th1 cell development by suppression of clonal expansion. *J Nutr* 136:2391-2398.

53. Kelley, D. S., P. C. Taylor, G. J. Nelson, and B. E. Mackey. 1998. Arachidonic acid supplementation enhances synthesis of eicosanoids without suppressing immune functions in young healthy men. *Lipids* 33:125-130.

54. Thomas, C. P., Z. Davison, and C. M. Heard. 2007. Probing the skin permeation of fish oil/EPA and ketoprofen-3. Effects on epidermal COX-2 and LOX. *Prostaglandins Leukot Essent Fatty Acids* 76:357-362.

55. Bagga, D., L. Wang, R. Farias-Eisner, J. A. Glaspy, and S. T. Reddy. 2003. Differential effects of prostaglandin derived from omega-6 and omega-3 polyunsaturated fatty acids on COX-2 expression and IL-6 secretion. *Proc Natl Acad Sci U S A* 100:1751-1756.

56. Smith, W. L. 2005. Cyclooxygenases, peroxide tone and the allure of fish oil. *Curr Opin Cell Biol* 17:174-182.

57. Lawrence, T., D. A. Willoughby, and D. W. Gilroy. 2002. Anti-inflammatory lipid mediators and insights into the resolution of inflammation. *Nat Rev Immunol* 2:787-795.

58. Arita, M., M. Yoshida, S. Hong, E. Tjonahen, J. N. Glickman, N. A. Petasis, R. S. Blumberg, and C. N. Serhan. 2005. Resolvin E1, an endogenous lipid mediator derived from omega-3 eicosapentaenoic acid, protects against 2,4,6-trinitrobenzene sulfonic acid-induced colitis. *Proc Natl Acad Sci U S A* 102:7671-7676.

59. Serhan, C. N., S. Yacoubian, and R. Yang. 2008. Anti-inflammatory and proresolving lipid mediators. *Annu Rev Pathol* 3:279-312.

60. Flower, R. J., and M. Perretti. 2005. Controlling inflammation: a fat chance? *J Exp Med* 201:671-674.

61. Mangino, M. J., L. Brounts, B. Harms, and C. Heise. 2006. Lipoxin biosynthesis in inflammatory bowel disease. *Prostaglandins Other Lipid Mediat* 79:84-92.

62. Hamazaki, T., S. Fischer, M. Urakaze, S. Sawazaki, S. Yano, and T. Kuwamori. 1989. Urinary excretion of PGI2/3-M and recent N-6/3 fatty acid intake. *Prostaglandins* 37:417-424.

63. Hontecillas, R., and J. Bassaganya-Riera. 2007. Peroxisome proliferator-activated receptor gamma is required for regulatory CD4+ T cell-mediated protection against colitis. *J Immunol* 178:2940-2949.

64. Xu, H. E., M. H. Lambert, V. G. Montana, D. J. Parks, S. G. Blanchard, P. J. Brown, D. D. Sternbach, J. M. Lehmann, G. B. Wisely, T. M. Willson, S. A. Kliewer, and M. V. Milburn. 1999. Molecular recognition of fatty acids by peroxisome proliferator-activated receptors. *Mol Cell* 3:397-403.

65. Kliewer, S. A., S. S. Sundseth, S. A. Jones, P. J. Brown, G. B. Wisely, C. S. Koble, P. Devchand, W. Wahli, T. M. Willson, J. M. Lenhard, and J. M. Lehmann. 1997. Fatty acids and eicosanoids regulate gene expression through direct interactions with peroxisome proliferator-activated receptors alpha and gamma. *Proc Natl Acad Sci U S A* 94:4318-4323.

66. Pascual, G., A. L. Fong, S. Ogawa, A. Gamliel, A. C. Li, V. Perissi, D. W. Rose, T. M. Willson, M. G. Rosenfeld, and C. K. Glass. 2005. A SUMOylation-dependent pathway mediates transrepression of inflammatory response genes by PPAR-gamma. *Nature* 437:759-763.

67. Balamuth, F., J. L. Brogdon, and K. Bottomly. 2004. CD4 raft association and signaling regulate molecular clustering at the immunological synapse site. *J Immunol* 172:5887-5892.

68. Webb, Y., L. Hermida-Matsumoto, and M. D. Resh. 2000. Inhibition of protein palmitoylation, raft localization, and T cell signaling by 2-bromopalmitate and polyunsaturated fatty acids. *J Biol Chem* 275:261-270.

69. Kabouridis, P. S., A. I. Magee, and S. C. Ley. 1997. S-acylation of LCK protein tyrosine kinase is essential for its signalling function in T lymphocytes. *EMBO J* 16:4983-4998.

70. Zeyda, M., G. Staffler, V. Horejsi, W. Waldhausl, and T. M. Stulnig. 2002. LAT displacement from lipid rafts as a molecular mechanism for the inhibition of T cell signaling by polyunsaturated fatty acids. *J Biol Chem* 277:28418-28423.

71. Zhu, M., S. Shen, Y. Liu, O. Granillo, and W. Zhang. 2005. Cutting Edge: Localization of linker for activation of T cells to lipid rafts is not essential in T cell activation and development. *J Immunol* 174:31-35.

72. Stulnig, T. M., M. Berger, T. Sigmund, D. Raederstorff, H. Stockinger, and W. Waldhausl. 1998. Polyunsaturated fatty acids inhibit T cell signal transduction by modification of detergent-insoluble membrane domains. *J Cell Biol* 143:637-644.

73. Stulnig, T. M., and M. Zeyda. 2004. Immunomodulation by polyunsaturated fatty acids: impact on T-cell signaling. *Lipids* 39:1171-1175.

74. Geyeregger, R., M. Zeyda, G. J. Zlabinger, W. Waldhausl, and T. M. Stulnig. 2005. Polyunsaturated fatty acids interfere with formation of the immunological synapse. *J Leukoc Biol* 77:680-688.

75. Stulnig, T. M. 2003. Immunomodulation by polyunsaturated fatty acids: mechanisms and effects. *Int Arch Allergy Immunol* 132:310-321.

76. Zeyda, M., A. B. Szekeres, M. D. Saemann, R. Geyeregger, H. Stockinger, G. J. Zlabinger, W. Waldhausl, and T. M. Stulnig. 2003. Suppression of T cell signaling by polyunsaturated fatty acids: selectivity in inhibition of mitogen-activated protein kinase and nuclear factor activation. *J Immunol* 170:6033-6039.

77. Fan, Y. Y., L. H. Ly, R. Barhoumi, D. N. McMurray, and R. S. Chapkin. 2004. Dietary docosahexaenoic acid suppresses T cell protein kinase C theta lipid raft recruitment and IL-2 production. *J Immunol* 173:6151-6160.

78. Chapkin, R. S., N. Wang, Y. Y. Fan, J. R. Lupton, and I. A. Prior. 2008. Docosahexaenoic acid alters the size and distribution of cell surface microdomains. *Biochim Biophys Acta* 1778:466-471.

79. Chapkin, R. S., D. N. McMurray, L. A. Davidson, B. S. Patil, Y. Y. Fan, and J. R. Lupton. 2008. Bioactive dietary long-chain fatty acids: emerging mechanisms of action. *Br J Nutr*:1-6.

80. Shaikh, S. R., V. Cherezov, M. Caffrey, W. Stillwell, and S. R. Wassall. 2003. Interaction of cholesterol with a docosahexaenoic acid-containing phosphatidylethanolamine: trigger for microdomain/raft formation? *Biochemistry* 42:12028-12037.

81. Shaikh, S. R., and M. Edidin. 2006. Polyunsaturated fatty acids, membrane organization, T cells, and antigen presentation. *Am J Clin Nutr* 84:1277-1289.

82. Shaikh, S. R., and M. A. Edidin. 2006. Membranes are not just rafts. *Chem Phys Lipids* 144:1-3.

83. Wassall, S. R., and W. Stillwell. 2008. Docosahexaenoic acid domains: the ultimate non-raft membrane domain. *Chem Phys Lipids* 153:57-63.

84. Soni, S. P., D. S. LoCascio, Y. Liu, J. A. Williams, R. Bittman, W. Stillwell, and S. R. Wassall. 2008. Docosahexaenoic acid enhances segregation of lipids between : 2H-NMR study. *Biophys J* 95:203-214.

85. Patra, S. K. 2008. Dissecting lipid raft facilitated cell signaling pathways in cancer. *Biochim Biophys Acta* 1785:182-206.

86. Deguchi, Y., A. Andoh, O. Inatomi, Y. Yagi, S. Bamba, Y. Araki, K. Hata, T. Tsujikawa, and Y. Fujiyama. 2007. Curcumin prevents the development of dextran sulfate Sodium (DSS)-induced experimental colitis. *Dig Dis Sci* 52:2993-2998.

87. Balasubramanian, S., and R. L. Eckert. 2007. Curcumin suppresses AP1 transcription factor-dependent differentiation and activates apoptosis in human epidermal keratinocytes. *J Biol Chem* 282:6707-6715.

88. Aggarwal, S., H. Ichikawa, Y. Takada, S. K. Sandur, S. Shishodia, and B. B. Aggarwal. 2006. Curcumin (diferuloylmethane) down-regulates expression of cell proliferation and antiapoptotic and metastatic gene products through

suppression of IkappaBalpha kinase and Akt activation. *Mol Pharmacol* 69:195-206.

89. Gertsch, J., M. Guttinger, J. Heilmann, and O. Sticher. 2003. Curcumin differentially modulates mRNA profiles in Jurkat T and human peripheral blood mononuclear cells. *Bioorg Med Chem* 11:1057-1063.

90. Pendurthi, U. R., J. T. Williams, and L. V. Rao. 1997. Inhibition of tissue factor gene activation in cultured endothelial cells by curcumin. Suppression of activation of transcription factors Egr-1, AP-1, and NF-kappa B. *Arterioscler Thromb Vasc Biol* 17:3406-3413.

91. Singh, S., and B. B. Aggarwal. 1995. Activation of transcription factor NF-kappa B is suppressed by curcumin (diferuloylmethane) [corrected]. *J Biol Chem* 270:24995-25000.

92. Chen, Y. R., and T. H. Tan. 1998. Inhibition of the c-Jun N-terminal kinase (JNK) signaling pathway by curcumin. *Oncogene* 17:173-178.

93. Surh, Y. J., S. S. Han, Y. S. Keum, H. J. Seo, and S. S. Lee. 2000. Inhibitory effects of curcumin and capsaicin on phorbol ester-induced activation of eukaryotic transcription factors, NF-kappaB and AP-1. *Biofactors* 12:107-112.

94. Milacic, V., S. Banerjee, K. R. Landis-Piwowar, F. H. Sarkar, A. P. Majumdar, and Q. P. Dou. 2008. Curcumin inhibits the proteasome activity in human colon cancer cells *in vitro* and *in vivo*. *Cancer Res* 68:7283-7292.

95. Hanai, H., T. Iida, K. Takeuchi, F. Watanabe, Y. Maruyama, A. Andoh, T. Tsujikawa, Y. Fujiyama, K. Mitsuyama, M. Sata, M. Yamada, Y. Iwaoka, K.

Kanke, H. Hiraishi, K. Hirayama, H. Arai, S. Yoshii, M. Uchijima, T. Nagata, and Y. Koide. 2006. Curcumin maintenance therapy for ulcerative colitis: randomized, multicenter, double-blind, placebo-controlled trial. *Clin Gastroenterol Hepatol* 4:1502-1506.

96. Holt, P. R., S. Katz, and R. Kirshoff. 2005. Curcumin therapy in inflammatory bowel disease: a pilot study. *Dig Dis Sci* 50:2191-2193.

97. Sharma, C., J. Kaur, S. Shishodia, B. B. Aggarwal, and R. Ralhan. 2006. Curcumin down regulates smokeless tobacco-induced NF-kappaB activation and COX-2 expression in human oral premalignant and cancer cells. *Toxicology* 228:1-15.

98. Zhang, M., C. S. Deng, J. J. Zheng, and J. Xia. 2006. Curcumin regulated shift from Th1 to Th2 in trinitrobenzene sulphonic acid-induced chronic colitis. *Acta Pharmacol Sin* 27:1071-1077.

99. Kang, B. Y., Y. J. Song, K. M. Kim, Y. K. Choe, S. Y. Hwang, and T. S. Kim. 1999. Curcumin inhibits Th1 cytokine profile in CD4+ T cells by suppressing interleukin-12 production in macrophages. *Br J Pharmacol* 128:380-384.

100. Vanamala, J., T. Leonardi, B. S. Patil, S. S. Taddeo, M. E. Murphy, L. M. Pike, R. S. Chapkin, J. R. Lupton, and N. D. Turner. 2006. Suppression of colon carcinogenesis by bioactive compounds in grapefruit. *Carcinogenesis* 27:1257-1265.

101. Tanaka, T., M. Maeda, H. Kohno, M. Murakami, S. Kagami, M. Miyake, and K. Wada. 2001. Inhibition of azoxymethane-induced colon carcinogenesis in male

F344 rats by the citrus limonoids obacunone and limonin. *Carcinogenesis* 22:193-198.

102. Shishodia, S., and B. B. Aggarwal. 2002. Nuclear factor-kappaB activation: a question of life or death. *J Biochem Mol Biol* 35:28-40.

103. Chiu, F. L., and J. K. Lin. 2008. Tomatidine inhibits iNOS and COX-2 through suppression of NF-kappaB and JNK pathways in LPS-stimulated mouse macrophages. *FEBS Lett* 582:2407-2412.

104. Yu, J., L. Wang, R. L. Walzem, E. G. Miller, L. M. Pike, and B. S. Patil. 2005. Antioxidant activity of citrus limonoids, flavonoids, and coumarins. *J Agric Food Chem* 53:2009-2014.

105. Harder, T., P. Scheiffele, P. Verkade, and K. Simons. 1998. Lipid domain structure of the plasma membrane revealed by patching of membrane components. *J Cell Biol* 141:929-942.

106. Anderson, R. G. 1998. The caveolae membrane system. *Annu Rev Biochem* 67:199-225.

107. Wilson, B. S., J. R. Pfeiffer, and J. M. Oliver. 2000. Observing FcepsilonRI signaling from the inside of the mast cell membrane. *J Cell Biol* 149:1131-1142.

108. Kenworthy, A. K., N. Petranova, and M. Edidin. 2000. High-resolution FRET microscopy of cholera toxin B-subunit and GPI-anchored proteins in cell plasma membranes. *Mol Biol Cell* 11:1645-1655.

109. Simons, K., and D. Toomre. 2000. Lipid rafts and signal transduction. *Nat Rev Mol Cell Biol* 1:31-39.

110. Gaus, K., E. Chklovskaia, B. Fazekas de St Groth, W. Jessup, and T. Harder. 2005. Condensation of the plasma membrane at the site of T lymphocyte activation. *J Cell Biol* 171:121-131.

111. Gaus, K., T. Zech, and T. Harder. 2006. Visualizing membrane microdomains by Laurdan 2-photon microscopy. *Mol Membr Biol* 23:41-48.

112. Rentero, C., T. Zech, C. M. Quinn, K. Engelhardt, D. Williamson, T. Grewal, W. Jessup, T. Harder, and K. Gaus. 2008. Functional implications of plasma membrane condensation for T cell activation. *PLoS ONE* 3:e2262.

113. Kang, J. X., J. Wang, L. Wu, and Z. B. Kang. 2004. Transgenic mice: fat-1 mice convert n-6 to n-3 fatty acids. *Nature* 427:504.

114. Jia, Q., J. R. Lupton, R. Smith, B. R. Weeks, E. Callaway, L. A. Davidson, W. Kim, Y. Y. Fan, P. Yang, R. A. Newman, J. X. Kang, D. N. McMurray, and R. S. Chapkin. 2008. Reduced colitis-associated colon cancer in fat-1 (n-3 Fatty acid desaturase) transgenic mice. *Cancer Res* 68:3985-3991.

115. Mittler, J. N., and W. T. Lee. 2004. Antigen-specific CD4 T cell clonal expansion and differentiation in the aged lymphoid microenvironment. I. The primary T cell response is unaffected. *Mech Ageing Dev* 125:47-57.

116. Murphy, K. M., A. B. Heimberger, and D. Y. Loh. 1990. Induction by antigen of intrathymic apoptosis of $CD4^{+}CD8^{+}TCR^{lo}$ thymocytes *in vivo*. *Science* 250:1720-1723.

117. Pompos, L. J., and K. L. Fritsche. 2002. Antigen-driven murine CD4+ T lymphocyte proliferation and interleukin-2 production are diminished by dietary (n-3) polyunsaturated fatty acids. *J Nutr* 132:3293-3300.

118. Kato, Y., T. Negishi, S. Furusako, K. Mizuguchi, and H. Mochizuki. 2003. An orally active Th1/Th2 balance modulator, M50367, suppresses Th2 differentiation of naive Th cell *in vitro*. *Cell Immunol* 224:29-37.

119. Hsieh, C. S., S. E. Macatonia, A. O'Garra, and K. M. Murphy. 1995. T cell genetic background determines default T helper phenotype development *in vitro*. *J Exp Med* 181:713-721.

120. Kearney, E. R., K. A. Pape, D. Y. Loh, and M. K. Jenkins. 1994. Visualization of peptide-specific T cell immunity and peripheral tolerance induction *in vivo*. *Immunity* 1:327-339.

121. Yip, H. C., A. Y. Karulin, M. Tary-Lehmann, M. D. Hesse, H. Radeke, P. S. Heeger, R. P. Trezza, F. P. Heinzel, T. Forsthuber, and P. V. Lehmann. 1999. Adjuvant-guided type-1 and type-2 immunity: infectious/noninfectious dichotomy defines the class of response. *J Immunol* 162:3942-3949.

122. Lyons, A. B., and C. R. Parish. 1994. Determination of lymphocyte division by flow cytometry. *J Immunol Methods* 171:131-137.

123. Moses, C. T., K. M. Thorstenson, S. C. Jameson, and A. Khoruts. 2003. Competition for self ligands restrains homeostatic proliferation of naive CD4 T cells. *Proc Natl Acad Sci U S A* 100:1185-1190.

124. Lee, K. H., A. R. Dinner, C. Tu, G. Campi, S. Raychaudhuri, R. Varma, T. N. Sims, W. R. Burack, H. Wu, J. Wang, O. Kanagawa, M. Markiewicz, P. M. Allen, M. L. Dustin, A. K. Chakraborty, and A. S. Shaw. 2003. The immunological synapse balances T cell receptor signaling and degradation. *Science* 302:1218-1222.

125. Thompson, B. S., and T. C. Mitchell. 2004. Measurement of daughter cell accumulation during lymphocyte proliferation *in vivo*. *J Immunol Methods* 295:79-87.

126. Laird, N. M., Ware, J.H. 1982. Random effects models for longitudinal data. *Biometrics* 38:963-974.

127. Harville, D. A. 1977. Maximun likelihood approaches to variance component estimation and to related problems. *J. Amer. Stat. Assoc.* 72:320-340.

128. Thompson, B. S., V. Mata-Haro, C. R. Casella, and T. C. Mitchell. 2005. Peptide-stimulated DO11.10 T cells divide well but accumulate poorly in the absence of TLR agonist treatment. *Eur J Immunol* 35:3196-3208.

129. Lingwood, D., and K. Simons. 2007. Detergent resistance as a tool in membrane research. *Nat Protoc* 2:2159-2165.

130. Sijben, J. W., and P. C. Calder. 2007. Differential immunomodulation with long-chain n-3 PUFA in health and chronic disease. *Proc Nutr Soc* 66:237-259.

131. Chapkin, R. S., L. A. Davidson, L. Ly, B. R. Weeks, J. R. Lupton, and D. N. McMurray. 2007. Immunomodulatory effects of (n-3) fatty acids: putative link to inflammation and colon cancer. *J Nutr* 137:200S-204S.

132. Chapkin, R. S., D. N. McMurray, and J. R. Lupton. 2007. Colon cancer, fatty acids and anti-inflammatory compounds. *Curr Opin Gastroenterol* 23:48-54.

133. Li, Q., L. Tan, C. Wang, N. Li, Y. Li, G. Xu, and J. Li. 2006. Polyunsaturated eicosapentaenoic acid changes lipid composition in lipid rafts. *Eur J Nutr* 45:144-151.

134. Zachowski, A. 1993. Phospholipids in animal eukaryotic membranes: transverse asymmetry and movement. *Biochem J* 294 (Pt 1):1-14.

135. Chow, S. C., L. Sisfontes, M. Jondal, and I. Bjorkhem. 1991. Modification of membrane phospholipid fatty acyl composition in a leukemic T cell line: effects on receptor mediated intracellular Ca2+ increase. *Biochim Biophys Acta* 1092:358-366.

136. Sasaki, T., Y. Kanke, K. Kudoh, Y. Misawa, J. Shimizu, and T. Takita. 1999. Effects of dietary docosahexaenoic acid on surface molecules involved in T cell proliferation. *Biochim Biophys Acta* 1436:519-530.

137. Tanner, M. J., W. Hanel, S. L. Gaffen, and X. Lin. 2007. CARMA1 coiled-coil domain is involved in the oligomerization and subcellular localization of CARMA1 and is required for T cell receptor-induced NF-kappaB activation. *J Biol Chem* 282:17141-17147.

138. Zidovetzki, R., and I. Levitan. 2007. Use of cyclodextrins to manipulate plasma membrane cholesterol content: evidence, misconceptions and control strategies. *Biochim Biophys Acta* 1768:1311-1324.

139. Tamir, A., M. D. Eisenbraun, G. G. Garcia, and R. A. Miller. 2000. Age-dependent alterations in the assembly of signal transduction complexes at the site of T cell/APC interaction. *J Immunol* 165:1243-1251.

140. Tavano, R., R. L. Contento, S. J. Baranda, M. Soligo, L. Tuosto, S. Manes, and A. Viola. 2006. CD28 interaction with filamin-A controls lipid raft accumulation at the T-cell immunological synapse. *Nat Cell Biol* 8:1270-1276.

141. Quah, B. J., H. S. Warren, and C. R. Parish. 2007. Monitoring lymphocyte proliferation *in vitro* and *in vivo* with the intracellular fluorescent dye carboxyfluorescein diacetate succinimidyl ester. *Nat Protoc* 2:2049-2056.

142. Owen, D. M., M. A. Neil, P. M. French, and A. I. Magee. 2007. Optical techniques for imaging membrane lipid microdomains in living cells. *Semin Cell Dev Biol* 18:591-598.

143. Gaide, O., B. Favier, D. F. Legler, D. Bonnet, B. Brissoni, S. Valitutti, C. Bron, J. Tschopp, and M. Thome. 2002. CARMA1 is a critical lipid raft-associated regulator of TCR-induced NF-kappa B activation. *Nat Immunol* 3:836-843.

144. Reynolds, L. F., C. de Bettignies, T. Norton, A. Beeser, J. Chernoff, and V. L. Tybulewicz. 2004. Vav1 transduces T cell receptor signals to the activation of the Ras/ERK pathway via LAT, Sos, and RasGRP1. *J Biol Chem* 279:18239-18246.

145. Moore, A. L., M. W. Roe, R. F. Melnick, and S. D. Lidofsky. 2002. Calcium mobilization evoked by hepatocellular swelling is linked to activation of phospholipase Cgamma. *J Biol Chem* 277:34030-34035.

146. Ma, D. W., V. Ngo, P. S. Huot, and J. X. Kang. 2006. N-3 polyunsaturated fatty acids endogenously synthesized in fat-1 mice are enriched in the mammary gland. *Lipids* 41:35-39.

147. Pike, L. J., X. Han, and R. W. Gross. 2005. Epidermal growth factor receptors are localized to lipid rafts that contain a balance of inner and outer leaflet lipids: a shotgun lipidomics study. *J Biol Chem* 280:26796-26804.

148. Blank, N., M. Schiller, S. Krienke, G. Wabnitz, A. D. Ho, and H. M. Lorenz. 2007. Cholera toxin binds to lipid rafts but has a limited specificity for ganglioside GM1. *Immunol Cell Biol* 85:378-382.

149. Sanderson, P., and P. C. Calder. 1998. Dietary fish oil appears to prevent the activation of phospholipase C-gamma in lymphocytes. *Biochim Biophys Acta* 1392:300-308.

150. Huse, M., L. O. Klein, A. T. Girvin, J. M. Faraj, Q. J. Li, M. S. Kuhns, and M. M. Davis. 2007. Spatial and temporal dynamics of T cell receptor signaling with a photoactivatable agonist. *Immunity* 27:76-88.

151. Mossman, K. D., G. Campi, J. T. Groves, and M. L. Dustin. 2005. Altered TCR signaling from geometrically repatterned immunological synapses. *Science* 310:1191-1193.

152. Varma, R., G. Campi, T. Yokosuka, T. Saito, and M. L. Dustin. 2006. T cell receptor-proximal signals are sustained in peripheral microclusters and terminated in the central supramolecular activation cluster. *Immunity* 25:117-127.

153. Ly, L. H., R. Smith, 3rd, R. S. Chapkin, and D. N. McMurray. 2005. Dietary n-3 polyunsaturated fatty acids suppress splenic CD4(+) T cell function in interleukin (IL)-10(-/-) mice. *Clin Exp Immunol* 139:202-209.

154. Wang, D., and R. N. Dubois. 2008. Pro-inflammatory prostaglandins and progression of colorectal cancer. *Cancer Lett*.

155. Engels, E. A. 2008. Inflammation in the development of lung cancer: epidemiological evidence. *Expert Rev Anticancer Ther* 8:605-615.

156. Maeda, S., and M. Omata. 2008. Inflammation and cancer: role of nuclear factor-kappaB activation. *Cancer Sci* 99:836-842.

157. Meydani, S. N., S. Endres, M. M. Woods, B. R. Goldin, C. Soo, A. Morrill-Labrode, C. A. Dinarello, and S. L. Gorbach. 1991. Oral (n-3) fatty acid supplementation suppresses cytokine production and lymphocyte proliferation: comparison between young and older women. *The Journal of nutrition* 121:547-555.

158. Stenson, W. F., D. Cort, J. Rodgers, R. Burakoff, K. DeSchryver-Kecskemeti, T. L. Gramlich, and W. Beeken. 1992. Dietary supplementation with fish oil in ulcerative colitis. *Annals of internal medicine* 116:609-614.

159. Fowler, K. H., R. S. Chapkin, and D. N. McMurray. 1993. Effects of purified dietary n-3 ethyl esters on murine T lymphocyte function. *J Immunol* 151:5186-5197.

160. Calder, P. C. 1998. Dietary fatty acids and the immune system. *Nutrition reviews* 56:S70-83.

161. Curtis, C. L., S. G. Rees, C. B. Little, C. R. Flannery, C. E. Hughes, C. Wilson, C. M. Dent, I. G. Otterness, J. L. Harwood, and B. Caterson. 2002. Pathologic indicators of degradation and inflammation in human osteoarthritic cartilage are abrogated by exposure to n-3 fatty acids. *Arthritis and rheumatism* 46:1544-1553.

162. Spector, A. A. 1999. Essentiality of fatty acids. *Lipids* 34 Suppl:S1-3.

163. Pike, L. J. 2006. Rafts defined: a report on the Keystone symposium on lipid rafts and cell function. *J Lipid Res* 47:1597-1598.

164. Park, K. R., J. H. Lee, C. Choi, K. H. Liu, D. H. Seog, Y. H. Kim, D. E. Kim, C. H. Yun, and S. S. Yea. 2007. Suppression of interleukin-2 gene expression by isoeugenol is mediated through down-regulation of NF-AT and NF-kappaB. *Int Immunopharmacol* 7:1251-1258.

165. Fantini, M. C., and F. Pallone. 2008. Cytokines: from gut inflammation to colorectal cancer. *Curr Drug Targets* 9:375-380.

166. Katsiari, C. G., and G. C. Tsokos. 2006. Transcriptional repression of interleukin-2 in human systemic lupus erythematosus. *Autoimmun Rev* 5:118-121.

167. Quintana, A., C. Schwindling, A. S. Wenning, U. Becherer, J. Rettig, E. C. Schwarz, and M. Hoth. 2007. T cell activation requires mitochondrial translocation to the immunological synapse. *Proc Natl Acad Sci U S A* 104:14418-14423.

168. Lin, Y. G., A. B. Kunnumakkara, A. Nair, W. M. Merritt, L. Y. Han, G. N. Armaiz-Pena, A. A. Kamat, W. A. Spannuth, D. M. Gershenson, S. K. Lutgendorf, B. B. Aggarwal, and A. K. Sood. 2007. Curcumin inhibits tumor

growth and angiogenesis in ovarian carcinoma by targeting the nuclear factor-kappaB pathway. *Clin Cancer Res* 13:3423-3430.

169. Kunnumakkara, A. B., S. Guha, S. Krishnan, P. Diagaradjane, J. Gelovani, and B. B. Aggarwal. 2007. Curcumin potentiates antitumor activity of gemcitabine in an orthotopic model of pancreatic cancer through suppression of proliferation, angiogenesis, and inhibition of nuclear factor-kappaB-regulated gene products. *Cancer Res* 67:3853-3861.

170. Li, L., B. B. Aggarwal, S. Shishodia, J. Abbruzzese, and R. Kurzrock. 2004. Nuclear factor-kappaB and IkappaB kinase are constitutively active in human pancreatic cells, and their down-regulation by curcumin (diferuloylmethane) is associated with the suppression of proliferation and the induction of apoptosis. *Cancer* 101:2351-2362.

171. Manners, G. D., R. A. Jacob, A. P. Breksa, 3rd, T. K. Schoch, and S. Hasegawa. 2003. Bioavailability of citrus limonoids in humans. *Journal of agricultural and food chemistry* 51:4156-4161.

172. Sharma, R. A., S. A. Euden, S. L. Platton, D. N. Cooke, A. Shafayat, H. R. Hewitt, T. H. Marczylo, B. Morgan, D. Hemingway, S. M. Plummer, M. Pirmohamed, A. J. Gescher, and W. P. Steward. 2004. Phase I clinical trial of oral curcumin: biomarkers of systemic activity and compliance. *Clin Cancer Res* 10:6847-6854.

173. Jain, J., C. Loh, and A. Rao. 1995. Transcriptional regulation of the IL-2 gene. *Curr Opin Immunol* 7:333-342.

174. Calame, K. 2008. Activation-dependent induction of Blimp-1. *Curr Opin Immunol* 20:259-264.

175. Macian, F., C. Lopez-Rodriguez, and A. Rao. 2001. Partners in transcription: NFAT and AP-1. *Oncogene* 20:2476-2489.

176. Magnani, M., R. Crinelli, M. Bianchi, and A. Antonelli. 2000. The ubiquitin-dependent proteolytic system and other potential targets for the modulation of nuclear factor-kB (NF-kB). *Curr Drug Targets* 1:387-399.

177. Liou, H. C., Z. Jin, J. Tumang, S. Andjelic, K. A. Smith, and M. L. Liou. 1999. c-Rel is crucial for lymphocyte proliferation but dispensable for T cell effector function. *Int Immunol* 11:361-371.

178. Rao, S., S. Gerondakis, D. Woltring, and M. F. Shannon. 2003. c-Rel is required for chromatin remodeling across the IL-2 gene promoter. *J Immunol* 170:3724-3731.

179. Lederer, J. A., J. S. Liou, M. D. Todd, L. H. Glimcher, and A. H. Lichtman. 1994. Regulation of cytokine gene expression in T helper cell subsets. *J Immunol* 152:77-86.

180. Umlauf, S. W., B. Beverly, O. Lantz, and R. H. Schwartz. 1995. Regulation of interleukin 2 gene expression by CD28 costimulation in mouse T-cell clones: both nuclear and cytoplasmic RNAs are regulated with complex kinetics. *Mol Cell Biol* 15:3197-3205.

181. Fulcher, D., and S. Wong. 1999. Carboxyfluorescein succinimidyl ester-based proliferative assays for assessment of T cell function in the diagnostic laboratory. *Immunol Cell Biol* 77:559-564.

182. Hilchey, S. P., and S. H. Bernstein. 2007. Use of CFSE to monitor ex vivo regulatory T-cell suppression of CD4+ and CD8+ T-cell proliferation within unseparated mononuclear cells from malignant and non-malignant human lymph node biopsies. *Immunol Invest* 36:629-648.

183. Venken, K., M. Thewissen, N. Hellings, V. Somers, K. Hensen, J. L. Rummens, and P. Stinissen. 2007. A CFSE based assay for measuring CD4+CD25+ regulatory T cell mediated suppression of auto-antigen specific and polyclonal T cell responses. *J Immunol Methods* 322:1-11.

184. Haglund, O., R. Wallin, R. Luostarinen, and T. Saldeen. 1990. Effects of a new fluid fish oil concentrate, ESKIMO-3, on triglycerides, cholesterol, fibrinogen and blood pressure. *J Intern Med* 227:347-353.

185. Feagan, B. G., W. J. Sandborn, U. Mittmann, S. Bar-Meir, G. D'Haens, M. Bradette, A. Cohen, C. Dallaire, T. P. Ponich, J. W. McDonald, X. Hebuterne, P. Pare, P. Klvana, Y. Niv, S. Ardizzone, O. Alexeeva, A. Rostom, G. Kiudelis, J. Spleiss, D. Gilgen, M. K. Vandervoort, C. J. Wong, G. Y. Zou, A. Donner, and P. Rutgeerts. 2008. Omega-3 free fatty acids for the maintenance of remission in Crohn disease: the EPIC Randomized Controlled Trials. *JAMA* 299:1690-1697.

186. Logan, A. C. 2005. Omega-3, omega-6 and psoriasis: a different view. *Int J Dermatol* 44:527-528; author reply 528-529.

187. Rackal, J., and B. Barankin. 2004. The role of fish oils in psoriasis. *Skinmed* 3:290-291.

188. Terano, T., T. Kojima, A. Seya, E. Tanabe, A. Hirai, H. Makuta, A. Ozawa, T. Fujita, Y. Tamura, S. Okamoto, and et al. 1989. The effect of highly purified eicosapentaenoic acid in patients with psoriasis. *Adv Prostaglandin Thromboxane Leukot Res* 19:610-613.

189. Kim, Y. J., T. Yokozawa, and H. Y. Chung. 2005. Effects of energy restriction and fish oil supplementation on renal guanidino levels and antioxidant defences in aged lupus-prone B/W mice. *Br J Nutr* 93:835-844.

190. Weinstock-Guttman, B., M. Baier, Y. Park, J. Feichter, P. Lee-Kwen, E. Gallagher, J. Venkatraman, K. Meksawan, S. Deinehert, D. Pendergast, A. B. Awad, M. Ramanathan, F. Munschauer, and R. Rudick. 2005. Low fat dietary intervention with omega-3 fatty acid supplementation in multiple sclerosis patients. *Prostaglandins Leukot Essent Fatty Acids* 73:397-404.

191. Nordvik, I., K. M. Myhr, H. Nyland, and K. S. Bjerve. 2000. Effect of dietary advice and n-3 supplementation in newly diagnosed MS patients. *Acta Neurol Scand* 102:143-149.

192. 1990. Lipids and multiple sclerosis. *Lancet* 336:25-26.

193. Bates, D. 1990. Dietary lipids and multiple sclerosis. *Ups J Med Sci Suppl* 48:173-187.

APPENDIX A

SUPPLEMENT DATA

A-1. DO11.10 Genotyping Results

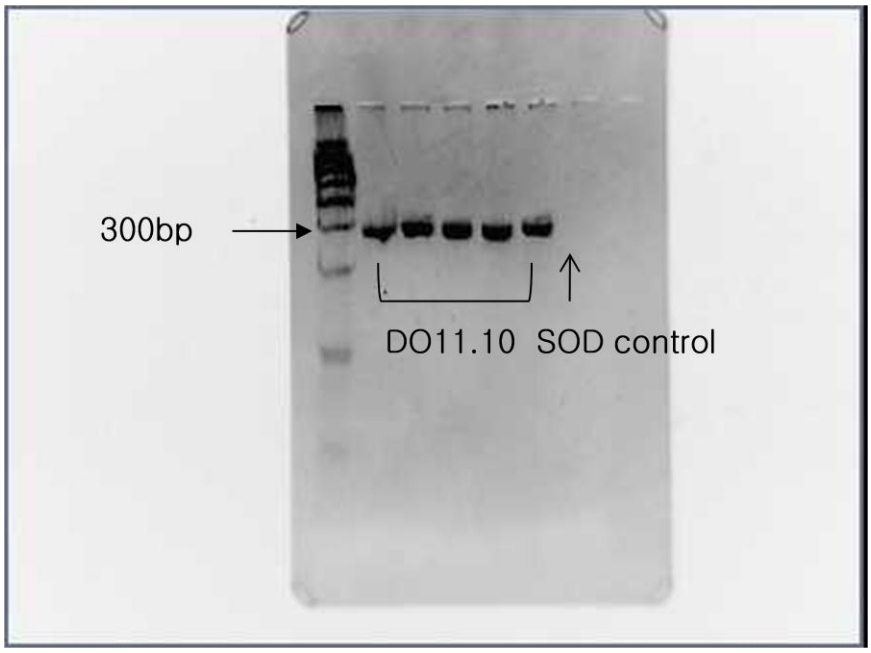

Objective: To test the genotype of DO11.10 breeders.

Methods: Detailed protocol is available in Appendix B-1.

Results: All five mice tested were identified as DO11.10 transgenic mice.

A-2. KJ1-26 staining controls

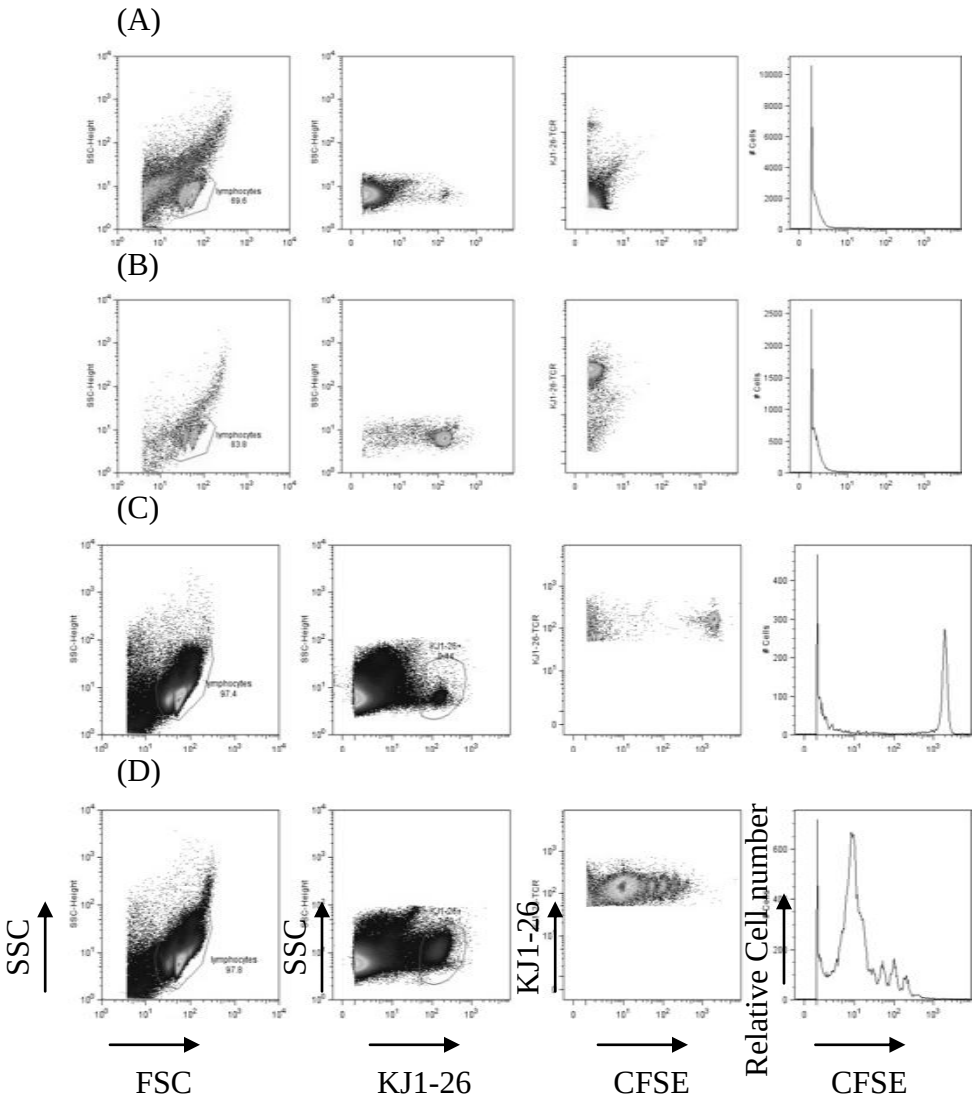

Objective: To test the DO11.10 specific staining of KJ1-26.

Methods: Single cell suspensions from lymph nodes of (A) KJ1-26 stained B10.D2 cells, (B) non-stained DO11.10 cells, (C) double stained DO11.10 cells without stimulation or (D) double stained DO11.10 cells with PMA/Ionomycin stimulation were analyzed by flow cytometry. Refer to Appendix B-2 for experimental details.

Results: KJ1-26 stains DO11.10 cells specifically (A vs B). In addition, KJ1-26 and CFSE are detected in different channels (B vs C).

A-3. Representative GC profiles of *Fat-1* phenotyping

(A) Representative chromatogram of a WT mouse

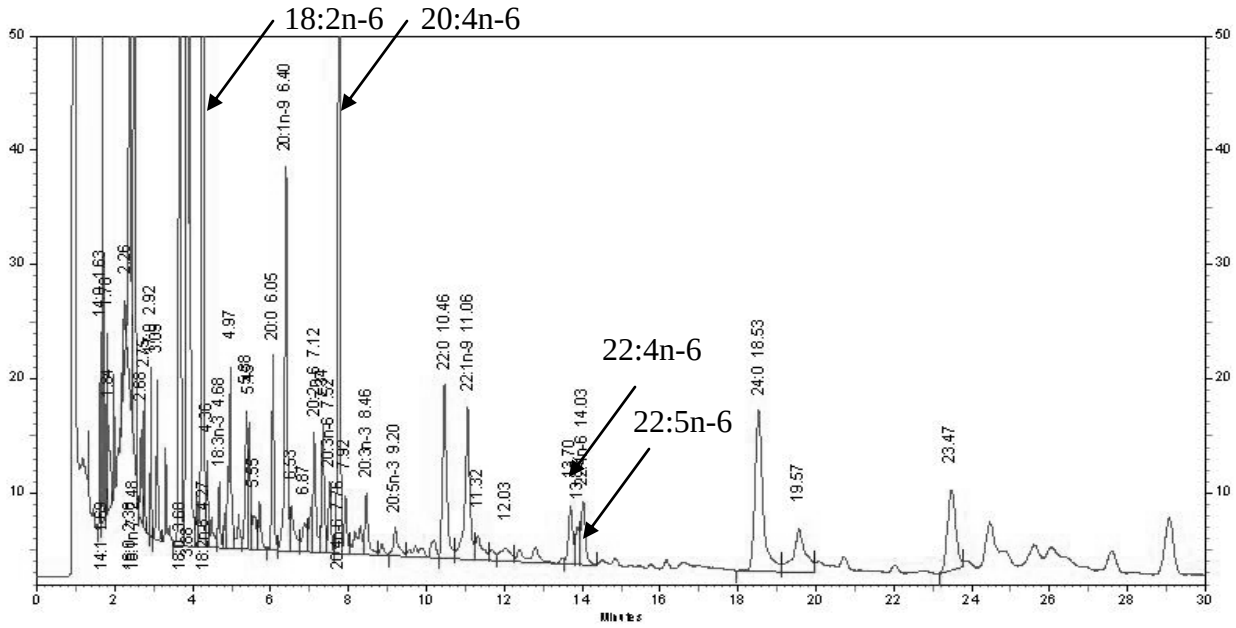

(B) Representative chromatogram of a *fat-1* mouse

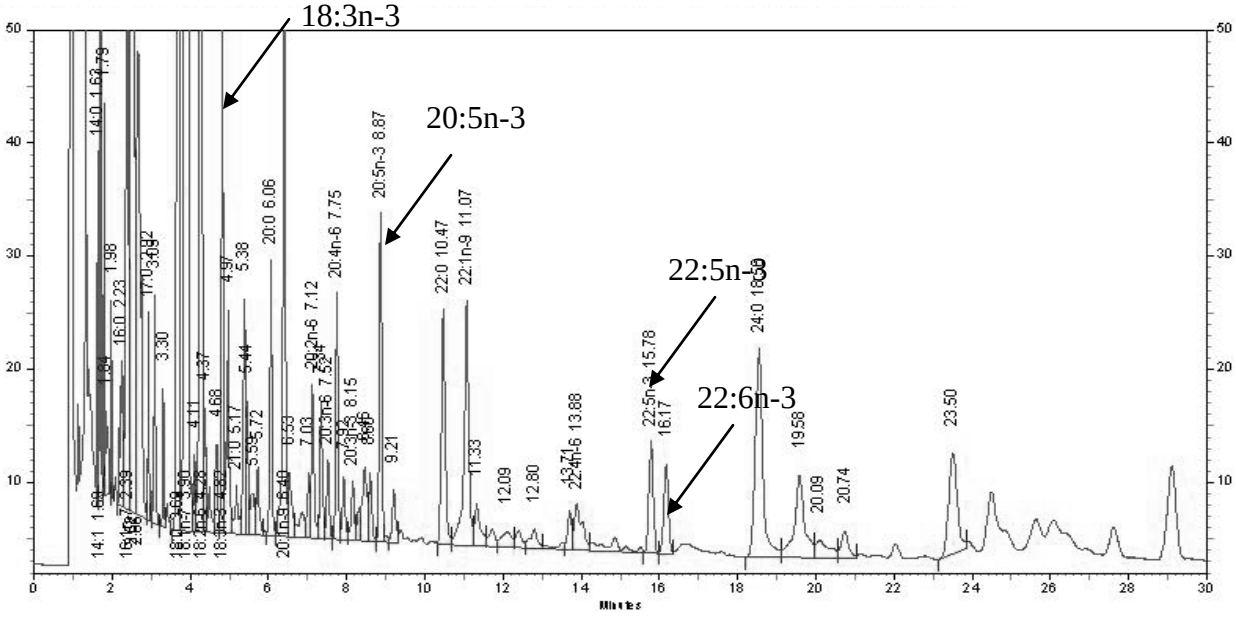

The protocol for *fat-1* phenotyping can be found in Appendix B-3.

(C) Examples of determining phenotypes by mol% of major tail snip fatty acids

ID	Sex	n-6 (mol%)					n-3 (mol%)					n-6:n-3 ratio*	Phenotype**
		18:2	20:4	22:4	22:5	Total n-6	18:3	20:5	22:5	22:6	Total n-3		
835	F	19.7	1.2	0.4	0.3	21.6	2.1	1.7	1.2	1.3	6.3	3.4	*Fat-1*
839	F	19.0	1.2	0.6	0.4	21.2	1.7	1.6	1.5	1.1	5.9	3.6	*Fat-1*
841	F	19.2	1.7	0.7	0.6	22.2	1.5	1.5	1.4	1.3	5.7	3.9	*Fat-1*
847	F	11.8	1.2	0	0	13.0	2.7	1.8	1.6	1.6	7.7	1.7	*Fat-1*
822	M	15.8	6.6	1.5	1.3	25.2	0.0	0.0	0.0	0.0	0.0		WT
830	M	13.7	6.1	1.6	1.2	22.6	0.0	0.0	0.0	0.0	0.0		WT
820	F	17.3	1.3	1.0	0.6	20.2	1.7	1.8	1.3	1.0	5.8	3.5	*Fat-1*
833	F	16.2	1.2	0.6	0.0	18.0	2.5	1.3	1.2	1.7	6.7	2.7	*Fat-1*
843	F	19.9	1.1	0.5	0.4	21.9	1.6	1.5	1.1	1.1	5.3	4.1	*Fat-1*
844	F	13.8	2.6	0	0	16.4	2.2	1.8	1.8	1.4	7.2	2.3	*Fat-1*
818	M	19.6	1.2	0.6	0.4	21.8	1.3	1.4	1.1	1.0	4.8	4.5	*Fat-1*
829	M	15.8	1.5	0.4	0.0	17.7	1.8	1.2	1.1	1.3	5.4	3.3	*Fat-1*
832	M	16.3	1.3	0.5	0.0	18.1	2.1	1.1	1.0	1.2	5.4	3.4	*Fat-1*
836	M	9.7	0.6	0.3	0.2	10.8	1.1	0.9	0.9	0.6	3.5	3.1	*Fat-1*
837	M	18.9	1.5	0.5	0.4	21.3	1.4	1.4	1.5	1.3	5.6	3.8	*Fat-1*
838	M	17.8	1.7	0.5	0.4	20.4	1.7	3.5	1.6	1.2	8.0	2.6	*Fat-1*
845	M	12.6	1.3	0.6	0	14.5	2.7	2.3	1.6	1.4	8.0	1.8	*Fat-1*
846	M	11.3	0	0.7	0.2	12.2	3.3	2.6	1.8	1.5	9.2	1.3	*Fat-1*
819	F	19.1	5.4	1.5	1.2	27.2	0.2	0.0	0.0	0.0	0.2	136.0	WT
826	F	18.7	0.6	1.5	1.3	22.1	0.5	0.0	0.0	0.3	0.8	27.6	WT
828	F	22.1	6.3	1.3	1.0	30.7	0.3	0.0	0.0	0.3	0.6	51.2	WT
840	F	20.2	5.6	1.4	1.3	28.5	0.2	0.0	0.0	0.0	0.2	142.5	WT
848	F	18.3	6.8	1.6	1.7	28.4	0	0	0	0	0.0		WT
825	M	16.2	5.9	1.5	1.2	24.8	0.3	0.0	0.0	0.3	0.6	41.3	WT
821	F	25.4	1.4	0.7	0.5	28.0	0.8	1.0	0.8	0.6	3.2	8.8	*Fat-1*
827	F	16.2	1.1	0.5	0.0	17.8	1.9	1.4	1.2	1.6	6.1	2.9	*Fat-1*
834	F	20.1	0.7	0.5	0.0	21.3	2.1	0.9	0.8	1.1	4.9	4.3	*Fat-1*
823	M	8.5	0.6	0.9	0.0	10.0	3.2	2.0	1.5	2.0	8.7	1.1	*Fat-1*
824	M	12.8	1.8	0.7	0.4	15.7	1.8	1.4	1.2	1.3	5.7	2.8	*Fat-1*

* Examplary calculation of n-6/n-3 ratio: 21.6 / 6.3 = 3.4 (Mouse ID 835)

** Phenotype is determined by n-6/n-3 ratio. Generally, n-6/n-3> 10 were identified as WT, whereas n-6/n-3 < 10 were classified as *fat-1*.

A-4. Representative RT-PCR plots of *Fat-1* genotyping

(A) Representative amplification plot of *fat-1* genotyping

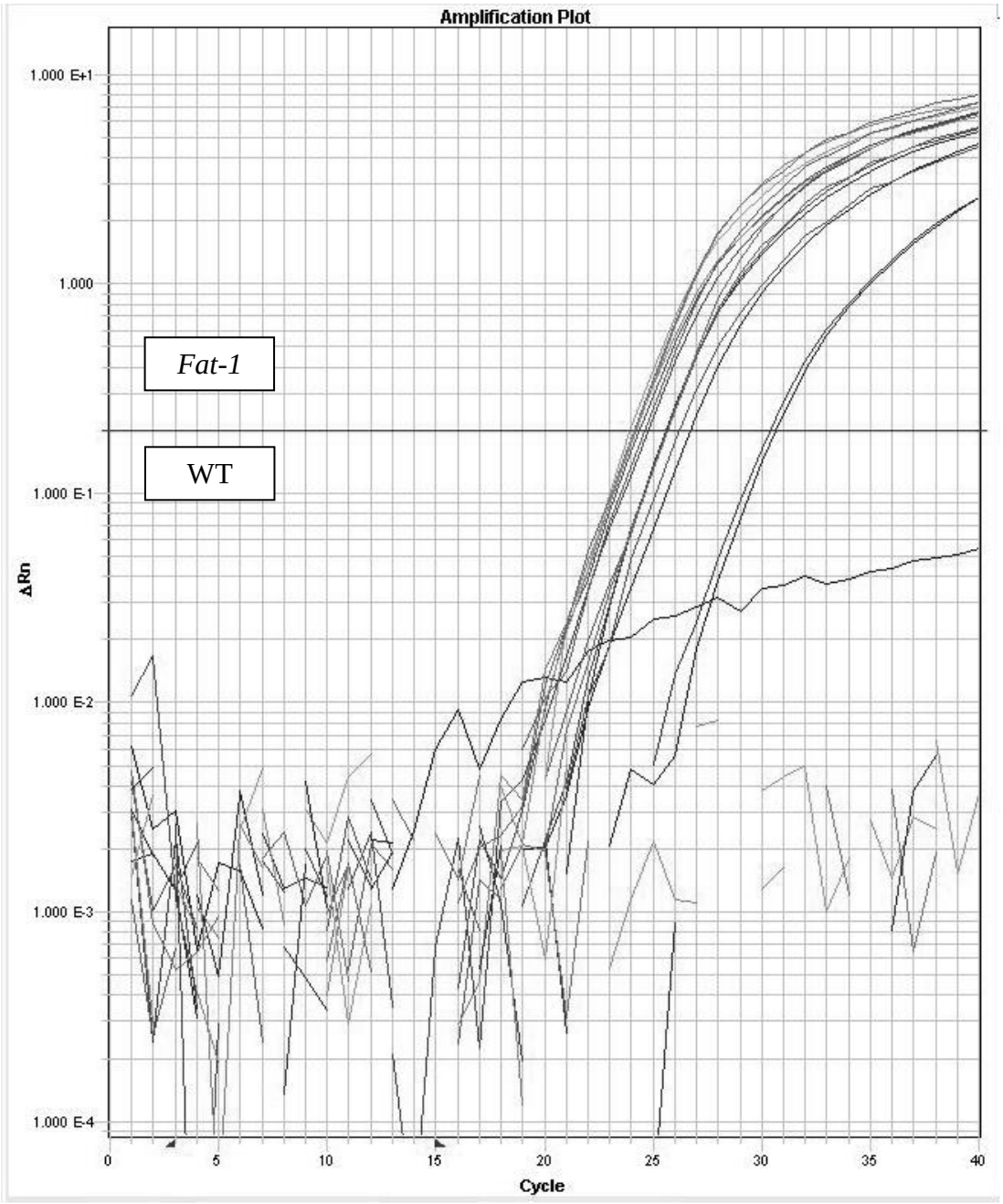

The detailed protocol of fat-1 genotyping can be found in Appendix B-4.

(B) CT values

ID	Sex	Ct (min)*	Genotype
835	F	25.814	*Fat-1*
839	F	25.519	*Fat-1*
841	F	24.200	*Fat-1*
847	F	23.966	*Fat-1*
822	M	38.180	WT
830	M	-	WT
820	F	23.491	*Fat-1*
833	F	26.199	*Fat-1*
843	F	24.550	*Fat-1*
844	F	26.330	*Fat-1*
818	M	23.931	*Fat-1*
829	M	33.698	*Fat-1*
832	M	26.494	*Fat-1*
836	M	27.693	*Fat-1*
837	M	25.153	*Fat-1*
838	M	26.719	*Fat-1*
845	M	22.910	*Fat-1*
846	M	23.854	*Fat-1*
819	F	-	WT
826	F	-	WT
828	F	-	WT
840	F	39.315	WT
848	F	35.729	WT
825	M	-	WT
831	M	36.570	WT
815			WT
816			WT
821	F	34.798	*Fat-1*
827	F	32.998	*Fat-1*
834	F	28.700	*Fat-1*
842	F	25.835	*Fat-1*
823	M	29.992	*Fat-1*
824	M	27.640	*Fat-1*

*In general, mice with Ct<30.000 min were classified as *Fat-1*.

A-5. Examples of GP-value calculation

The detailed protocol can be found in Appendix B-8.

A) Animal ID: 730W

IS			Contact whole cell			Non-contact whole cell		
I_{Blue}	I_{Green}	GP-value	I_{Blue}	I_{Green}	GP-value	I_{Blue}	I_{Green}	GP-value
205.89	107.48	0.31	172.10	104.86	0.24	193.46	140.44	0.16
Ex) (205.89-107.48) =0.31			212.85	149.02	0.18	231.25	166.58	0.16
(205.89+107.48)			213.35	156.37	0.15	198.51	141.94	0.17
211.53	107.84	0.32	157.78	81.92	0.32	223.29	159.90	0.17
240.93	127.06	0.31	158.71	82.52	0.32	195.39	132.65	0.19
177.72	59.56	0.50	183.08	122.51	0.20	186.15	116.11	0.23
168.14	94.74	0.28	200.68	136.23	0.19	182.58	125.51	0.19
235.22	134.63	0.27	191.54	117.14	0.24	186.19	130.28	0.18
225.80	124.22	0.29	162.55	99.04	0.24	194.30	133.93	0.18
218.85	112.44	0.32	190.58	110.59	0.27	191.54	138.68	0.16
233.16	116.52	0.33	177.23	113.63	0.22	189.02	120.28	0.22
224.20	120.02	0.30	164.79	94.51	0.27	211.60	176.78	0.09
213.68	123.52	0.27	182.00	125.21	0.18	188.91	115.67	0.24
241.68	144.41	0.25	182.79	122.86	0.20	202.74	141.64	0.18
212.40	97.74	0.37	173.73	115.03	0.20	200.09	139.12	0.18
244.27	101.93	0.41	201.83	131.76	0.21	207.31	153.61	0.15
218.98	122.83	0.28	200.51	126.87	0.22	205.56	145.09	0.17
183.43	90.99	0.34	179.62	130.63	0.16	180.95	115.27	0.22
181.98	87.57	0.35	189.30	133.59	0.17	214.76	150.62	0.18
207.66	112.49	0.30	177.73	120.91	0.19	203.60	134.70	0.20
189.74	86.16	0.38				195.13	142.63	0.16
234.90	110.56	0.36				196.95	138.54	0.17

B) Animal ID: 705F

IS			Contact whole cell			Non-contact whole cell		
I_{Blue}	I_{Green}	GP-value	I_{Blue}	I_{Green}	GP-value	I_{Blue}	I_{Green}	GP-value
89.93	40.37	0.38	82.50	35.40	0.40	85.14	36.12	0.40
169.01	51.45	0.53	96.05	38.88	0.42	70.39	24.49	0.48
100.59	50.02	0.34	83.84	36.34	0.40	83.23	30.22	0.47
169.49	82.83	0.34	73.63	29.32	0.43	82.57	29.86	0.47
65.24	17.83	0.57	58.55	19.17	0.51	79.57	33.02	0.41

56.54	25.53	0.38	61.60	24.38	0.43	56.80	22.05	0.44
133.69	35.23	0.58	83.76	30.00	0.47	93.39	34.47	0.46
171.27	43.87	0.59	73.68	29.48	0.43	110.63	42.85	0.44
109.11	41.49	0.45	50.67	19.36	0.45	79.22	30.92	0.44
154.13	52.45	0.49	74.76	28.73	0.44	65.10	21.60	0.50
124.75	26.99	0.64	52.63	18.72	0.48	53.85	25.91	0.35
137.26	41.25	0.54	55.24	21.03	0.45	68.24	26.51	0.44
122.38	28.33	0.62	62.08	22.70	0.46	82.49	31.96	0.44
74.12	23.49	0.52	47.74	14.60	0.53	77.60	28.70	0.46
						91.91	35.36	0.44
						76.15	27.79	0.47

A-6. Calculation of % patching of signaling proteins

Protein	Phenotype	# patching	# nonpatching	# total	% patching	SEM	p-value
F-actin	*Fat-1*	35	66	101	34.653	4.735	0.020
			Ex) 35 / 101 × 100 = 34.653 %				
	WT	20	17	37	54.054	8.193	
LAT	*Fat-1*	27	47	74	36.486	5.596	0.193
	WT	23	29	52	44.231	6.887	
p-LAT	*Fat-1*	19	26	45	42.222	7.363	0.464
	WT	16	21	37	43.243	8.145	
PLCg1	*Fat-1*	24	68	92	26.087	4.578	0.081
	WT	16	26	42	38.095	7.493	
p-PLCg1	*Fat-1*	27	32	59	45.763	6.486	0.034
	WT	27	15	42	64.286	7.394	
CARMA1	*Fat-1*	17	32	49	34.694	6.800	0.399
	WT	25	52	77	32.468	5.336	
PKCθ	*Fat-1*	28	71	99	28.283	4.526	0.055
	WT	24	35	59	40.678	6.395	

The details of the microscope setting are described in Materials and Methods of Chapter III.

A-7. GM1 relative relocaliztion index (RRI) calculation

Mouse ID	Genotype	Intensity at synapse	Intensity in whole cell	RRI	Mouse ID	Genotype	Intensity at synapse	Intensity in whole cell	RRI
818F	*Fat-1*	99.97	45.99	2.173733	838F	*Fat-1*	37.68	43.78	0.860667
		Ex) 99.97 / 45.99 = 2.173733			828W	WT	61.29	52.59	1.165431
818F	*Fat-1*	74.83	76.42	0.979194	828W	WT	43.86	36.8	1.191848
818F	*Fat-1*	33.89	35.42	0.956804	828W	WT	74.74	39.33	1.900331
818F	*Fat-1*	71.03	46.91	1.514176	828W	WT	48.53	32.33	1.501083
818F	*Fat-1*	86.16	55.32	1.557484	828W	WT	74.06	34.4	2.152907
818F	*Fat-1*	79.93	63.49	1.258938	828W	WT	32.14	32.79	0.980177
818F	*Fat-1*	75.22	38.15	1.971691	828W	WT	56.49	51.91	1.08823
818F	*Fat-1*	94.46	62.3	1.516212	828W	WT	47.06	37.06	1.269833
818F	*Fat-1*	52.73	35.77	1.47414	828W	WT	56.15	42.47	1.32211
818F	*Fat-1*	70.57	65.87	1.071353	828W	WT	68.14	46.26	1.472979
818F	*Fat-1*	58.71	57.74	1.016799	828W	WT	68.5	56.8	1.205986
818F	*Fat-1*	116.86	54.15	2.158079	828W	WT	31.36	51.44	0.609642
818F	*Fat-1*	83.65	52.33	1.598509	848W	WT	50.3	27.51	1.828426
838F	*Fat-1*	55.37	23.87	2.319648	848W	WT	45.33	31.54	1.437223
838F	*Fat-1*	45.91	27.57	1.665216	848W	WT	36.05	26.46	1.362434
838F	*Fat-1*	27.59	24.32	1.134457	848W	WT	50.77	36.71	1.383002
838F	*Fat-1*	34.9	20.41	1.709946	848W	WT	61.83	30.37	2.035891
838F	*Fat-1*	37.32	21.74	1.716651	848W	WT	47.13	29.77	1.583137
838F	*Fat-1*	45.99	24.68	1.863452	848W	WT	56.54	30.52	1.852556
838F	*Fat-1*	53.64	28.42	1.887403	848W	WT	50.1	29.24	1.713406
838F	*Fat-1*	53.32	25.74	2.071484	848W	WT	151.06	65.82	2.295047
838F	*Fat-1*	47.51	27.47	1.729523	848W	WT	116.86	58.99	1.981014
838F	*Fat-1*	84.31	34.28	2.459452	848W	WT	145.9	59.8	2.439799
838F	*Fat-1*	127.85	69.06	1.851289	848W	WT	134.82	52.18	2.583749
838F	*Fat-1*	41.15	36.98	1.112764	848W	WT	88.92	46.66	1.905701
838F	*Fat-1*	63.4	37.01	1.713051	848W	WT	94.43	52	1.815962
838F	*Fat-1*	65.71	45.46	1.445447	848W	WT	83.82	68.16	1.229754
838F	*Fat-1*	103.93	75.43	1.377834	848W	WT	109.86	52.2	2.104598
838F	*Fat-1*	133.43	76.07	1.754042	848W	WT	123.12	68.09	1.808195
838F	*Fat-1*	91.79	62.55	1.467466	848W	WT	91.51	52.04	1.758455
838F	*Fat-1*	185.76	102.41	1.813885	848W	WT	103.91	53.96	1.925686

A-8. Analysis of CFSE profiles using ModFit^{LT}

Animal ID	Phenotype	Stimulation	% of cells Gen1	Gen2	Gen3	Gen4	Gen5	Gen6	Gen7	Gen8	Sum
843F	*Fat-1*	anti-CD3/28	26.53	11.13	21.64	23.23	14.24	3.07	0.15	0.00	99.99
843F	*Fat-1*	anti-CD3/28	31.00	11.66	20.41	21.13	13.34	2.35	0.10	0.00	99.99
844F	*Fat-1*	anti-CD3/28	17.93	11.09	21.39	29.35	16.42	3.39	0.42	0.00	99.99
844F	*Fat-1*	anti-CD3/28	26.56	11.68	20.58	24.48	13.79	2.43	0.48	0.00	100.00
845F	*Fat-1*	anti-CD3/28	19.45	5.96	9.42	16.62	25.51	17.47	4.65	0.92	100.00
845F	*Fat-1*	anti-CD3/28	21.71	8.23	10.54	17.51	23.13	14.83	3.95	0.09	99.99
846F	*Fat-1*	anti-CD3/28	39.05	6.44	10.41	14.68	16.74	9.11	3.12	0.43	99.98
846F	*Fat-1*	anti-CD3/28	37.69	6.44	10.02	15.27	16.88	10.23	3.41	0.07	100.01
829F	*Fat-1*	anti-CD3/28	48.72	6.49	10.25	13.40	14.22	6.66	0.26	0.00	100.00
829F	*Fat-1*	anti-CD3/28	52.60	7.25	9.28	12.11	12.37	5.67	0.58	0.15	100.01
832F	*Fat-1*	anti-CD3/28	46.04	6.53	10.93	14.47	14.64	6.79	0.60	0.00	100.00
832F	*Fat-1*	anti-CD3/28	54.52	6.40	8.84	11.37	11.97	6.21	0.69	0.00	100.00
Mean			35.15	8.28	13.64	17.80	16.10	7.35	1.53	0.14	100.00
SEM			3.79	0.63	1.45	1.48	1.11	1.29	0.45	0.07	0.00
825W	WT	anti-CD3/28	21.42	12.23	25.16	27.30	12.77	1.09	0.00	0.00	99.97
825W	WT	anti-CD3/28	18.47	12.24	25.26	28.96	13.38	1.51	0.18	0.00	100.00
840W	WT	anti-CD3/28	22.63	9.17	18.77	26.01	18.82	4.16	0.43	0.00	99.99
840W	WT	anti-CD3/28	27.60	10.27	18.98	24.90	17.03	1.22	0.00	0.00	100.00
815W	WT	anti-CD3/28	24.36	8.90	14.76	22.62	19.75	7.39	2.09	0.10	99.97
815W	WT	anti-CD3/28	23.70	10.92	16.33	20.77	19.47	6.93	1.79	0.10	100.01
816W	WT	anti-CD3/28	23.14	11.27	15.17	20.34	19.15	8.41	2.52	0.00	100.00
816W	WT	anti-CD3/28	27.53	12.13	15.79	19.00	16.59	6.92	1.67	0.37	100.00
819W	WT	anti-CD3/28	37.29	6.91	10.81	14.55	16.55	10.62	3.09	0.17	99.99
831W	WT	anti-CD3/28	45.24	6.68	10.29	14.90	14.65	6.96	1.29	0.00	100.01
831W	WT	anti-CD3/28	52.40	6.00	9.16	11.94	12.31	6.39	1.76	0.04	100.00
Mean			29.43	9.70	16.41	21.03	16.41	5.60	1.35	0.07	99.99
SEM			3.27	0.70	1.63	1.68	0.83	0.96	0.32	0.03	0.00
843F	*Fat-1*	Hybridoma	66.49	16.29	10.71	5.12	1.11	0.28	0.00	0.00	100.00
843F	*Fat-1*	Hybridoma	56.27	20.08	13.12	6.87	3.30	0.36	0.00	0.00	100.00
844F	*Fat-1*	Hybridoma	60.32	17.14	12.86	6.49	3.19	0.00	0.00	0.00	100.00
844F	*Fat-1*	Hybridoma	56.40	18.51	13.53	7.71	3.20	0.65	0.00	0.00	100.00
845F	*Fat-1*	Hybridoma	19.44	21.53	23.99	23.82	9.09	2.02	0.11	0.00	100.00
845F	*Fat-1*	Hybridoma	17.64	22.72	25.55	22.83	8.86	1.78	0.63	0.00	100.01

846F	*Fat-1*	Hybridoma	16.15	20.01	24.84	24.25	11.74	2.63	0.39	0.00	100.01
846F	*Fat-1*	Hybridoma	17.30	20.35	25.75	23.09	10.62	2.37	0.53	0.00	100.01
829F	*Fat-1*	Hybridoma	50.76	29.66	13.07	4.17	1.80	0.45	0.08	0.00	99.99
829F	*Fat-1*	Hybridoma	50.77	27.52	9.81	6.14	4.27	1.21	0.30	0.00	100.02
832F	*Fat-1*	Hybridoma	40.51	29.91	21.36	5.99	1.81	0.38	0.05	0.00	100.01
832F	*Fat-1*	Hybridoma	40.86	31.08	21.15	5.01	1.21	0.60	0.09	0.00	100.00
Mean			41.08	22.90	17.98	11.79	5.02	1.06	0.18	0.00	100.00
SEM			5.42	1.52	1.82	2.51	1.13	0.26	0.06	0.00	0.00
825W	WT	Hybridoma	75.44	13.18	7.15	2.45	1.65	0.13	0.00	0.00	100.00
825W	WT	Hybridoma	82.42	9.49	1.83	4.67	1.59	0.00	0.00	0.00	100.00
840W	WT	Hybridoma	57.04	20.93	6.12	6.57	6.76	2.58	0.00	0.00	100.00
840W	WT	Hybridoma	49.81	20.52	1.15	13.61	10.55	4.35	0.00	0.00	99.99
815W	WT	Hybridoma	26.86	23.26	23.54	17.52	7.03	1.63	0.15	0.00	99.99
815W	WT	Hybridoma	24.99	25.61	23.21	18.03	6.54	1.34	0.28	0.00	100.00
816W	WT	Hybridoma	27.51	23.23	21.70	16.97	7.66	2.40	0.53	0.00	100.00
816W	WT	Hybridoma	30.21	24.22	22.24	15.23	5.89	1.74	0.47	0.00	100.00
819W	WT	Hybridoma	40.85	29.82	20.19	6.03	1.96	0.84	0.30	0.00	99.99
831W	WT	Hybridoma	47.34	28.36	17.47	4.60	1.59	0.51	0.14	0.00	100.01
831W	WT	Hybridoma	43.12	30.91	17.97	5.86	1.77	0.35	0.04	0.00	100.02
Mean			45.96	22.68	14.78	10.14	4.82	1.44	0.17	0.00	100.00
SEM			5.85	1.99	2.67	1.83	0.96	0.39	0.06	0.00	0.00
843F	*Fat-1*	PMA/Iono	2.60	8.35	33.65	40.88	13.65	0.88	0.00	0.00	100.01
844F	*Fat-1*	PMA/Iono	1.29	7.91	33.55	42.83	13.29	0.94	0.18	0.00	99.99
845F	*Fat-1*	PMA/Iono	1.35	6.16	16.94	32.77	32.75	8.98	1.05	0.00	100.00
846F	*Fat-1*	PMA/Iono	1.45	5.24	16.49	35.22	32.80	7.88	0.91	0.00	99.99
829F	*Fat-1*	PMA/Iono	1.81	5.59	16.19	33.60	31.33	9.73	1.75	0.00	100.00
829F	*Fat-1*	PMA/Iono	1.80	5.27	15.78	34.04	31.18	10.08	1.85	0.00	100.00
832F	*Fat-1*	PMA/Iono	2.22	6.98	19.47	35.04	27.34	7.94	1.02	0.00	100.01
832F	*Fat-1*	PMA/Iono	2.21	7.72	20.84	34.22	26.51	8.02	0.47	0.00	99.99
Mean			1.84	6.65	21.61	36.08	26.11	6.81	0.90	0.00	100.00
SEM			0.17	0.44	2.69	1.30	2.88	1.32	0.24	0.00	0.00
825W	WT	PMA/Iono	1.97	6.92	29.85	47.05	13.29	0.93	0.00	0.00	100.01
840W	WT	PMA/Iono	2.02	7.66	29.38	47.04	2.44	11.46	0.00	0.00	100.00
815W	WT	PMA/Iono	0.84	4.69	19.20	39.67	27.69	6.83	1.07	0.00	99.99
816W	WT	PMA/Iono	1.44	5.82	21.37	40.20	24.25	6.40	0.52	0.00	100.00
819W	WT	PMA/Iono	1.62	5.58	19.10	32.23	29.18	9.89	1.40	0.00	99.00
831W	WT	PMA/Iono	2.28	7.98	22.82	35.87	24.22	6.20	0.63	0.00	100.00
831W	WT	PMA/Iono	2.65	8.64	24.66	34.67	22.38	6.15	0.85	0.00	100.00
Mean			1.83	6.76	23.77	39.53	20.49	6.84	0.64	0.00	99.86
SEM			0.22	0.54	1.68	2.20	3.57	1.26	0.20	0.00	0.14

A-9. Calculation of proliferation index using [^{3}H]-thymidine labeling

Animal ID	Pheno type	Stimulation	DPM	Proliferation index	Animal ID	Pheno type	Stimulation	DPM	Proliferation index
820F	*Fat-1*	Basal	300.89		837F	Fat-1	Basal	437.08	
820F	*Fat-1*	Basal	333.98		837F	Fat-1	Basal	528.47	
820F	*Fat-1*	anti-CD3/28	22940.86	72.27	837F	Fat-1	anti-CD3/28	17075.63	35.37
		Ex) 22940.86 / [(300.89+333.98)/2] = 72.27			837F	Fat-1	anti-CD3/28	17263.07	35.76
820F	*Fat-1*	anti-CD3/28	23364.47	73.60	837F	Fat-1	Hybridoma	924.66	1.92
820F	*Fat-1*	Hybridoma	1333.45	4.20	837F	Fat-1	Hybridoma	992.24	2.06
820F	*Fat-1*	Hybridoma	1380.92	4.35	837F	Fat-1	PMA/Iono	28419.30	58.87
820F	*Fat-1*	PMA/Iono	32469.71	102.29	837F	Fat-1	PMA/Iono	35842.43	74.24
820F	*Fat-1*	PMA/Iono	33314.80	104.95					
836F	*Fat-1*	Basal	452.23		671W	WT	Basal	254.12	
836F	*Fat-1*	Basal	281.70		671W	WT	Basal	269.56	
836F	*Fat-1*	anti-CD3/28	16431.50	44.78	671W	WT	anti-CD3/28	19185.40	73.27
836F	*Fat-1*	anti-CD3/28	17455.79	47.57	671W	WT	anti-CD3/28	19315.09	73.77
836F	*Fat-1*	Hybridoma	826.34	2.25	671W	WT	Hybridoma	1290.44	4.93
836F	*Fat-1*	Hybridoma	689.81	1.88	671W	WT	Hybridoma	1082.17	4.13
836F	*Fat-1*	PMA/Iono	28658.36	78.10	671W	WT	PMA/Iono	28383.79	108.40
836F	*Fat-1*	PMA/Iono	28043.95	76.42	671W	WT	PMA/Iono	32508.94	124.16
826W	WT	Basal	180.96		614F	Fat-1	Basal	409.99	
826W	WT	Basal	327.74		614F	Fat-1	Basal	573.26	
826W	WT	anti-CD3/28	14433.01	56.74	614F	Fat-1	anti-CD3/28	10166.86	20.68
826W	WT	anti-CD3/28	14907.45	58.61	614F	Fat-1	anti-CD3/28	14552.08	29.60
826W	WT	Hybridoma	1297.22	5.10	614F	Fat-1	Hybridoma	681.57	1.39
826W	WT	Hybridoma	1194.43	4.70	614F	Fat-1	Hybridoma	712.15	1.45
826W	WT	PMA/Iono	34598.12	136.03	614F	Fat-1	PMA/Iono	25079.85	51.01
826W	WT	PMA/Iono	30501.95	119.92	614F	Fat-1	PMA/Iono	29053.75	59.10
821F	*Fat-1*	Basal	366.18		671W	WT	Basal	75.49	
821F	*Fat-1*	Basal	443.66		671W	WT	Basal	175.88	
821F	*Fat-1*	anti-CD3/28	11501.18	28.40	671W	WT	anti-CD3/28	11928.80	94.91
821F	*Fat-1*	anti-CD3/28	11890.73	29.37	671W	WT	anti-CD3/28	12752.29	101.46
821F	*Fat-1*	Hybridoma	1109.09	2.74	671W	WT	Hybridoma	871.90	6.94
821F	*Fat-1*	Hybridoma	1337.15	3.30	671W	WT	Hybridoma	805.28	6.41
821F	*Fat-1*	PMA/Iono	28729.87	70.95	671W	WT	PMA/Iono	31679.00	252.05
821F	*Fat-1*	PMA/Iono	29416.13	72.65	671W	WT	PMA/Iono	34437.94	274.00

A-10. Mouse body weight change during curcumin and limonin diet feeding

(g/mouse, mean±SEM)

	Initial	after 1wk control CO diet	after 2wk experimental diets
CO* (n=4)	23.5±1.7	23.6±1.6	24.6±1.4
CC (n=5)	23.0±1.6	22.9±1.8	23.9±1.4
CL (n=5)	22.5±1.5	22.5±1.7	23.6±1.7
FO (n=5)	21.8±1.3	22.0±1.7	22.7±1.8
FC (n=5)	21.2±0.8	20.4±0.8	21.8±0.8
FL (n=5)	21.1±1.9	21.4±1.9	23.0±1.6

*CO, corn oil; CC, corn oil+curcumin; CL, corn oil+limonin, FO, fish oil; FC, fish oil+curcumin, FL, fish oil+limonin

Conclusion: Mouse body weight gain was not statiscally (P>0.05) altered by experimental diet feeding.

A-11. Comparison of $CD4^+$ T cell isolation kits (Miltenyi vs R&D sytems)

($x10^6$ cells*/mouse, mean±SEM)

	Miltenyi**		R&D systems
	After column	After CFSE staining	After column
DO11.10	5.11±0.90 (n=4)	2.19±0.33 (n=4)	0.44±0.215 (n=2)
Balb/C	15.34 (n=1)	10.07 (n=1)	2.71 (n=1)

* Viable $CD4^+$ T cells were counted by Trypan Blue exclusion method using hemacytometer (Appendix B-2, Section I.5)

** Detailed procedures of $CD4^+$ T cell isolation using either R&D Systems or Miltenyi are described in Appendices B-2 and B-5, respectively.

A-12. Purity of $CD4^+$ T cells isolated using Miltenyi system

$CD4^+$ T cell purity (C57BL/6, analyzed by BD FACSCalibur)

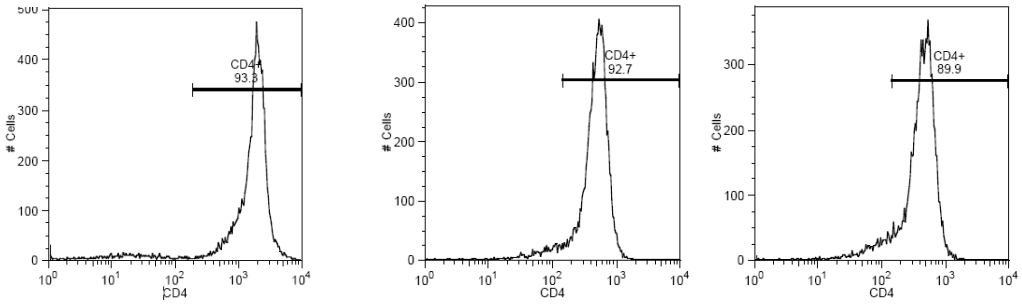

Methods: $CD4^+$ T cells were isolated as described in Appendix B-5. Purified cells were stained with 1 µg/ml rat anti-mouse CD4-FITC (Invitrogen, cat# MCD0401) at the cell density of 1×10^7 cells/ml.

Resultis: $CD4^+$ T cell purity = 91.97 ± 1.05 % (n=3)

A-13. Optimization of antigenic stimulation of DO11.10 $CD4^+$ T cells

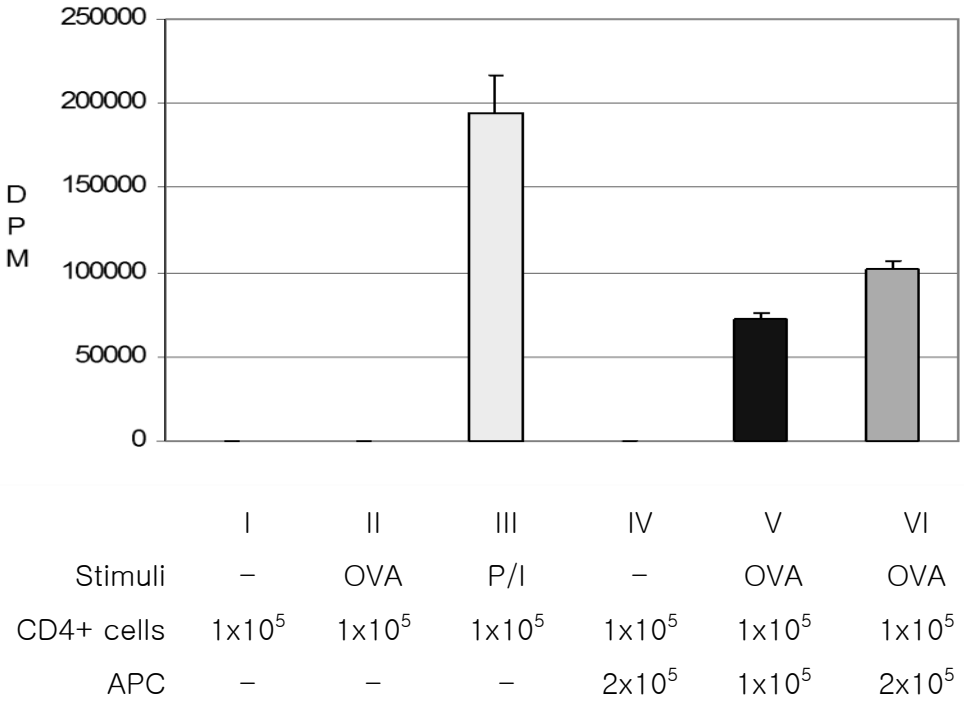

Objective: To set the optimum cell concentrations for antigenic DO11.10 $CD4^+$ T cell proliferation.

Methods: Purified $CD4^+$ T cells were purified by Miltenyi beads (refer to Appendix B-5 for details). APC were prepared from Balb/C spleens by lympholyte-M. Cells were co-cultured in total 200µl complete RPMI medium in 96-well plates at different concentrations as indicated, in the presence of OVA peptide for 72 h at 37°C. (The detailed protocol for APC preparation and OVA stimulation can be found in Appendix B-10). For the last 6 h of culture, cells were pulsed with 4 µCi [^{3}H]-thymidine/well. Following culture, cells were harvested and thymidine uptake was counted using liquid scintilation.

Results: $1x10^5$ $CD4^+$ T cell and $2x10^5$ $CD4^+$ T cell exhibited the maximal stimulation. We decided to use $2.5x10^5$ $CD4^+$ T cells in future studies.

A-14. Test to evaluate the effect of CFSE labeling on $CD4^+$ T cell proliferation

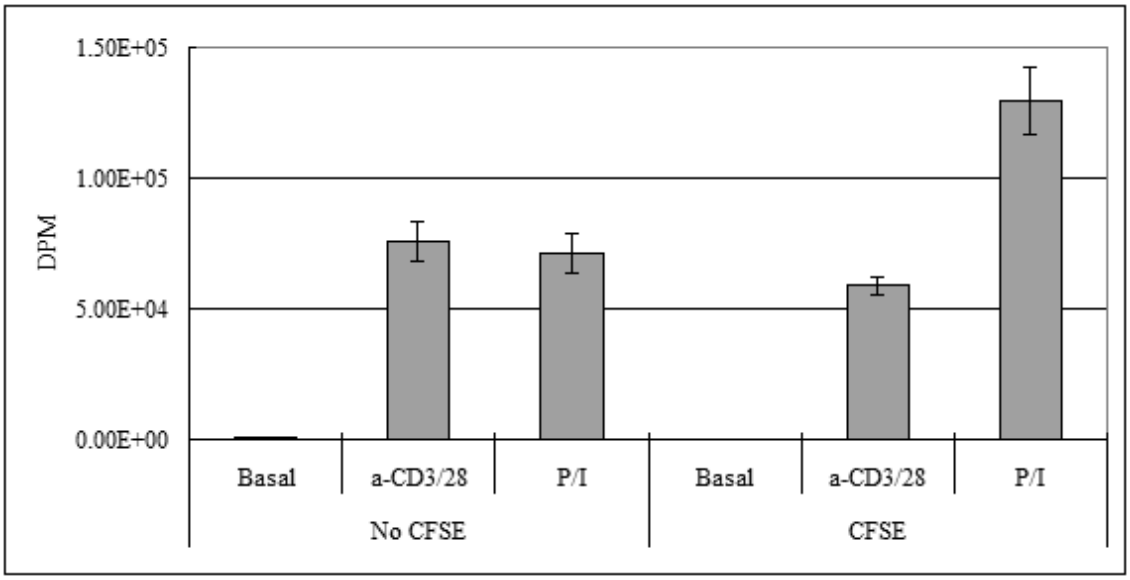

Objective: To test the cytotoxicity of CFSE on $CD4^+$ T cell proliferation.

Methods: $CD4^+$ T cells were purified from C57BL/6 by Miltenyi beads. Cells (at $>10^7$ cells/ml) were labeled with 5 µM CFSE in the presence of 5% FBS in PBS. Washed cells were stimulated for 72 hr by either control media, plate bound anti-CD3 Ab+soluble anti-CD28 Ab or PMA+Ionomycin. Following stimulation, 4µCi [^{3}H]-thymidine was added in the culture for 6 hr. Cells were harvested and thymidine incorporation was measured by liquid scintilation counting. Data are expressed as disintegrations per minute (DPM).

Results: CFSE labeled $CD4^+$ T cells were responding to anti-CD3/28 mAbs and PMA/Ionomycin, indicationg that CFSE was not toxic to cells at this concentration in the presence of 5 % FBS in PBS. We decided to use FBS to protect cells from cytotoxicity of CFSE and the protocol was modified as Appendix B-10.

A-15. Jurkat cell Laurdan labeling test

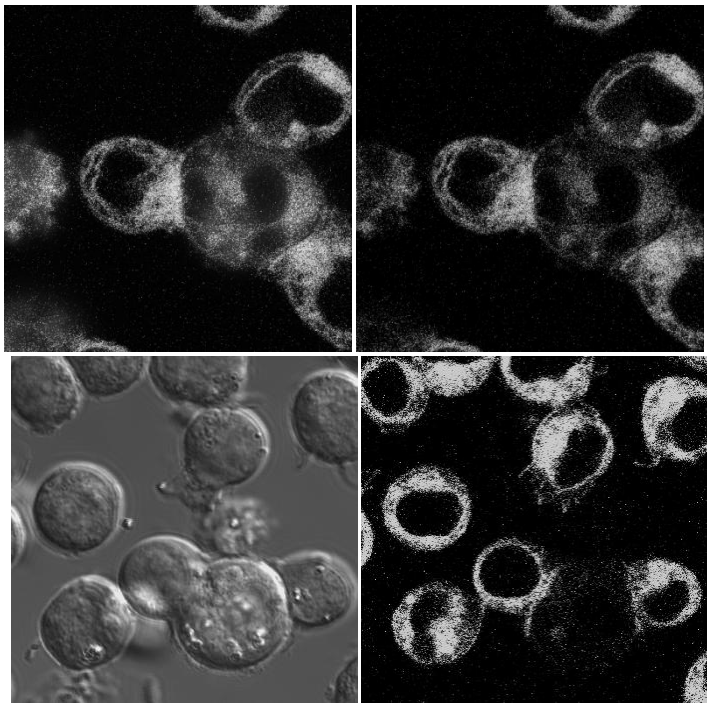

Objective: 1) To set the Laurdan labeling protocol for Jurkat cells.
2) To confirm Jurkat (clone E6-1, ATCC, cat# TIB-52) cells and Raji (ATCC, cat# CCL-86)+SEE (Toxin Technology, cat# ET404) form an immunological synapse (IS).

Methods: Raji cells ($10x10^6$ cells) were labled with 5μM CMTMR (Molecular Probe, cat# C2927) for 15 min and treated with 10 μM mitomycin C (Sigma, cat# M0503) in PBS for 20 min. Jurkat cells were washed and labeled by 10 μM Laurdan for 10 min. Excess Laurdan was washed out and Jurkat cells were cocultured with SEE pulsed Raji cells for 30 min at 37^{o}C. Following incubation, 2-photon microscopy was performed. (The detailed Laurdan labeling protocol can be found in Appendix B-7).

Results: Laurdan labeling was acceptable to measure GP-values. Jurkat and Raji cells formed an IS.

A-16. The effect of n-3 PUFA on GP-values at the IS of Jurkat-Raji co-culture

(GP-value, mean±SEM, n=12-22 cells)

	Noncontact whole cell	Immunological synapse
AA	0.087±0.012	0.131±0.013
DHA	0.089±0.009	0.163±0.023
EPA	0.085±0.008	0.163±0.017

Objective: To confirm the enhancement of lipid raft formation at the IS as shown in Chapter II using Jurkat-Raji co-culture system.

Methods: Jurkat T cells (clone E6.1, ATCC) were treated with BSA complex of either control AA, DHA or EPA [50 μM] for 72 hr. 10 μM Laurdan labeled cells (detailed protocol can be found in Appendix B-6) were washed and co-cultured with [5 μg/ml] superantigen Staphylococcal Enterotoxin E (SEE, Toxin Technology) pulsed Raji cells for 30 min. 2-Photon microscopy was applied to capture Laurdan images (n=12-19 cells). GP-values at the IS or noncontact whole cells were calculated as described in Appendix B-8.

Results: The formation of IS resulted in an increase in lipid rafts consistent with previous observations (110). In accordance with the results in Chapter III, n-3 PUFA (DHA and EPA) tended to increase GP-values at the IS compared to control n-6 PUFA. Further studies are required to draw statistical conclusion.

A-17. Kinetics of GP-value increase following IS formation by Jurkat-Raji cells

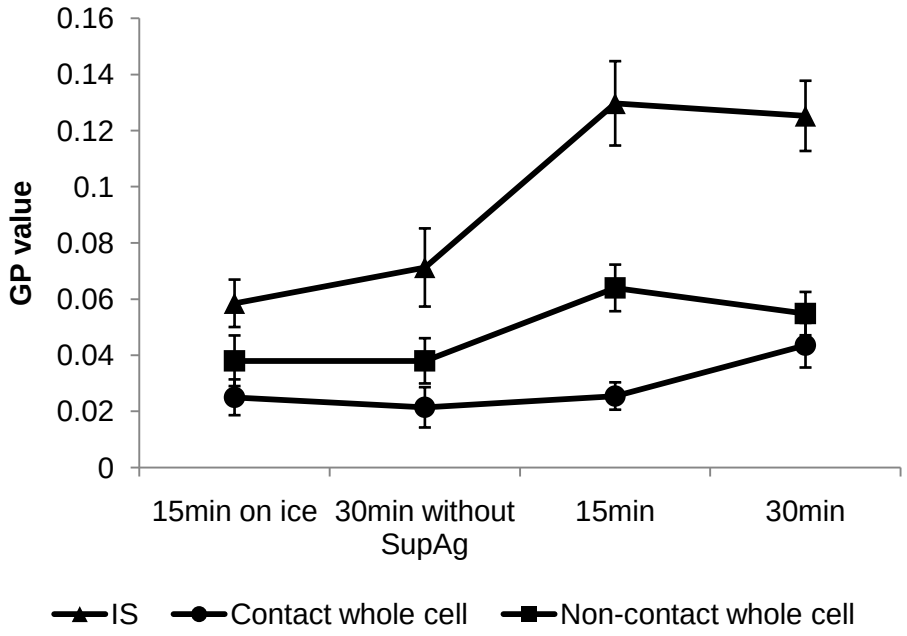

Objective: To test if the increase of the GP-value at the IS is dependent on IS formation and physiological cellular function.

Methods: Laurdan labeled Jurkat T cells were co-cultured with Raji cells, which were either pulsed with SEE or a control medium. Mixed cells were incubated on the ice to block cellular function or 37 ^{o}C incubator for 15 or 30 min prior to imaging. Laurdan images were captured and GP-values were calculated as described in Appendix B-8.

Results: GP-values at the IS increased only in the presence of SEE at 37 ^{o}C, indicating that the index is dependent on IS formation and cellular function. GP-values at the IS were not significantly ($P>0.05$) different at both time points (15 or 30 min).

A-18. Comparison of cell count by hemocytometer and Coulter counter

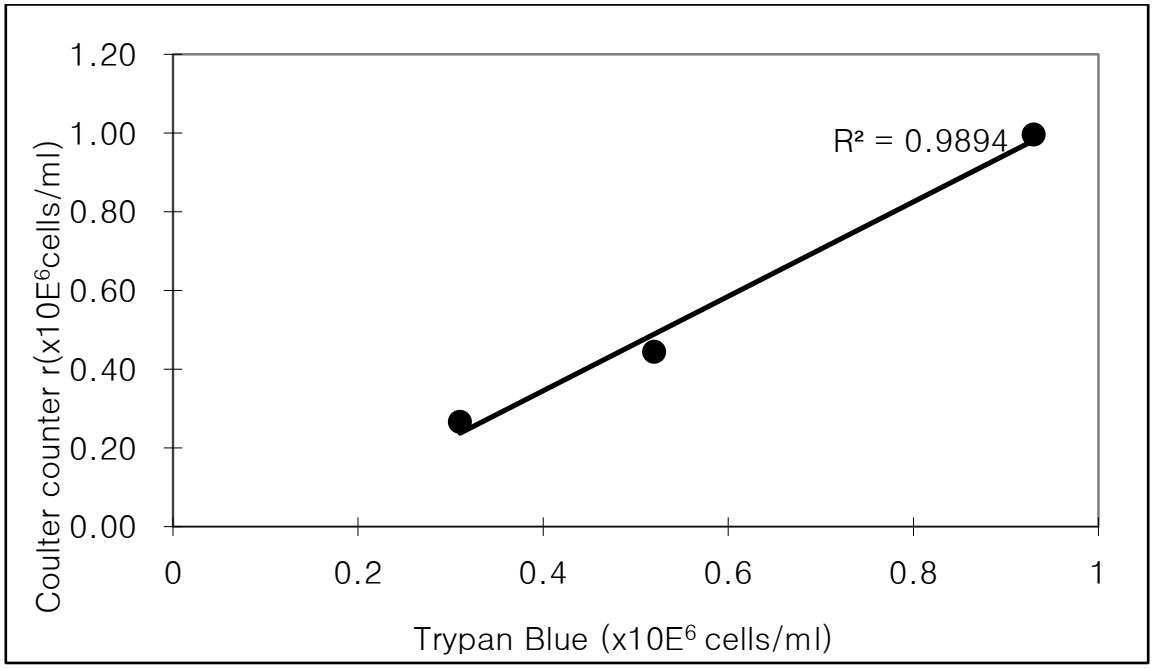

Objective: To test if the Coulter counter can be used for T cell quantification.

Methods: Purified $CD4^+$ T cells by Miltenyi beads were resuspended in 1ml medium. Cells were subsequently counted by either Trypan Blue exclusion method using hemocytometer or Coulter counter (4 µm) as described in Appedice B-2 and B-6 (n=3).

Results: The cell numbers counted by the two different methods correlate at R^2=0.9894. We concluded that Coulter counter can be used to count $CD4^+$ T cells.

A-19. Controls for nuclear factor activation measurements

(A) NF-κB

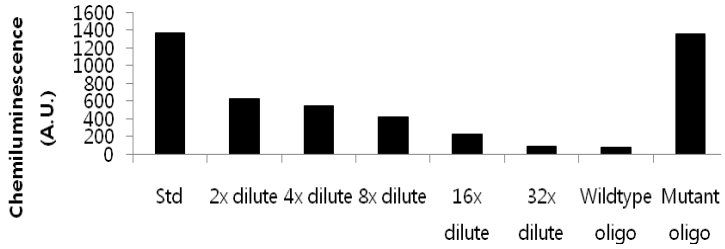

(B) NFAT

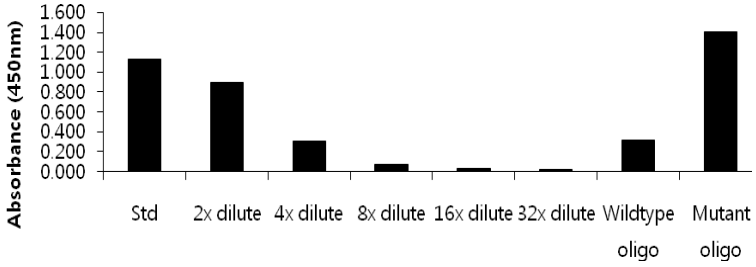

(C) AP-1

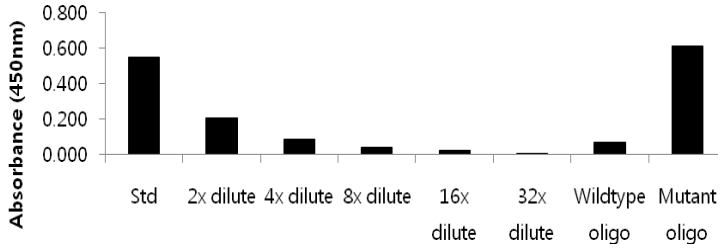

Objective: To confirm the sensitivity of nuclear factor detection ELISA kits (Active Motif, cat# 40097, NF-κB p65; 40296, NFATc1; 46096, AP-1 c-Jun).

Methods: Standard nuclear extracts (provided in the kit) were quantified using kits as described in the Methods. Extracts were serially diluted in order to measure the dose-dependent colorimetric readouts. Wild-type or mutant oligonucleotides, which were included in the kits, were added into buffer to confirm the specificity of each kit.

Results: The readouts were affected in a dose-dependent manner and selectively responded to nuclear factors.

A-20. Standard curve of IL-2 secretion measurements

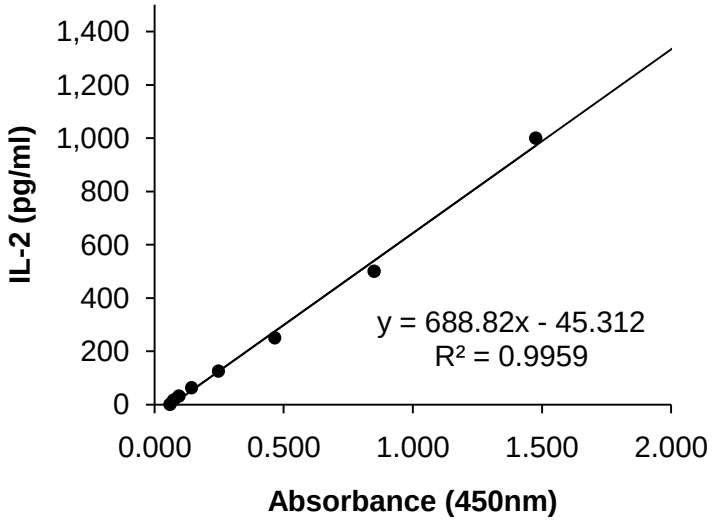

Objective: To confirm the sensitivity of IL-2 detection ELISA kit (R&D Sytems, cat# M2000).

Methods: IL-2 standard solution was serially diluted and measured by linear regression of spectrophotometry readouts according to the manufacturer's manual.

Results: The IL-2 detection kit responded in dose-dependent manner.

A-21. Propidium iodide uptake of APC as determined by flow cytometry

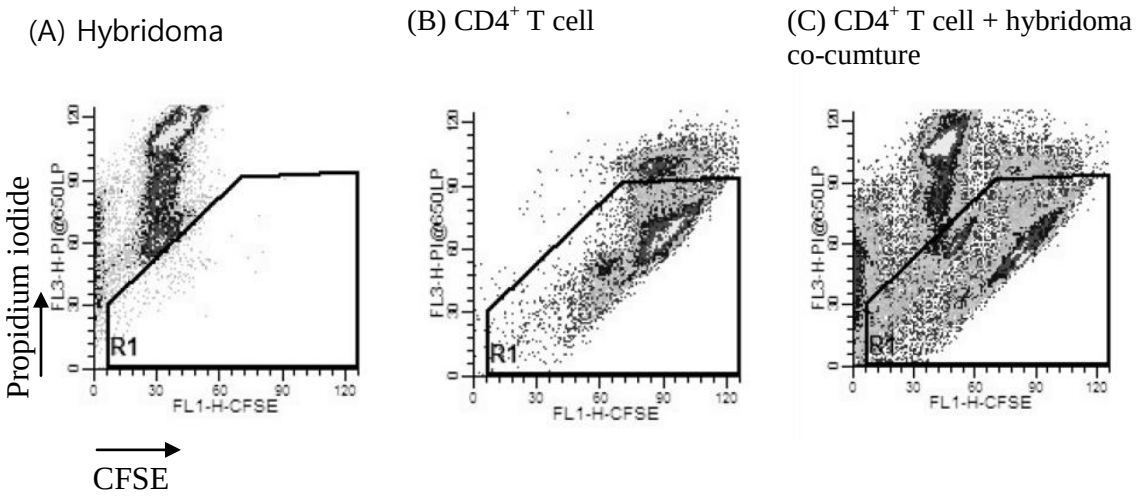

Objective: To gate viable $CD4^+$ T cells from non-viable cells and APC.

Results: Hybridoma exhibited propodium iodide (PI, 1mg/ml) uptake in red channer (A) and a subpopulation of $CD4^+$ T cells were PI^+ (B). Overall, viable $CD4^+$ T cells were gated by drawing a polygon (C).

A-22. Gating of viable lymphocytes by side scatter properties using flow cytometry

(A) FSC vs SSC

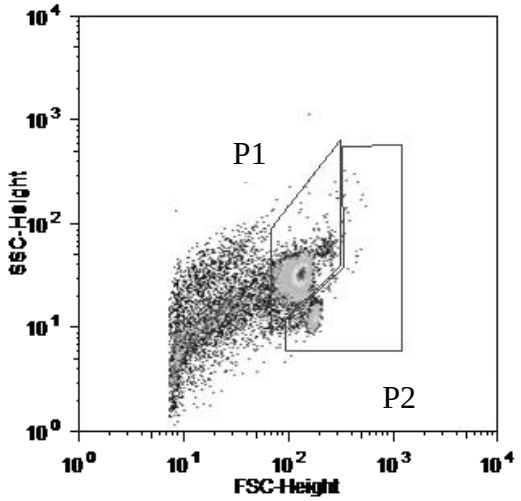

(B) Propidium iodide uptake

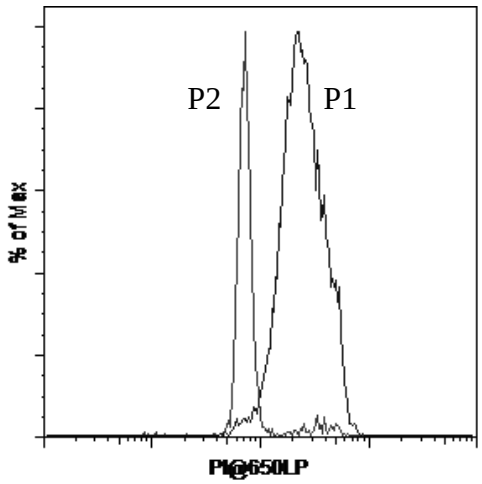

Objective: To gate viable lymphocytes by flow cytometry.

Results: Population 1 (P1) determined by FSC vs SSC property exhibited higher propidium iodide uptake properties, indicating that P1 is non- or less viable. Therefore, we decided to use P2 for further analyses.

A-23. Images of $CD4^+$ T cell culture

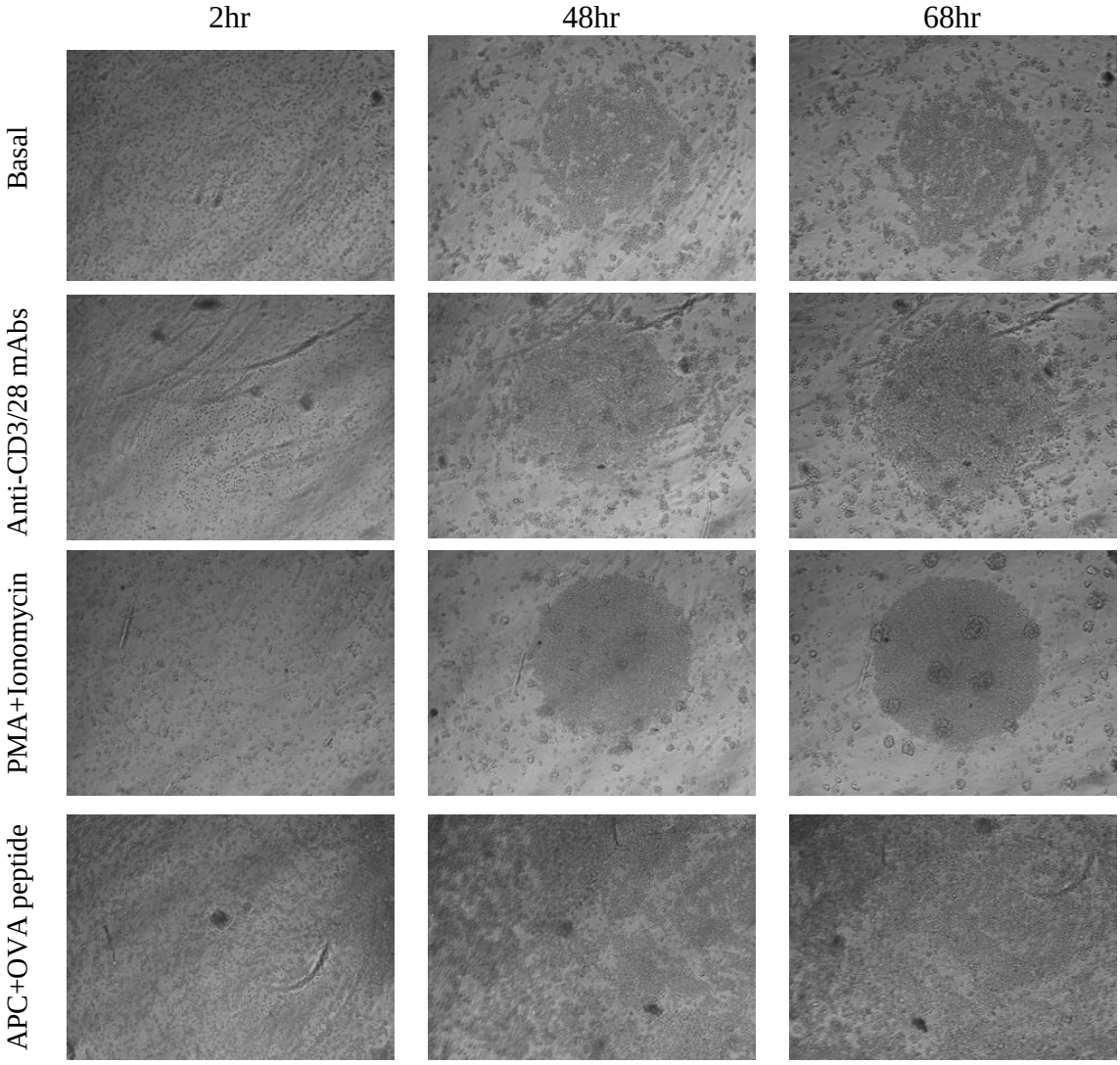

Methods: Purified $CD4^+$ T cells were labeled with 5 μM CFSE (Appendix B-10) to trace cell division in PBS with 5% FBS. $1x10^5$ cells were cultured in total 200 μL complete medium in 96-well plates with or without stimuli. Representative images were captured at 2 h, 48 h and 68 h (10x objective).

APPENDIX B

EXPERIMENTAL PROTOCOLS

B-1. DO11.10 Genotyping
(From Ping Zhang)

Primers:

#0786 CAG GAG GGA TCC AGT GCC AGC
#0787 TGG CTC TAC AGT GAG TTT GGT

Reaction Mix:

PCR Platinum supermix	45 µl
#0786 (10pmol/ul each)	0.5 µl
#0787 (10pmol/ul each)	0.5 µl
~75 to 100 ng DNA	~75-100 ng
Water	To 50 µl total volume

PCR Parameters:

94°C 6 min

30 cycles of:
94 °C 1 min
64 °C 1 min 30 sec
72 °C 2 min

72 °C 10 min
4 °C ∞

DNA Gel

10 µl PCR product
1.1 µl 10x sample dye,
quick mix. Heat at 65°C for 5 min. Run at 4% EtBr-agarose gel (Reliant Gel System, Cambrex, #54927) (with 0.5X TAE running buffer) at 200V in cold room for 1 to 1.5 hr. Also, include 5 µl MW marker (Hyperladder IV, Bioline#BIO-33029)

Band is approx. 300 bp
Refer to Appendix A-1 for a representative image.

B-2. Protocol for Adoptive Transfer Study

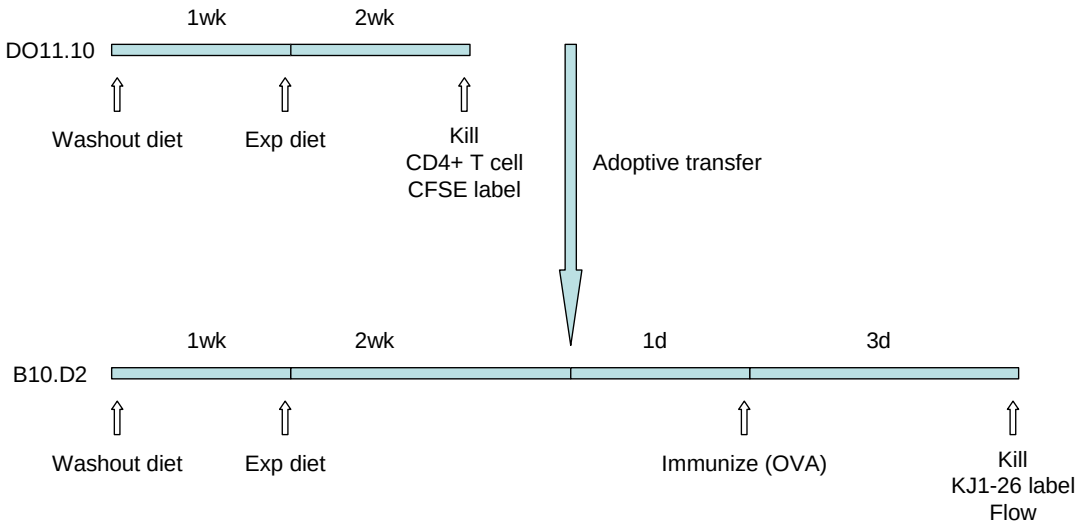

I. Isolate splenocytes and $CD4^+$ T cells

1. Spleen and Lymph nodes Isolation

A. Materials

i) DO11.10 mice.
ii) Sterile tools (scissors and forceps).
iii) 70% EtOH.
iv) Labeled 15 ml conical tube filled with 3 ml complete RPMI.

B. Methods

i) Sacrifice mice by CO_2.
ii) Place a mouse with abdomen facing up.
iii) Apply 70% alcohol to the abdomen area.
iv) Grab the skin of the abdomen with forceps and make a small incision.
v) Peel the skin to expose the membrane underneath.
vi) Find the lymph nodes under the arms. Pinch the lymph nodes off and tease off the connect fat, put them in a tube containing complete RPMI.
vii) Make an incision in the membrane at abdomen and find the mesenteric node. Get it and put in the above tube.
viii) Turn the mice around and find the spleen.
ix) Remove the spleen with forceps while cutting the fat tissue with scissors.
x) Carefully remove as much fat as possible.

xi) Place the spleens in a conical tube containing complete RPMI.

2. Spleen and lymph node cells preparation
   A. Materials
      i) Sterile glass-in-glass homogenizers.
      ii) Sterile wire filters.
      iii) 5 ml syringes.
      iv) 20 gauge needles.
      v) 15 ml conical tubes.
   B. Methods
      i) Transfer spleen and lymph nodes into corresponding glass-in-glass homogenizers.
      ii) Homogenize spleens until completely broken up (5-7 strokes) and homogenize the lymph nodes in the same way (only 3-4 strokes will be enough).
      iii) Assemble a 5 ml syringe, wire filter and 20 gauge needle unit and place on top of a newly labeled 15 ml conical tube.
      iv) Remove the syringe plungers and transfer the appropriate spleen and lymph node suspension into the assembled units.
      v) Slowly reinsert the plunger to filtrate the suspension into the corresponding tube (be gentle with this step).
      vi) Fill each tube with RPMI for washing and centrifuge at 200x g (acc/bcc=6) for 5 min at RT.
      vii) After the spinning, carefully aspirate the RPMI.
      viii) Resuspend cells in 3 ml complete medium.

3. Isolation of lymphocytes by Lympholyte-M
   A. Materials
      i) Lympholyte-M (Cedarlane Laboratories, Cat# CL5030) warmed to RT .
      ii) 1x column buffer (Provided in column kit).
      iii) Monoclonal antibody (Provided in column kit).
      iv) PBS/5% FBS (<u>regular, not heat-inactivated</u>).
   B. Methods
      i) Add 3 ml of Lympholyte-M by layering it beneath the suspended cells (insert the pipet tip into the bottom of the conical tube then dispense

the Lympholyte-M slowly and carefully in order to see 2 distinct layers).

ii) Centrifuge the cells at 500x g for 15 min (deactivate centrifuge break by setting acc/dcc=0) at RT.

iii) After spinning, 2 distinct layers (white on top and pink on bottom) and an interface band should be seen.

iv) Carefully remove the interface band with a pipette and dispense into a new conical tube.

v) Fill the conical tube with RPMI, mix and centrifuge at 200x g for 5 min at RT.

vi) Aspirate off the RPMI.

vii) Combine all lymph node cells with 1 ml PBS/5% FBS. Lymph node cells are ready for CFSE staining (previous studies confirmed that more than 90% of lymph node cells are $CD4^+$ T-cells).

viii) Mix 1 vial (0.5 ml) of antibody cocktail to every splenocyte tube, and incubate at RT for 15min. (At this point, begin column washing).

ix) Wash cells with 10 ml of 1x column buffer at 200x g for 5 min.

x) Resuspend in 1ml of 1x column buffer.

4. $CD4^+$ T cell purification

A. Materials:

i) R&D $CD4^+$ columns-small (Cat# MCD4C-1000) at RT.

ii) R&D column rack.

iii) 70% EtOH.

iv) Waste receptacle.

v) Timers.

vi) Sterile 15 ml conical tubes.

B. Methods:

i) Place the T cell columns in the R&D column rack and place a waste receptacle beneath the columns.

ii) To prepare the columns, remove the top cap first, and then remove the bottom cap.

iii) Allow the fluid within the column to drain until dripping stops; meanwhile rinse the outside of the column tip with 70% EtOH.

iv) Wash the column with 6 ml of 1x column buffer.

v) Replace the waste receptacle with a newly labeled sterile 15 ml conical tube.

vi) Apply 1 ml cell suspension to the top of the column.

vii) Allow the cells to sit in the column for 10 min at RT.
viii) Apply 8 ml of 1x column wash buffer to the column to elute the $CD4^+$ T cells.
ix) Once all the T cells have been collected, centrifuge at 200x g for 5 min at RT.
x) Aspirate the supernatant, and combine purified splenocytes with lymph node cells in 1 ml PBS/5% FBS.
xi) Now cells are ready to be counted (lymph node cells are thought as $CD4^+$ T cells).

5. Cell counting by hemacytometer
   A. Materials:
      i) Trypan blue (Sigma, cat# T8154).
      ii) Eppendorf tubes.
      iii) Hemacytometer.
   B. Methods:
      i) Add 180 μL H_2O and 10 μL Trypan blue to an epi-tube.
      ii) Mix the T cells and remove 10 μL to add to a sample tube with Trypan blue.
      iii) Mix by pipetting up and down several times.
      iv) Remove about 20 μL from the suspension and put in a hemacytometer.
      v) Count the viable white cells by microscope at 10x magnification (count at least 200 cells)

$$\text{Cell concentration (cells/ml)} = (\text{cell count})/(\text{squares}) \times 10^4 \times 20$$

II. CFSE labeling of $CD4^+$ T cells
   A. Materials
      i) BSA: IgG free, Boehringer Mannheim Laboratory Reagents, 100018 (non-sterile).
      ii) PBS/0.1% BSA : filter thorough 0.2 μm filter to sterilize.
      iii) Carboxyfluorescein succinimidyl ester (CFSE, Molecular probes V-12883).
         - To prepare 10 mM CFSE, dissolve one vial (50 μg) in 90 μl DMSO.
         - Aliquot 10 μl in epi-tubes.
         - Store at -20 ^oC up to a month.

iv) RPMI 1640/10% FBS (regular).

B. Methods;

i) Add 1µl of 10mM CFSE in the tube containing cells. Vortex IMMEDIATELY.

ii) Incubate at 37 ^{o}C. (in water bath) for 10 min .

iii) Add 5 ml of ice-cold RPMI 1640/10% FBS and incubate for 5 min on ice.

iv) Fill the tube with sterile PBS, spin down (200x g, 5min) and aspirate supernatant.

v) Resuspend cells at $3x10^{7}$ cells/ml in PBS and load 100 µl into 30 gauge insulin syringes (BD, cat# 328438).

vi) Put syringes on ice and bring over to LARR for tail injection.

III. Immunization (D+1)

A. Materials

i) Sterile PBS.

ii) OVA323-339 peptide (ISQAVHAAHAEINEAGR, synthesized by Biosource, Inc) needs to be warmed to RT before use.

iii) Complete Freund's adjuvant (CFA), Sigma #F-5881.

iv) Micro-emulsifying needles 73mm, Popper & Sous, Inc., New Hyde Park, N.Y., #7973.

v) 1 ml BD Luer-Lok syringe, #309585.

vi) 3 ml BD Luer-Lok syringe, #309628.

vii) 25 5/8 G needle BD #305122.

B. Methods

i) One day after tail injection, dissolve OVA peptide in PBS. (We want final concentration 6 mg/ml, 1mg in a bottle, thus dissolve 6 bottles in 1 ml PBS).

ii) Emulsify with 1 ml CFA (Add OVA peptide in a syringe at one end of the mixing tube, then add 1 ml of CFA to another syringe attached to the other end of the mixing tube, push through the mixing tubes until it is really hard to push, which means it is ready).
→ OVA peptide conc. is diluted half (3 mg/ml).

iii) Inject subcutaneously in a total volume of 0.1 ml (300 µg OVA peptide per mouse) distributed between two dorsal sites on the back with 25 5/8 needle.

IV. Flow detection of antigen-specific cells

A. Materials

i) 0.2um Nylon membrane filter, Gelman Laboratory, #4433.

ii) Staining buffer.

- Sterile PBS.
- 1% heat-inactivated FBS.
- 0.09% sodium azide.
- adjust pH to 7.4-7.6, filter, store at 4 ^{o}C.

iii) Fc Block (5 µg/ml).
: diluted from Fc Block stock (0.5 mg/ml, Pharmingen, cat# 553142) (4 µl Fc Block + 396 µl staining buffer).

iv) KJ1-26 anti-TcR-Cy5.5 (0.2 mg/ml), Caltag Laboratories #MM7506.

v) 1.5 ml microtubes.

vi) 12x75 mm Polystyrene tubes (BD, cat# 352054).

B. Methods

i) Sacrifice B10.D2 recipient mice and get draining lymph nodes in 3 ml complete RPMI (15 ml conical tube).

ii) Sacrifice 2 B10.D2 control mice (without donor cells), and get draining lymph nodes (for KJ1-26 negative control).

iii) Sacrifice 2 DO11.10 mice, and get draining lymph nodes (for KJ1-26 positive control)

iv) Homogenize lymph nodes and wash with complete RPMI medium.

v) Count viable cells by Trypan blue exclusion.

vi) Resuspend cells in 100 µl of 5 µg/ml Fc Block and incubate at 4 ^{o}C. for 15min.

vii) Add 5 ml staining buffer, centrifuge (200x g, 5 min, RT) and aspirate supernatant.

viii) Resuspend cells in 100 µl KJ1-26 antibody diluted in staining buffer (KJ1-26 dilute to 2 µg/ml: 4 µl KJ1-26 + 396 µl staining buffer) and incubate in dark at 4 ^{o}C for 30 min.

ix) Add 5 ml staining buffer into the tube, spin down (200x g, 5 min, RT) and aspirate.

x) Resuspend cells in 500 µl staining buffer and transfer to FACS tubes.

xi) Promptly take samples for flow cytometer analysis in ice.

B-3. *Fat-1* phenotyping
(modified from Yang-Yi Fan's protocol)

*Always keep the samples in ice.

I. Prepare leak proof tubes (D-1)
1. Put 1 ml acetone in 12 ml glass tubes with black Teflon caps.
2. Evaporate for 1hr in 80 ^{o}C oven.
3. Check if acetone has evaporated.

II. Extract total lipid (D-0)
1. Preset centrifuge at 4 ^{o}C.
2. Clean 12 ml tubes.
   A. Work in hood.
   B. Pour out acetone (into brown waste bottle).
   C. Put upside down on the rack (don't mix the caps).
   D. Clean the tubes with 1 ml methanol (GC grade) using glass pipette.
   E. Dry down the tube.
3. Put 1 ml 0.1 M KCl (in walk-in refrigerator) with plastic pipette into 2 ml epi-tubes.
4. Cut the mouse tail to small pieces using glass plate and blade, into the tube from #3.
5. Homogenize the sample with Polytron blade (Ultra-Turrax T8, IKA Labortechnik) at speed 5 for 15 sec. (Put the sample tube on ice during the homogenization). The tail mixture will turn brownish color.
6. Add 5 ml of Folch ($CHCl_3$/MeOH, 2:1, v/v) into 12 ml glass tube, then transfer the sample to the tube.
7. Vortex the sample for 1min.
8. Centrifuge the sample at 3000rpm for 5min at 4 ^{o}C. (Put the glass tube inside plastic tube wrapper to avoid breaking during the centrifugation). After centrifugation, set centrifuge temp. at 20 ^{o}C.
9. Transfer lower phase to a leak-proof 12 ml glass vial with Pasteur glass pipette. Push the bulb to make bubbling during passing the upper phase to avoid contamination. After getting out the pipette, throw away 1-2 drops.
10. Wipe the needles of N_2 dryer with MeOH in the hood.
11. Dry sample under N_2
12. Mix 6% HCl-MeOH under the hood near walk in freezer. (HCl is under the hood, and GC-grade MeOH is near the balance). Use mass cylinder to measure.
13. Add 3 ml 6% HCl-MeOH to the tube.
14. Flush sample with N_2, close cap tight.

15. Vortex and incubate at 76 ^{o}C oven for ~15 hrs.
16. Prepare 4 ml tubes with labels. (Recap with green Teflon caps).

III. Extract FAME (D+1)

1. At this time, turn on GC
2. Set centrifuge at 4 ^{o}C.
3. Extract FAME by adding 1 ml cold 0.1M KCl and 2 ml Hexane to the methylated sample. Vortex for 1min, centrifuge at 3000rpm for 5min at 4 ^{o}C.
4. Transfer upper phase to 4 ml glass vial.
5. Dry FAME under N_2.
6. Redissolve the sample in 25ul methylene chloride (CH_2Cl_2) using wiretrol.
7. Vortex the tubes in order to dissolve all the FAME on the wall.
8. Ready for running on GC.

IV. GC analysis

1. Turn on GC, stabilize for 15min.
2. Turn on computer, open 32 Karat 7.0
3. Click on GC, then OK.
4. Click on single run icon (Blue single arrow), the screen shows "waiting for trigger"
5. Then, inject std (68A std, Nuchek)
   A. Find the tube with yellow tag in -20 ^{o}C. freezer
   B. Vortex.
   C. Rinse the inject needle with CH_2Cl_2.
   D. Load 0.5 µl std in the needle: avoid any bubble.
   E. Push the needle into injector inlet, the push the plunger.
   F. Pull back the needle, then press "start" button on GC machine.
   G. After injection, flush the tube with N_2.
   H. Put back in -20 ^{o}C. freezer.
6. Vortex the sample and inject in the same way.
7. For the report,
   A. Click "3.2 Karat", then "offline GC".
   B. Data → Open (D\GC\GCdata\wooki).
   C. Method → integration events → minimum area → adjust → green (analyze).
   D. Ctrl+z : escape highlight.
   E. Method → custom report.
   F. Double click on graph to change the Y axis range.

B-4. *Fat-1* genotyping
(modified from Yang-Yi Fan and Evelyn Callaway's protocols)

I. Isolation of total DNA from mouse tail.

1. Material.
   A. Mouse tail (~1cm), frozen in liquid nitrogen.
   B. DNeasy Tissue Kit (Qiagen, cat# 69504).
   C. Other buffers are provided in the kit.

2. Preparation of reagent.
   A. For the first time use, add appropriate amounts of 100% EtOH to Buffers AW1 and AW2 as indicated on the bottles.
   B. Prewarm 55 ^{o}C shaking water bath (set at 75 rpm).

3. Procedure (It is better to do this in the late afternoon).
   A. Perform all steps in RT, vortex for 5-10 sec. unless specified.
   B. Allow the frozen tail to warm to RT. Put the tail on a new glass slide.
   C. Cut the tail into smaller pieces using brand new or DNA away-zapped razor blade.
   D. Transfer the tail pieces to a new 2 ml sterile epi-tube.
   E. Add 180 uL Buffer ATL to the tube.
   F. Add 20 uL proteinase K to the tube and vortex (make sure all pieces are down)
   G. Incubate the tube (on a floating platform) in 55 ^{o}C. shaking water bath (75 rpm) overnight (~16-18 hr).

---------- Overnight----------

   H. Mix 200 uL Buffer AL and 200 uL 100% EtOH to make Buffer ALE for each sample, using DNase free pipette-tips. (Make fresh)
   I. Remove the tube from the water bath. Vortex for 15 sec.
   J. Add 400 uL Buffer ALE to the sample, and mix vigorously by vortexing (make sure it mixes thoroughly)
   K. Pipette the mixture into DNeasy Mini spin column placed in a 2ml collection tube (kit provided).
   L. Centrifuge at >6000 x g (8000 rpm) for 1 min. (Eppendorf centrifuge 5414D)
   M. Discard flow-through and collection tube.
   N. Place the DNeasy Mini spin column in a new 2 ml collection tube (provided).

O. Add 500 uL Buffer AW1, and centrifuge for 1 min at >6000 x g (8000 rpm).
P. Discard flow-through and collection tube.
Q. Place the DNeasy Mini spin column in a new 2 ml collection tube (provided).
R. Add 500uL Buffer AW2, and centrifuge for 3 min at 20,000 x g (14,000 rpm) to dry the DNeasy membrane. (Centrifuge 5417R) It is important to completely dry the membrane, since EtOH will interfere with subsequent reactions.
S. Discard flow-through and collection tube.
T. Place the DNeasy Mini spin column in a new sterile 2 ml collection tube with lid (not provided). Pipette 200 uL of Buffer AE directly onto the DNeasy membrane.
U. Incubate at RT for 1 min, then centrifuge for 1 min at >6000 x g (8000 rpm) to elute the DNA
V. Pipette 200 uL of Buffer AE directly onto the DNeasy membrane, in the same 2 ml tube.
W. Incubate at RT for 1 min, then centrifuge for 1 min at >6000 x g (8000 rpm) to elute the DNA in the same tube.

II. DNA quantification

1. Handle Quartz plate with lens cleaner, ALWAYS!! → Avoid "any" scratch !!
2. Turn on Spectra Max and the Mac computer connected. (Prewarm 10-15 min)
3. Find the "Spectra Max" icon on the Desktop, and double click it.
4. Click "Set up" → Wavelength Lm1: 260 / Lm2: 280 → Calibrate: On
5. Place Quartz plate on the machine
6. Find "Control" toolbar on menu → close tray
7. Control → Run → Pre-read → OK
8. The machine reads the plate, then the Quartz plate comes out.
9. Save, and bring the plate to the bench table.
10. Make 1X TE with 0.1% Tween 20
11. Put 95 uL TE buffer into designated wells (duplicate is better)
12. Make sure the first two wells are "Blank"
13. Use DNA quantification control (~115 µg/ml, in Laurie's freezer)
14. Put 5 uL of DNA samples into appropriate wells.
15. Bring the plate to the Spectra Max, and load the plate.
16. Click Control → Close Tray → Read → Experiment → OK
17. The machine reads the plate
18. After the reading, click "Template"
19. Drag wells which are used → Unknown

20. Group number: 2
21. Drag first two wells → Blank
22. Then, look into result part
23. Delete any unnecessary columns
24. Calculate "MeanValues" for duplicates
25. Calculate "DNA quantity (µg/ml) by formulation: MeanValues*20 (dilution factor)*214 (Correction)

Correction table

Volumn in Quartz plate	DNA	RNA
200 uL	93.6	83.0
150 uL	131.0	115.8
100 uL	214.0	191.3
50 uL	597.0	523.8

(1) Dilute DNA to make 10 uL of 15 µg/ml DNA with ddH_2O.

III. RT-PCR (SYBR Green real time PCR, 7900HT)

1. Per Reaction:

2X SYBR Master Mix	6.25 uL
Forward primer (300 nM)	1 uL
Reverse primer (300 nM)	1 uL
DNA (~15 µg/ml)	0.5 uL
ddH_2O	3.75 uL

2. Make a cocktail with Maser Mix, both primers, and ddH2O.

Master Mix	6.25 uL x	=	uL
F primer	1 uL x	=	uL
R primer	1 uL x	=	uL
ddH_2O	3.75 uL x	=	uL
		Total cocktail volume	uL

A. Add 12 uL of cocktail to plate and 0.5uL diluted DNA (Do in the hood for PCR, plate part# 4346906)
B. Cover the plate with plastic cover.
C. Squeeze with a rubber to ensure all wells are completely sealed. (If any well is not sealed, the material evaporates during PCR cycle).
D. Centrifuge the plate several seconds. (when the centrifuge reaches up to 1000 rpm, turn off).
E. Run RT-PCR

3. RT-PCR running

F. Turn on machine and computer
G. Click SDS 2.2.2 on desktop
H. File → new
   Assay: Absolute quantification
   Container: 96 well
   Template: Blank → OK
I. Designate sample-containing wells by clicking and dragging on plate map
J. (Use CTRL key if you need to add/drop wells)
K. Setup → add detector → SYBR → copy to plate documents → done
L. Mark "X" on detector SYBR
M. (Make sure that all sample-containing wells are designated and marked as SYBR)
N. Instrument → Mode → Standard → Sample volume (µl) → 13
O. Connect → open → load plate → close → start

4. After RT-PCR is done
   A. Designate wells → analysis → analyze
   B. Open → take out sample → done

B-5. $CD4^+$ T cell Positive Isolation by Miltenyi® Beads and Column (Modified from Qian Jia's protocol)

I. Preparation (D-1)
1. Prepare media/tubes
   A. Fill conical tubes with 3 ml MACS buffer (cat# 130-091-221).
   B. Prepare scissors, forceps, 70% EtOH squeeze bottle, 5 ml syringes.

II. Kill/Co-culture (D-0)
1. Isolate $CD4^+$ T cells from spleens
   A. Sacrifice mice by CO2.
   B. Place mice on their right side so that the left side faces you.
   C. Apply alcohol to the abdomen area.
   D. Grab the skin of the abdomen with forceps and make a small incision.
   E. Peel back the skin/fur with fingers to expose the membrane underneath.
   F. Grab the membrane with forceps and cut the membrane to expose the organs.
   G. Remove the spleen (dark red organ) with forceps.
   H. Carefully remove as much fat from the exterior of the spleen as possible.
   I. Place a spleen in a 15 ml conical tube containing 3 ml MACS buffer, transfer to cell culture room.
2. Preparing single-cell suspension
   A. Place a Falcon cell strainer (70 μm mesh, BD, # 35-2350), on the 100mm petri dish, and pre-wet with 5 ml MACS® buffer.
   B. Transfer spleens into cell strainer.
   C. Gently press spleen against the bottom of the strainer with a plunger from a 5 ml syringe. Use up and down motion (not grinding), being careful not to damage cells.
   D. When only the spleen connective tissue remains in the strainer, remove the plunger.
   E. Transfer the cell suspension from the dish to the original 15ml conical tube.
   F. Wash strainer with 5 ml MACS buffer, and transfer to the same tube to collect the remaining cells.
   G. Spin down at 300x g for 10 min.
   H. Aspirate the supernatant.
   I. Take 10 ml MACS buffer and pre-wet the 30 μm filter (Miltenyi, cat# 130-041-407, on a 15 ml conical tube) with 2 ml buffer.
   J. Resuspend cells in 8 ml buffer and pass the cells through the filter.
   K. Remove 10 μl to a Coulter Counter tube for counting.
   L. Centrifuge the cells at 300x g for 10 min.

M. Remove the supernatant and resuspend the pellet by flicking the tube or ratcheting the tube over a tube rack.
N. Count the cell number during waiting for centrifuge by Coulter Counter with 4 μm cut-off.

3. Mixing with magnetic bead/column separation
   A. Resuspend cells with 90 μl cold MACS buffer per 10^7 total cells.
   B. Add 10 μl of CD4 (L3T4) Microbeads (Miltenyl Biotec, cat# 130-049-201) per 10^7 total cells.
   C. Mix well and incubate for 15 min at 4-8 ℃ (refrigerator, not ice!!) (No shaking needed)
   D. Wash cells by adding MACS buffer up to 12 ml, and centrifuge at 300x g rpm for 10 min.
   E. Aspirate the supernatant. Flick the tube to loosen the pellet.
   F. Resuspend up to 10^8 cells in 500 μl cold MACS buffer. If cell number exceeds 10^8, multiply the volume by cell number.
   G. Place MS** column at Octo MACS Separator.

   (**The following buffer volume is for MS column only.)
   H. Rinse MS column with 500 μl MACS buffer. Let the buffer slowly drip to drop, wait until dry (very quick, less than 1 min).
   I. Apply cell suspension to the column.
   J. Let unlabeled cells pass through, and wash MS column with 500 μl MACS buffer 3 times.
   K. Let the column drip completely dry between washes.
   L. Remove total column from the separator, and place it on a collection 15 ml conical tube.
   M. Pipette 1 ml of sterile MACS buffer onto the column. Immediately flush out fraction with the magnetically labeled cells by firmly applying the plunger supplied with the column.
   N. Now, $CD4^+$ T cells are ready in 1ml buffer.
   O. Count $CD4^+$ T cells by Coulter Counter with 4 μm cut-off.

B-6. Counting Cells with Coulter Counter
(modified from Evelyn Callaway's)

I. Prepare sample cups 24-48 hrs ahead: De-gas Isotone: turn red lever to the left and lift dispensing pump twice. Turn red lever so it is parallel to the arm. Fill Coulter vials with 10 ml per vial (one pump of Isotone).

II. On the counting day,

1. Turn power on, open door, lower stage.
2. Remove vial of Coulter Clenz, replace with Isotone/Isoflow, raise stage.
3. Readout: Setup #1 (S1). Scroll down to last line and set cell size. This measurement is to be set for the smallest cell of acceptable range. Our laboratory usually sets 4 µm for $CD4^+$ T-cells.
4. Select: FUNCTIONS on keypad. Scroll to Flush Asperature. Hit: START/STOP to flush. Repeat flush, then replace Isotone. Flush twice more.
5. Select: OUTPUT on keypad. Scroll to Count/Concentration and select one., If "concentration" is selected, readout will be in #cells/ml. Scroll to Dilution and enter dilution factor. Leave units on um.
6. Add 10 µl sample to Coulter vial (for 1:1,000 dilution) Place vial on stage, raise, and press START/STOP on keypad to count. Count each sample 2-3 times and average.
7. To shut down machine, replace vial of blue Coulter Clenz and flush aperature (under FUNCTIONS) 2-3 times. When flush is complete, turn off power.

B-7. Laurdan study protocol

I. Poly-L-Lysine precoating (D-1)

1. Dilute 0.1%(w/v) Poly-L-Lysine solution (Sigma, cat# P8920) to 0.01% with sterile water.
2. Fill the chambered coverglass (Nunc, cat# 155380) wells with 0.01% Poly-L-Lysine solution (1 ml), allow it to sit for 30 min, then aspirate excess solution and allow the coverglass wells to air dry. Sterilize the coverglass slides under UV light for 1 hr.

II. Isolate $CD4^+$ T cells from spleens (D-0)

1. After $CD4^+$ T cell isolation (Appendix B-5), centrifuge cells at 300x g for 5 min, RT.
2. Resuspend cells in 1 ml complete medium and count cells using Coulter counter (4 µm).
3. Adjust cell concentration at $1x10^6$ cells/ml in the complete medium.
4. Keep cells in 37 ^oC., 5% CO_2 incubator with the cap loosen.

III. Hybridoma (anti-CD3 expressing, clone 145-2C11) cell preparation.

1. Pipette cell suspension up/down several times to detach cells from bottom of flask.
2. Transfer cell suspension to a 50 ml conical tube.
3. Wash the flask with 10 ml RPMI twice and transfer to the 50ml conical tube containing cells.
4. Centrifuge at 200x g for 5 min at RT.
5. Aspirate supernatant and resuspend cells in 1 ml Leibovitz's media (Gibco cat# 21083-02).
6. Count cells by Coulter counter with 4 µm cut-off.
7. Adjust cell concentration at $0.2x10^6$ cells/ml.
8. In optional experiments, anti-DNP expressing hybridoma (clone UC8-1B9) can serve as a negative control.
9. Now cells are ready.

IV. Cell Tracker CMTPX Invitrogen, (M.W. 686.25, 50 µg/vial) stock solution preparation (optional)

1. In some experiments, hybridoma cells are stained with CMTPX to be distinguished from $CD4^+$ T cells under microscope
2. Dissolve one vial in 728.6 µl DMSO
   → 50 µg / 728.6 uL * 1 umole / 686.25 µg = 100 µM
3. Aliquot 20 µl and keep in -20 ^oC.
4. Transfer 10 ml hybridoma cells ($0.2x10^6$ cells/ml) into a 15 ml conical tube.
5. Spin down cells at 200x g for 5 min, RT.
6. Resuspend cells in 2 ml serum-free RPMI medium.
7. Add 1 µl of [100 µM] CMTPX stock solution → [0.05 µM].
8. Incubate at 37 ^oC for 15 min (water bath).
9. Following incubation, add 10 ml serum-free RPMI and spin down cells at 200x g for 10 min, aspirate supernatant.
10. Resuspend cells in 1 ml Leibovitz medium.
11. Count cells using Coulter counter (4 µm).
12. Adjust cell concentration at $0.2x10^6$ cells/ml

V. Material to bring to Image lab:
1. Poly-L-Lysine coated plates
2. $CD4^+$ T cells in 15 ml conical tubes ($1x10^6$ cells/ml)
3. Hybridoma cells in 15 ml conical tubes ($0.2x10^6$ cells/ml)
4. Laurdan stock (Invitrogen, cat# D250, 10 mM in EtOH) on ice covered by aluminum foil
5. 1000p pipette + tips
6. 200p pipette + tips
7. 10p pipette + tips
8. Timer
9. Empty glass vials.
10. Aluminum foil
11. Empty 15 ml conical tubes
12. Sterile 2 ml epi-tubes
13. FBS

VI. Lipid-raft specific cholesterol depletion by Methyl-β-cyclodextrin treatment (optional).
1. Prepare [10 mM] methyl-beta-cyclodextrin (MβCD, Sigma cat# C4555).
   A. Take 10 mg in (1000x10)/(1320x10) ml serum-free RPMI medium.
   B. Dissolve (1000x10)/(1320x10) mg FA-free BSA (Boeringer Mannheim)

2. Transfer 2 ml of $CD4^+$ T-cells to a 15 ml conical tube.
3. Spin down at setting 5 of centrifuge in Dr. Berghardt Lab for 5 min, then resuspend cells in 2 ml [10 mM] MβCD.
4. Incubate at 37 ^oC for 3 min, and wash with 10 ml serum-free RPMI (centrifuge at setting 5 for 5 min).
5. Resuspend cells in 2 ml serum-free RPMI.

VII. T cell labeling of Laurdan

1. Trasnfer 2 ml $CD4^+$ T cells ($1x10^6$ cells/ml) into a 15 ml conical tube.
2. Add 2 µl of [10 mM] Laurdan solution into 2 ml $CD4^+$ T-cell suspension.
3. Vortex at dial setting 7 for 2 sec.
4. Incubate at 37 ^oC for 10 min.
5. Spin down at the speed 5 by the centrifuge at Imaging Lab for 5 min.
6. Resuspend cells in 2 ml Leibovitz's medium.

VIII. Mix cells (T cell:hybridoma = 5:1)

7. Mix 0.4 ml hybridoma into 2 ml T-cell suspension.
8. Incubate the tube on ice for 1 min.
9. Rinse Poly-L-Lysine pre-coated chambered coverglass slides with 1 ml warm Leibovitz's medium once.
10. Transfer 1.2 ml of cell suspension from the tube to each of 2 chambered slide wells.
11. Capture images after 30 min incubation at 37 ^oC., 5% CO_2.

B-8. GP-value calculation

1. Capture Laurdan images and save the image files as 8-bit TIFF format.
2. Open the image file in Adobe Photoshop® CS (v.8.0).
3. Using a marquee tool, make a circle to select cell-cell contact region.
4. In “Histogram” panel, we can choose each channel of RGB.
5. Once blue channel is selected, the panel displays “mean intensity” of marquee-se lected region.
6. Histogram also shows the pixels chosen by marquee tool. We generally choose 8 00-1200 pixels for contact region.
7. If you change the channel to green, mean intensity is changed, while pixel is not.
8. For non-contact control cells, select whole cell by marquee tool.
9. Histogram shows green/blue mean intensities.
10. Record green and blue intensities to calculate GP-values by fomula $GP= (I_{Blue}-I_{Green})/(I_{Blue}+I_{Green})$. Example calculation is shown in Appendix A-5).

B-9. Immunofluoresence protocol
(modified from Dr. Yang-Yi Fan's protocol)

Materials:

1. FITC-CTx (Sigma, cat# C1655), make [250 µg/ml stock in dd-H2O], store at 4℃
2. Rabbit anti-LAT (Millipore, cat# 06-807, Lot# 22622, 1,000 µg/ml)
   *Ref: Fan *et al*., J Immunol. 2004 Nov 15;173(10):6151-60
3. Rabbit anti-phospho-LAT (Tyr 191) (Millipore, cat# 04-467, Lot# JBC1371310, 100-500 µg/ml)
4. Alexa 568 goat anti-rabbit IgG(H+L), [2 mg/ml] (Molecular Probe, cat# A-11036)
5. ProLong Antifade Kit (Molecular Probe, cat# P-36931)
6. 0.1%(w/v) Poly-L-Lysine solution (Sigma, cat#P8920)
7. Coverglass (No. 1, 22 x 50 mm, Corning)
8. Fresh 4% PFA in PBS (dilute from 20% PFA, EMS#15713-S)
9. Lab-Tek II 2-well glass chamber slide (Nalge, cat# 154461)

Procedure:

1. Precoat Lab-Tek II 2-well glass chamber slides with 0.01% poly-L-Lysine (10x diluted from 0.1%(w/v) Poly-L-Lysine solution with sterile H_2O) (2 wells/slide) the day before assay: Add 2 ml of 0.01% poly-L-Lysine/well for 30 min, then aspirate excess solution and allow the chamber slides to air dry. Sterile the coverglasses under UV light for 1 hr.
2. Prewarm the coated chamber slides at 37℃ for 30 min before use.
3. Prepare T cells resuspend in complete RPMI at $2x10^6$ cells/ml (See Appendix B-5)
4. Prepare hybridoma cells resuspend in complete DMEM at $2x10^6$ cells/ml (See Appendix B-10)
5. For each well, we want 2×10^6 T cells + 0.4×10^6 Hybridoma

(For each 2-well samples)

6. Wash the coated chamber slides with warm medium 3 times.
7. For each sample (2 wells), mix 2 ml T cells with 0.4 ml Hybridoma in 15 ml conical tube.
8. Mix 4 ml T cells/mouse with 0.8 ml Hybridoma
9. Mix 2 ml WT T cells with 0.4 ml Hybridoma for Ctrl
10. Centrifuge at 300 g for 5 min.
11. Resuspend the cell mix pellet in 4 ml complete RPMI.
12. Seed 1 ml/well section (dropwisely add cell suspension onto the well).
13. Incubate at 37℃ for 30 min.
14. While incubation, make 4% PFA. (4 ml of 20X PFA + 16 ml PBS => 4% PFA)
15. Wash cells (on the chamber slide) with PBS 3x, then immediately fix in Fresh 4% paraformaldehyde in PBS for 20 min at RT.
16. Rinse samples with PBS 2x, incubate cells with 10 mM glycine in PBS for 10 min at RT to quench the aldehyde groups.

17. Wash chamber slides with PBS 2x, permeabilize cells in PBS/0.2% Triton X-100 for 5 min at RT, followed by PBS wash 3x.
18. Incubate cells in Blocking solution (1% BSA/0.1% NaN_3 in PBS) at 4℃ overnight
19. Wash chamber slides with PBS 3x.
20. Dilute all Ab in Blocking solution
    For 1 well:
    A. (anti-LAT) 1°Ab mix: 8 µl of GM1 [stock 250 µg/ml] (25x dil) + 5 µl of anti-LAT [stock 1,000 µg/ml] (40x dil) + 187 µl buffer
       ➔ 80 µL GM1 + 50 µL a-LAT + 1870 µL buffer
    B. (anti-phospho-LAT) 1°Ab mix: 8 µl of GM1 [stock 250 µg/ml] (25x dil) + 5 µl of anti-phospho-LAT [stock 100-500 µg/ml] (40x) + 187 µl buffer
       ➔ 80 µL GM1 + 50 µL a-p-LAT + 1870 µL buffer
21. Incubate all cells with 200 µl AB/well, incubate at room temp for 1 hr (Protect from light)
22. After 1 hr incubation, wash slide chamber with PBS 3x, and the last wash with blocking solution.
23. For 1 well: 2° Ab 1 µl of Alexa 568 goat anti-rabbit IgG [stock 2 mg/ml] (1:200 dil) + 199 µl buffer
24. 20 µL Alexa 568 + 3980 µL Buffer
25. Incubate cells with 200 µl/well 2° Ab (Alexa 568 goat anti-rabbit IgG [10µg/ml] at RT for 1 hr at a humidity chamber.

** Prepare the ProLong medium and labeling slides during the 1 hr incubation

- Mix 2 ml of ProLong mounting medium (Component B) to two brown vials of Prolong antifade reagent (Component A). (Mix well by pipetting or vortexing, remove bubbles that have formed during the mixing procedure by sonication)

26. Use the slide separator to remove the chamber. Put the slides on the metal slide holder for the following wash.
27. Wash coverglass with PBS 3x.
28. Incubate coverglass in 70% ethanol 1x.
29. Incubate coverglass in 95% ethanol 1x.
30. Incubate coverglass in 100% ethanol 1x.
31. Incubate coverglass in fresh xylene 1x.
32. Apply a small amount of antifade reagent/mounting medium mixture to the coverglass, cover the slide while it is still wet. (Use glass rod to put a line of medium on the side of the coverglass, then cover the slide at 45° angle to avoid bubbles) use razor blade to help coverslipping.
33. Place the coverglass/slide on a flat surface in the dark to dry overnight at RT.
34. Once dry, seal the coverglass to the slide with fingernail polish, to prevent shrinkage of the mounting medium and subsequent sample distortion.
35. After sealing, store the coverglass/slide upright in a covered slide box at -20 ℃. Desiccant may be added to the box to ensure that the slide remains dry.
36. Examine sample under Fluorescence microscopy.

B-10. Curcumin/Limonin study protocol

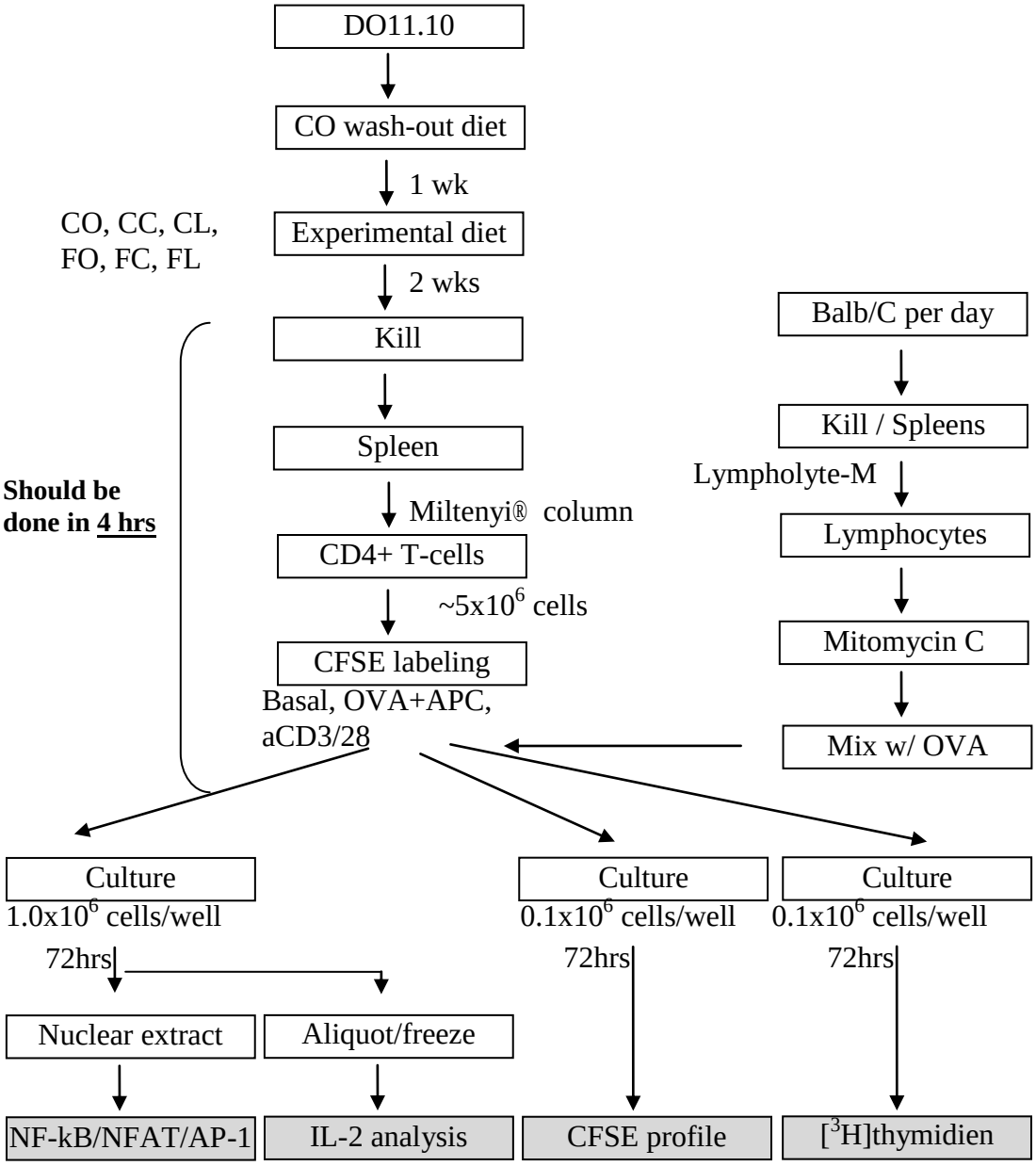

I. D-1: Reagents preparation
   1. OVA stock preparation
      1) Prepare 0.5% acetic acid solution: 500 µl HPLC grade acetic acid in 100 ml sterile water, then split into two 50 ml conical tube.
      2) Dissolve 1 mg lyophilized OVA peptide in 0.5 ml sterile water.
      3) To a low retention eppi tube, add 360 µl sterile water and 90 µl 0.5% acetic acid.

4) To the same tube, add 450 µl dissolved peptide.
5) Aliquote to 20 µl and store < -70 ^{o}C.

Stock concentration: (OVA M.W. 1774 g/mole)
1 mg/500 µl x 1/2 x mole/1774 g = 563.698 µM

2. 25 µg/ml Mitomycin preparation
   1) Mitomicyn C (Sigma, MW 334.3, cat# M4287) contains total 50 mg of 2mg mitomycin C and 48mg sodium chloride.
   2) Measure 10 mg → 2*10/50 mg mitomycin C
   3) Dissolve in 16 ml sterile PBS → 25 µg/ml

II. D-0: Kill/Co-culture
1. APC preparation
   1) Sacrifice Balb/C mouse by CO_2.
   2) Place the mouse on their right side so that the left side is facing up.
   3) Apply 70% EtOH to the abdomen area.
   4) Grab the skin of the abdomen with forceps and make a small incision.
   5) Peel the skin to expose the membrane underneath.
   6) Grab the membrane with forceps and cut the membrane to expose the organs.
   7) Remove the spleen with forceps while cutting the fat tissue with scissors.
   8) Carefully remove as much fat as possible.
   9) Place the spleen in a conical tube containing MACS buffer.
   10) Bring the tube into cell culture room.

-----Do the below in the HOOD----

1) Place a Falcon cell strainer (70 µm mesh, BD, # 35-2350) on the 100mm petri dish, and pre-wet with 5 ml MACS buffer.
2) Transfer spleens into cell strainer.
3) Gently press spleen against the bottom of the strainer with a plunger from a 5 ml syringe. Use up and down motion (not grinding), being careful not to damage cells.
4) When only the spleen connective tissue remains in the strainer, remove the strainer.
5) Place a 30 µm filter on the top of a new 15 ml conical tube, and pre-wet with 2 ml Miltenyi buffer.
6) Transfer the cell suspension from the dish to the filter.

7) Wash strainer with 5 ml MACS buffer to collect the remaining cells. Transfer to the filter
8) Spin down at 300x g for 10 min.
9) Aspirate supernatant, and resuspend the pellet in 3 ml complete RPMI (w/o 2-ME).
10) Shake-mix Lympholyte-M before use. Lay 3 ml Lympholyte-M down by putting pipette tip into the bottom of tube.
11) Centrifuge at 500x g for 15 min, RT with acc/brake=0.
12) Transfer the interface band by pipetting up into a 15 ml conical tube.
13) Wash with 10 ml RPMI (300x g for 10 min, RT), then aspirate the supernatant.
14) Resuspend cells in 1 ml of 25 µg/ml mitomycin C solution.
15) Incubate at 37 ^{o}C. (water bath) for 20 min.
16) Add 10 ml complete media, and transfer 2 ml to a new conical tube for APC control. (no OVA)
17) Wash with complete RPMI (300x g for 10 min, RT).

2. OVA preparation with APC

--- for OVA stimulation ---

1) Dilute OVA stock into 0.1 µM
: 4.43 µl OVA stock into 25 ml complete RPMI with 2-ME.
2) Resuspnd cells in 5 ml complete RPMI with OVA.

--- for APC control ---

3) Resuspedn cells in 1 ml complete media (w/o OVA)
4) Count cells by Coulter Counter.
5) Adjust cell concentrations at 2.5x10^{6} cells/ml.
6) Now APC are ready for co-culture, keep cells at 37 ^{o}C in 5% CO_2 chamber.

III. Isolate CD4+ T cells from spleens of DO11.10 mice following Appendix B-5.
IV. Culture for with stimuli

7) Count CD4^{+} T-cell by Coulter counter.
8) Adjust cell concentration to 1x10^{6} cells/ml.
9) Transfer 1 ml cell suspension into each well of 24-well plate for cytokine/nuclear extration.
10) Transfer 100 µL cell suspension into each well of 96-well plate for cell proliferation assays.
11) Tape the plate then place into 37 ^{o}C in 5% CO_2 incubator for 72 hr.

B-11. Hybridoma Handling (145-2C11, UC8-1B9)
(modified from Dr. L. Davidson's protocol and Product Info Sheet from ATCC)

1. Reagents
   A. Complete medium

	Vol(ml)	%	Stock Conc	Final Conc	Vendor	Cat#
DMEM	500.00	86.03			Gibco	11960-44
FBS	58.00	9.98			Invitrogen	16000
Glutamax	11.60	2.00	200mM	4mM	Gibco	35050-061
Na pyruvate	5.80	1.00	100mM	1mM	Cellgro	25-000-CI
Pen-Strep	5.80	1.00	10,000U/ml P 10,000µg/ml S	100U/ml P 100µg/ml S	Gibco	15140-148
Total	581.20	100.00				

   B. <u>During critical period (ie. After thawing), add 80u/ml hrIL-6</u>
      hrIL-6 stock is 200,000U/ml. Mix 50 ml complete media with 20 µl hrIL-6.
      (Roche, Cat# 11-138-600-001, Lot# 93320322)
   C. Cryoprotectant medium
      : complete medium with 5% (v/v) sterile DMSO
   D. Hybridoma
      i) 145-2C11: ATCC Cat# CRL-1975, Lot# 3048198
      ii) UC8-1B9: ATCC Cat# CRL-1968, Lot# 1375980

2. Handling frozen cells
   A. Prepare 45 ml and 14 ml complete media (with IL-6, see reagents) for 145-2C11 and UC8-1B9, respectively, in T-75 flask (the volumes differ to each batch. Confirm to Specific Batch Info)
   B. Place the flask into 5% CO2 inculbator at 37 ^{o}C for at least 15min.
   C. Thaw the vial by gentle agitation in a 37 ^{o}C water bath. To reduce the possibility of contamination, keep the O-ring and cap out of the water. Thawing should be rapid (approx. 30 sec).
   D. Move the vial to sterile hood, and spray 70% EtOH to the vial.
   E. Transfer the vial contents to a 15 ml conical tube.
   F. Wash with 10 ml complete medium by centrifuge at 200x g for 5 min.
   G. Aspirate supernatant and resuspend cell in 1 ml complete medium.
   H. Transfer cell suspension to the pre-warmed T-75 flask.
   I. Incubate in 5% CO_2 inculbator at 37^{o}C.
   J. After thawing, cells generally become confluent in 5 days (UC8-1B9) or 7 days (145-2C11).
   K. Renew the medium 2-3 times weekly (If media look yellow-it means acidic-, replace media immediately)
   L. A number of cells are adherent to the flask bottom. The viability was 93.66% (suspending cells) and 77.77% (adherent cells) determined by trypan blue exclusion method. Therefore, use only suspending cells by pipetting up the media,

not touching the flask bottom.

2. Passaging
   A. Prepare 18 ml complete media in a T-75 flask and keep the flask in the 37 ^{o}C incubator for ~15 min.
   B. Harvest suspending cells by pipette into a 50 ml conical tube. (Try to avoid mixing adherent cells by shaking flask or touching the flask bottom). Centrifuge cells at 200x g for 5 min. Aspirate the supernatant and resuspend cells in 5 ml complete DMEM media.
   C. Count cell concentration by Coulter Counter. Adjust conc. to $1x10^{6}$ cells/ml by adding complete DMEM.
   D. Transfer 2 ml cell suspension into the pre-warmed T-75 flask.
   E. Place the flask in the 37 ^{o}C 5% CO_2 incubator.

B-12. PMA/Ionomycin preparation

PMA (Sigma #P8139-1MG, Light sensitive)

1. Inject 1 ml sterile filtered DMSO into container using 1 ml syringe.
2. Wait until all powder dissolves
   → This is 1 mg/ml solution (too concentrated)
3. Take 2 µl of [1 mg/ml] soln, and add to 1 ml sterile DMSO
   → This is 2 µg/ml soln.
4. Aliquot 15 µl, and store at -20 ^{o}C.
5. Save remaining [1 mg/ml] at -20 ^{o}C.

Ionomycin (Calbiochem #407952)

1. Add 1.33 ml sterile filtered DMSO to 1mg powder
   0.001 g x 1 mole/747.1 g x 1000 mM/1 mole = 1.33×10^{-3} mM
   1.33×10^{-3} mMole/1.33 ml = 1mM
2. Mix and let sit for 5 min.
3. Aliquot 15 µl, and store at -20 ^{o}C.

VITA

Name Wooki Kim

Address Rm 321 Kleberg Biotechnology Center, TAMU 2253
College Station, TX 77843-2253

Email Address bbock76@gmail.com

Education B.S. in Biotechnology, Yonsei University, Seoul, Korea, 2002

Awards

04/ 2008	ASNS/Procter & Gamble graduate student research award competition- overall winner of the oral completion, travel award
03/ 2007	ASNS/McNeil Nutritionals predoctoral fellowship
07/ 2006	Texas public education grant- international
09/ 2004	Regent's fellowship, Texas A&M University
09/ 2004	Graduate study abroad scholarship, Korea Science and Engineering Foundation
2006, 2007, 2008	Competitive scholarship, Intercollege Faulty of Nutrition, Texas A&M University

Publications

- Kim, W., Fan, Y., Barhoumi, S., Smith, R., McMurray, D. N., and Chapkin, R. S. 2008. N-3 polyunsaturated fatty acids suppress the localization and activation of sign aling proteins at the immunological synapse in murine $CD4^+$ T-cells by affecting lipi d raft formation. *J. Immunol.* 181:6236-6243
- Kim, W., McMurray, D. N., and Chapkin, R. S. 2008. Chemotherapeutic properties o f n-3 polyunsaturated fatty acids - Old concepts and new insights. *Immunol., Endocri nol. & Metabol. Agents in Medicin. Chem.* (In press)
- Fan, Y., Kim, W., Callaway, E., Jia, Q., Zhou, L., McMurray, D. N., and Chapki n, R. S. 2008. Fat-1 transgene expression prevents cell culture-induced loss of memb rane n-3 fatty acids in $CD4^+$ T-cells. *Prostag. Leukotr. Ess.* (In press)
- Jia, Q., Lupton, J. R., Smith, R., Weeks, B. R., Callaway, E., Davidson, L. A., Ki m, W., Fan, Y., Yang, P., Newman, R. A., Kang, J. X., McMurray, D. N., and Chapk in, R. S. 2008. Reduced colitis-associated colon cancer in Fat-1 (n-3 fatty acid desatu rase) transgenic mice. *Cancer Res.* 68: 1-7
- Zhang, P., Kim, W., Zhou, L., Wang, N., Ly, L. H., McMurray, D. N., and Chapki n, R. S. 2006. Dietary fish oil inhibits antigen-specific murine Th1 cell development by suppression of clonal expansion. *J. Nutr*. 136: 2391-2398